REPORT DOCUMENTATION PAGE

Form Approved
OMB No. 0704-0188

1. AGENCY USE ONLY *(Leave blank)*

2. REPORT DATE
29.Sep.03

3. REPORT TYPE AND DATES COVERED
DISSERTATION

4. TITLE AND SUBTITLE
"BIOMOLECULAR PATTERNING ON MICRO AND NANOFABRICATED SURFACES FOR BIOSENSOR APPLICATION AND CELL-BASED RESEARCH"

5. FUNDING NUMBERS

6. AUTHOR(S)
CAPT ORTH REID N

7. PERFORMING ORGANIZATION NAME(S) AND ADDRESS(ES)
CORNELL UNIVERSITY

8. PERFORMING ORGANIZATION REPORT NUMBER
CI02-1289

9. SPONSORING/MONITORING AGENCY NAME(S) AND ADDRESS(ES)
THE DEPARTMENT OF THE AIR FORCE
AFIT/CIA, BLDG 125
2950 P STREET
WPAFB OH 45433

10. SPONSORING/MONITORING AGENCY REPORT NUMBER

11. SUPPLEMENTARY NOTES

12a. DISTRIBUTION AVAILABILITY STATEMENT
Unlimited distribution
In Accordance With AFI 35-205/AFIT Sup

DISTRIBUTION STATEMENT A
Approved for Public Release
Distribution Unlimited

12b. DISTRIBUTION CODE

13. ABSTRACT *(Maximum 200 words)*

20031015 019

14. SUBJECT TERMS

15. NUMBER OF PAGES
176

16. PRICE CODE

17. SECURITY CLASSIFICATION OF REPORT

18. SECURITY CLASSIFICATION OF THIS PAGE

19. SECURITY CLASSIFICATION OF ABSTRACT

20. LIMITATION OF ABSTRACT

BIOMOLECULAR PATTERNING ON MICRO- AND NANOFABRICATED SURFACES FOR BIOSENSOR APPLICATIONS AND CELL-BASED RESEARCH

A Dissertation

Presented to the Faculty of the Graduate School

of Cornell University

in Partial Fulfillment of the Requirements for the Degree of

Doctor of Philosophy

by

Reid Nelson Orth

May 2003

BIOMOLECULAR PATTERNING AT MICRO- AND NANOMETER SCALE DIMENSIONS FOR BIOSENSOR APPLICATIONS AND CELL-BASED RESEARCH

Reid Nelson Orth, Ph.D.

Cornell University 2003

In this thesis research, biomaterials are patterned at the micro- and nanometer scale for biosensor applications and cell-based research. Two enabling technologies were photoactivatable biotin and the polymer lift-off technique. Avidin-biotin complexes have been immobilized on planar silicon substrates and to the inner surfaces of capillary tubes. The latter serves as a model for patterning inside microfluidic systems. Several biomaterials have been patterend using the polymer lift-off method including lipids, metal, microspheres, biotin, and proteins (e.g., antibodies, protein A, and NeutrAvidin). The patterned lipids formed supported lipid bilayers with diffusion coefficients comparable to cell membranes as confirmed by fluorescence recovery after photobleaching (FRP). My tailored patterns comprised 2, 4-dinitrophenyl (DNP) or biotin functionalized lipids with features ranging from 1.3 μm to 76 μm. Non-lipid molecules were patterned in features as small as 700 nm. A characterization of the surfaces has shown a highly uniform patterning. Several of these materials were also applied in patterned regions inside microtrenches.

Micro- and nanometer scale patterns of functionalized biomaterials served as spatially controlled stimuli for cell surface ligands in this research. This technology has been applied to the rat basophilic leukocytes (RBL) cells, eosinophils, lymphocytes, macrophages, and fibroblasts. For RBL experiments, DNP-conjugated lipids have been incorporated in the lipid bilayers with fluorescent lipid $DiIC_{16}$ and used to stimulate RBL cells sensitized with anti-DNP IgE on the F_c receptors (FcϵRI). Receptor aggregation was observed with confocal microscopy. This technique allows

researchers to study the effect of antigen density on cellular response, the binding kinetics, and the redistribution after individual binding events. SEM imaging provided a nanometer scale view of the intricate cell-cell and cell receptor-ligand interactions. Mitogens and bacteria were used to stimulate immune responses of macrophages and lymphocytes. Confocal fluorescence microscopy and scanning electron microscopy (SEM) allow visualization of the proliferative responses, morphological changes, and the spatial distribution of mitogen-stimulated lymphocytes. Patterned complexes of BSA:anti-BSA IgG (equine) serve as stimuli initiating eosinophil immobilization, activation and degranulation. These spatially defined, micron scale biomaterial arrays serve as biomimetic membrane models that can be used to stimulate and analyze cellular and subcellular responses to environmental cues.

ACKNOWLEDGMENTS

TABLE OF CONTENTS

LIST OF TABLES

LIST OF FIGURES

CHAPTER 1

MAKING IT SMALL IN A BIG WORLD--INTRODUCTION TO BIOMATERIAL MICROPATTERNING

Nature has taken advantage of the physical, chemical, and biological properties of atoms and molecules at the nanometer scale over the past several billion years to generate life and living systems as we know them today. The physical, chemical, and biological properties have been exploited and optimized to create everything from single cell bacteria, to geometric diatoms, to 10 meter dinosaurs. Over the past several hundred years, scientists have enhanced their ability to control materials interactions at smaller resolutions through a better understanding of chemistry, physics, and other sciences. Careful control of material microfabrication has progressed steadily over the past several decades. Steady progress has occurred over recent years to enable materials to be patterned at the micro- and nanometer length scales offers the ability to shape materials to tens of nanometers. The advent of tools such as atomic force microscopy (AFM), electron beam microscopy (EM), and transmission electron microscopies have enabled materials to be viewed at low nanometer resolutions. AFM and EM have also been used to pattern materials at the nanometer length scale and provided researchers a means to analyze more precisely biological, chemical, and physical interactions found in nature. The ever-changing technology environment strives to produce commercial and benchtop devices that are faster, cheaper, and smaller. Nanofabrication technology is rapidly becoming the central technology that enables these three objectives to be achieved.

Biosensors offer a means to detect or measure biological and chemical molecules and acquire real-time information for monitoring and analyzing chemical, biological, and biophysical processes. Advances in biomedical research have come a long way over the past 100 years. At a scientific meeting held on biosensors in 1986,

the Royal Society in London defined biosensors as "a device that recognizes an analyte in an appropriate sample and interprets its concentration as an electrical signal via a suitable combination of a biological recognition system and an electrochemical transducer" [1]. The basic premise behind most biosensors is their ability to detect an analyte interacting with a surface. Technological advances developed after the invention of the transistor have enabled the development of microfabricated electronic devices. Refined processing techniques have improved the patterning capabilities to allow patterning with submicron resolution. Chapters 2-5 provide an overview of avidin-biotin technology and patterning using the polymer lift-off technique that can be applied to biosensor applications.

Physical, chemical, and biological principles often form the foundation and framework for innovative research. Recent technological advances have been made through interdisciplinary efforts that married once discrete fields into new areas of study. This thesis details how equipment commonly used in the highly optimized nanofabrication industry is applied to biological research studies. The first part of this thesis reviews the technologies involved in biomaterial patterning. The second part of the thesis details several cell-based applications.

Introduction to Biomaterial Patterning

My initial experimental efforts focused on developing protocols for patterning biomaterials on silicon substrates. A critical need was for the patterned proteins to retain their functionality. The avidin-biotin technology was selected since it lets the biomaterials maintain their functionality after patterning, ease of use without a need for complex chemical experimentation, and portability with the small chip size. The avidin-biotin method has added stability with robust avidin and biotin molecules. The next experimental efforts involved coupling these techniques with surface

modification techniques for biosensor applications designed to detect antigen, protein, and other biomolecules.

Avidin-biotin affinity molecules offered a generic building block onto which other molecules could be spatially distributed. Use of avidin and biotin molecules in research is an increasingly popular method for biomolecule immobilization. The avidin and biotin molecules are naturally occurring molecules with strong binding affinity for each other; this offers the essential physical-to-biological link that is needed when working with bioincompatible substrates. The high affinity of the two molecules offers potential for numerous research applications detailed later in this thesis. The avidin-biotin technology was also used for its ability to retain functionality after patterning and to withstand a wide range of pH, salinity, temperature, and other biological environmental conditions. Avidin-biotin technology offers precise and quantifiable control over molecules onto which they can bind, ranging in size from sub-micron to several centimeters. Any limitations in pattern size arise from the minimum feature resolution of the photolithography process. Substances that could be patterned include enzymes, antigens, antibodies, receptors, cell organelles, bacteria whole cells, and nucleic acids.

In addition to microcontact printing, photolithography and analytical chemistry steps were used to spatially distribute photobiotin onto silicon wafers and inside microfluidic tubes. The biotin-avidin-biotinylated-antibody complex was immobilized on a substrate with a self-assembled monolayer and the NHS ester of photobiotin. The antibodies were anchored through their biotinylation link and were subsequently bound to target antigen (protein A-covered spheres and bacterial cells). Each layer of patterning was characterized visually with fluorescent molecules. This research improved upon previously performed avidin-biotin patterning with its sharper feature resolution, first successful patterning of cells and spheres on patterned antibodies

using photobiotin, and an extensive characterization of the patterned biomolecule levels with fluorescence. In the second avidin-biotin study, photobiotin and avidin were patterned inside capillary tubes. This was a novel research technique that offered the first photolithographic means to pattern inside already enclosed microfluidic systems.

Introduction to Avidin-Biotin Technology

Avidin-biotin technology has progressed significantly since the seminal research performed by Green in 1975 [20]. This research detailed the characteristics of the avidin and biotin molecules and their applicability to chemical and biological experiments.

Avidin-biotin complexes are a preferred component of protein immobilization since they are easy to use, modify, and incorporate into experiments that have harsh environments [61]. Chemical biotinylation methods of many macromolecules have been described in the literature. Avidin-biotin technology is a useful experimental tool since biotinylated molecules retain their biological, chemical, and physical characteristics after binding to immobilized or soluble avidin [62].

The avidin and biotin molecules are an excellent linking pair since they have a strong association constant. Wilchnek, *et al.,* (1988 and 1990) determined the association constant of avidin and biotin to be $K_a = 1 \times 10^{15} \ M^{-1}$ [18], [61] and streptavidin to biotin to be $K_a = 1 \times 10^{13} \ M^{-1}$ [62]. This strong affinity allows the bond to survive conditions that would normally dissociate weaker bonds. The strength of the avidin-biotin bond and the generic nature of the biotinylation of proteins, DNA, or polysaccharide make avidin-biotin technology widely applicable to patterning [23]. The avidin-biotin complex bond is very stable and can withstand the following extreme conditions: a brief exposure to 132°C temperature, pH values between 2 and

13, guanidine-HCl up to 8 M at neutral pH, and detergents (only mildly affected by them) [52].

Avidin-biotin technology for microchip fabrication involves linking biotin to a silicon surface through an aminated silane, binding avidin to the biotin, and subsequently binding a biotinylated molecule to the avidin. Biotinylated molecules can subsequently bind to the avidin through the biotin link. Avidin is a tetrameric molecule consisting of four homologous subunits that bind biotin [20]. Streptavidin and NeutrAvidin are refined forms of avidin that have decreased nonspecific binding to substances other than biotin [52].

The ability to covalently bind molecules to polymer surfaces provides better control of the performance of the assay [23]. Protein patterning, the defined spatial localization of molecules on a surface, is a powerful approach for bioelectric applications.

Photobiotin

Photopatterning has been used to spatially distribute biomolecules, i.e., enzymes, antibodies, and nucleic acids, which are used in the development of biochips [15]. Several forms of photobiotin have been created to bond biotin to a substrate and overcome this deficit. Photoactivatable biotin [nitro(aryl)azide derivative of biotin, MW 533.65, 3 nm in size]; photocleavable biotin [NHS-Iminobiotin, MW 421.32, 1.35 nm]; and caged biotin [N-(4-azido-2-nitrophenyl)-N-(3-biotinylaminopropyl)-N-methyl-1-3-propanediamine)] have been used primarily to label proteins and nucleic acids [15], [16]. Photoactivatable biotin is the salt form of photobiotin. While biotin is useful for its strong binding to avidin, it cannot form a strong bond to hydrophobic substrates. Therefore, the samples are plasma cleaned prior to photobiotin application.

Photobiotin binds covalently to an organic surface when exposed to UV light [23]. In these experiments, the photoactivatable NHS group nitrene binds on the silane molecule. Exposure of photoactivatable biotin to UV light induces a photochemical reaction that generates a nitrene, which readily inserts into C-H bonds and other chemical groups as well [15]. During UV photolysis the aromatic nucleus absorbs light, which is followed by a vibrational transition to the azide group [27]. Elimination of nitrogen occurs and generates a reactive, uncharged singlet or triplet nitrene [58]. Singlet nitrenes react preferentially by insertion into O-H or N-H bonds, but if intersystem crossing occurs to form a triplet, insertion into a C-H bond to form a secondary arylamine is favored [58]. After the azide group of photobiotin has been activated by UV light, it subsequently binds covalently to the silane on the substrate surface.

A related technology is the use of caged biotin that is photodeprotected when UV light irradiates the photosensitive reagents [56]. Subsequently, an inactive form of biotin is converted into a form that actively reacts to a substrate and subsequently immobilizes the biotin along with molecules bound to the biotin to the substrate.

Avidin-Biotin Technology Applications

Numerous citations in the literature of avidin-biotin applications demonstrate the versatility and utility of this technology. An application for caged biotin, a non-binding derivative of biotin, was first demonstrated by Sundberg [56]. The method of uncaging the biotin converts it into a form that can actively bind avidin. Uncaged biotin can be covalently bound to a substrate and then photochemically activated to induce binding to a target molecule [48]. Yang, *et al.* (2000) deprotected caged biotin in regions irradiated by masked UV light, and subsequently incubated the samples with streptavidin resulting in selective binding of streptavidin to the irradiated regions [64].

Dortha, *et al.* (1997) used photopatterning of caged biotin to achieve spatial distribution of biomolecules, i.e., enzymes, antibodies, and nucleic acids, which are used in the development of biochips [15]. Interference patterns from the 325 nm UV laser shown through a diffraction pattern form patterns of APase enzymes onto the carbon electrode surface. Some portions of a carbon fiber were left underivitized to facilitate electron transfer reaction of redox mediators. Fluorescent images of the modified carbon surfaces were obtained by passing the light from the mercury arc lamp through an excitation filter specific for Texas Red absorption band (595 nm) and collecting all fluorescence at wavelengths greater than 615 nm with a 1-second camera collection time. A 50% beam splitter was used to produce the line spacings with light from the HeCd laser. 10 μm and 5 μm spacings were created. The average line width for the patterned 5 μm lines was 4.95 μm $\pm$ 0.19 μm (n = 5). The samples were irradiated with light at 325 nm (~1 W/cm^2 for 30-200 sec); irradiation for 60 sec produced the desired array pattern. Florescence dye added for 30 min. The average width with avidin added was 5.05 μm $\pm$ 0.1 μm. Exposures lasting up to 30 min were performed using a mask with a 50-mesh copper grid. Use of the grid required a tight seal between the grid and substrate. These experiments showed that derivitization of carbon surfaces degraded electron transfer characteristics. This method segregated the sites of enzyme immobilization from the electron transfer on the same electrode surface. It was also demonstrated that maskless photolithography could be used for photodeprotection chemistries.

Brooks, *et al.* (1999) used laser scanning confocal optics in conjunction with avidin-biotin technology to make micrometer-sized patterns of biomolecules on glassy carbon and fused silica surfaces [9]. A 325-nm HeCd laser (1 W/cm^2) was focused with 25X and 100X microscope objectives to make 5-20 μm patterns. The light was shown at varying scan speeds onto caged photobiotin, resulting in photodeprotection

(activation of photosensitive reagents to immobilized proteins). The integrity of immobilized biotin was confirmed by subsequent derivitization with fluorescently-labeled avidin. Laser use allowed writing different patterns without multiple masks. Polished carbon wafers with 45 nm z-direction difference were used. Tunneling electron microscopy grids (100 mesh square copper) were used as masks. The optimal exposure was found to be 1.5 min at 90 J/cm^2. The focused beam intensified light to 6 orders of magnification higher than unfocused; the writing was conducted with a 5% neutral density transmission filter producing a 5 kW/cm^2 intensity (90 J/cm^2).

Pritchard, *et al.* (1995) immobilized avidin to the surface of thiol-covered gold and silica substrates and then added photobiotin, which bound strongly to immobilized avidin [49]. They used carbodiimide and silanization methods for the immobilization. They used photolithography masks with patterns as small as 1.5 μm spacing on a silicon wafer.

Kossek, *et al.* (1996) developed an immunosensor for electrochemical detection that used estradiol as an antigen [33]. Ferrocene-labeled antibodies were used in a competitive assay to recognize the estradiol. The ferrocene redox centers were detected electrochemically by the gold electrodes on the silicon surface. The silicon chip was designed to be integrated into micromachined fluid transport systems. Streptavidin molecules were immobilized on silicon in a density of up to half of a theoretical monolayer, assuming a size of 4 x 4 nm per molecule. The surface density of 160 ng/cm^2 (2.7 $pmol/cm^2$) of streptavidin corresponding to 40% of a monolayer was achieved using 32 μg of streptavidin/chip. The immobilized streptavidin was fully functional, as proven by ELISA. The maximum surface density of biotin estradiol, determined by I^{125}-iodinated streptavidin [2] and confirmed with SFM, was ~2 $pmol/cm^2$. This was also the optimal antigen surface density for biorecognition. An immunoanalytical test was performed and demonstrated that the amount of

immobilized streptavidin decreased with further reuse treatments. This immunosensor transduced the antigen-antibody recognition directly into an electrochemical signal.

Hengsakul, *et al.* (1996) performed experiments with photobiotin dried onto polystyrene or nitrocellulose surfaces and exposed to white light [23]. This research demonstrated that enzymes retained catalytic activities as visualized through the formation of color or fluorescent products. Factors such as concentration, irradiation time, and light intensity were used to determine the amount of active enzyme that bound through photobiotinylation. The general patterning procedure involved irradiation of a dried film of photobiotin (20 µL/mg) with intense visible light (350-370 nm) of 5 min exposure on the polymer surface. This lead to the conversion of the aryl azide to a reactive aryl nitrene [16], which then inserted into the bond of the polymer [54], resulting in the formation of a covalent linkage between the two [23]. The controls to check for nonspecific binding were performed by irradiating plates in the absence of photobiotin and by adding photobiotin to plates kept in the dark. Nonspecific binding to suitably blocked surfaces was only about 8% of the specifically bound value and was quite independent of either irradiation time. Intensities measured were as follows: the unmaked portions were 24.5 ± 1.6 arbitrary units, the masked portions were 3.8 ± 0.3 units, and the control with no photobiotin was 3.4 ± 0.3 units. Optimum irradiation time was 20 min. For the nitrocellulose experiments, the optimum irradiation time was 10 min. The intensities measured were as follows: the exposed portions were 89.5 ± 2.2 units while the unexposed was 42.5 ± 3 units. Two controls were used. The first was a photobiotin-treated membrane with no light that was washed extensively, had no visible pattern and had an intensity of 19.4 units. The second sample was biotin-free and used had an intensity of 15.2 units. Completely untreated samples had an intensity of 1-2 units, indicating that the light reflected or scattered had an impact. A Fourier transform IR spectra was obtained to confirm that

the azide had been converted to a reactive nitrene and inserted into organic surfaces; the IR spectra initially showed the characteristic azide adsorption at 2138 cm^{-1} and did not contain this peak after being exposed to light.

Microcontact Printing Process Introduction

Many patterning techniques use lithographic methods, most often borrowed from microelectronics technology, to reproduce a mask pattern using biologically relevant chemicals [7]. A popular form of patterning materials at the micron scale is microcontact printing as described by Kumar, *et al.* (1993). They reviewed microcontact utility for several applications: creation of heterogeneous substrates for scanning probe microscopy, the formation of microelectrodes, the formation of microstructures of silicon, the preparation of substrates for the study of condensation and the preparation of substrates for patterned formation of microcrystals [36]. Microcontact printing (μCP) is an extremely versatile method for patterning micrometer size patterns on silicon, glass, or plastic substrates. The polymer polydimethylsiloxane (PDMS) forms the patterned stamp for μCP. Two examples of its use include printing alkanethiols [42] and polyethylene glycol (PEG) on gold to control cell growth on an inorganic substrate [53]. Over the past several years, there has been a dramatic increase in technologies allowing biological and biocompatable materials to be patterned on inorganic surfaces. Of particular interest are patterning of amino acids, antibodies, and proteins. These patterned molecules serve as an intermediate link that can actively bind biological cells and tissues. Furthermore, these patterned molecules can be configured to control cell attachment and growth [7].

Self-assembled monolayers (SAMs) are molecules that spontaneously bind to a solid surface and form a uniform monolayer [45]. SAMs are frequently used to serve as a link between a substrate and the molecules that are patterned. The chemical and

physical properties of SAMs are well characterized and, therefore, provide a surface that has pre-defined characteristics. Furthermore, the molecules in SAMs can be controlled to create a specific platform onto which other molecules can be bound. The thickness of the organic layer and chemical properties of the exposed interface can be manipulated by varying the length of the alkene chains in the SAM [36]. Microcontact printing is an attractive micropatterning method since the samples do not degrade over time, as analyzed by the reusability of the patterns in the study after 9 months [36].

Two of the most attractive features of patterning the formation of SAMs using the rubber stamping technique are the simplicity of the procedure and the accuracy of transferring the pattern [36]. Once a master is created, multiple impressions can be made routinely and quickly without further access to lithographic facilities. Furthermore, the pattern master can be reused numerous times to produce several rubber stamps.

Microcontact printing makes use of the PDMS elastomeric stamp to spatially distribute biomolecules, chemicals, molecules, or amino acids on a normally bioincompatable substrate. Having a biocompatible material on the surface can provide specificity to target molecules in a solution. This technique develops a favorable adhesive island of precisely set dimensions surrounded by an unfavorable nonadhesive surface [10]. An example of μCP using this principle is the patterning of polylysine on a biologically incompatible glass surface to control the neurite growth of hippocampal cells [23].

Identifying biomolecules that will discourage cell growth and adhesion is as important as identifying ones that promote cell growth. Hydrophobic silanes are frequently used to discourage cell attachment and growth in culture. Bovine serum albumin (BSA) is a commonly used protein to bind free amine groups and other molecules that promote binding [25]. The following is an evaluation of two

nonpermissive background molecules: polyethylene glycol (PEG) and the amino acid serine ($C_3H_7NO_3$) [9]. PEG is frequently used to reduce nonspecific protein adsorption onto biomedical devices [22]. In a study using two nonspecific blocking agents (serine and PEG), serine prevented neurite binding on 40% of the area at midculture and 5.5% after 29 days. PEG, in comparison, blocked 55% at midculture and 12% after 29 days. PEG was determined to be more effective as a nonpermissive substrate.

Charged biomolecules, proteins, and specific peptide sequences are used to achieve cytophilic and cytophobic neuron-to-substrate interactions. For example, Kleinfeld, *et al.* (1988) demonstrated how the hydrophilic and positively charged organosilanes [N-(2-aminoethyl) (3-aminopropyl) triethoxysilane] (EDA) and diethulenetriaminepropyltrimethoxysilane (DETA) have proven effective in promoting cell adhesion [31]. In a related paper, Branch, *et al.* (1998) used microstamping techniques for depositing biomolecules on glass surfaces for controlling neuronal cells [8]. Another paper written by Branch, *et al.* (2000) focused on the important issue of controlling background materials that deter cell growth for long periods, which is essential for stable biological experiments [7]. He used a grid of proteins (poly-D-lysine) printed on silicon substrate, resulting in a substrate onto which hippocampal cells actively bound, thus promoting neural attachment and neurite growth.

Lahiri, *et al.* (1999) used μCP to pattern ligands onto SAMs of alkothiolates on gold. Mixed SAMs allowed control over surface binding: SAMs high in -COOH led to decreased nonspecific binding. SAMs present both patterned ligand and oligo (ethylene glycol) triethylene glycol ((EG)$_3$) resist protein adsorption. Carboxylic acid groups of pentafluorophenyl ester groups have a reactivity ~10 times greater than N-hydroxysuccinimidyl esters (23). Use of living cells benefited from the ligands that cause adhesion of cells or of protein adhesion factors recognized by cells. Fresh

PDMS was oxidized with plasma treatment, covered with primary amine, and brought into contact with activated SAMs. The smallest features resolved were 5 μm on a side. μCP yield of anti-biotin was ~90% of that by immersion of the substrate into the avidin solution (~75% for carbonic anhydrase). This procedure was conducted in a two-step process: the -COOH terminal groups were converted to reactive groups and were then stamped using the PDMS elastomeric stamp. Two molecules were stamped, then tested with anti-biotin antibody (fluorescently-labeled). Alkanethiolates were patterned on the gold surface with feature sizes ranging from 0.2 to 100 μm, with feature sizes of 1 to 100 μm easily reproducible showing the adsorption of multiple SAMs on a single substrate [36].

Zhang, *et al.* (1999) used μCP to engineer biological surfaces and pattern two oligopeptides containing a cell adhesion motif $(RADS)_n$ (n=2 and 3) at the N-terminus, followed by an oligo (alanine) linker and a cysteine residue at the C-terminus. The thiol at the C-terminus enabled the oligopeptides to bind covalently to the gold surface and form a SAM [65]. Patterns were derivitized on the surface using the cell adhesion peptides and hexa-ethelene glycol thiolate, which resists non-specific adsorption of proteins and cells [65]. The cells patterned were human epidermal carcinoma A431, mouse fibroblast NIH 3T3, and bovine aortic endothelial cells that were all in linear array and geographic patterns.

Immunology Considerations and Research Methods Available for Detecting Antigen-Antibody Binding

Antibodies are molecules that are manufactured by an organism's immune system to serve a surveillance function and attack substances identified as "foreign." The antibody is composed of a constant and a variable region. The latter becomes specialized and specific to a particular antigen as B and T lymphocytes of an organism

mature and provide signals for specific antibody production. The antibodies are specific so that they do not attack host cells indiscriminately. Therefore, the antibody looks for specific characteristics of particles, including amino acid, carbohydrate, fatty acid, or toxic particles which could potentially harm the organism.

The kinetics of antibody-antigen interactions are important properties to understand when using antibodies in research. The binding of antibodies and antigens reaches a state of equilibrium after a certain degree of binding has taken place. The following equation details this phenomena [55]: $Ab + Ag \rightleftarrows Ab\text{-}Ag$. In this equation the forward reaction is the association of the antibody (Ab) and the antigen (Ag) and is quantified by "a", the association rate. The reverse reaction is the disassociation of the antibody and antigen is quantified by "b", the disassociation rate. The following equations detail the equilibrium constant "K", the association constant "K_a", and the dissociation constant "K_b" [55]: $K = K_a/K_b = [Ab\text{-}Ag]/([Ab][Ag])$. In this research, the antibodies used are specific to the O157:H7 serotype *E.coli*.

One research method that utilizes the enzyme-linked immunosorbant assay (ELISA) protocol involves three monoclonal antibody panels against three epitopes of *E.coli* [31]. The three epitopes were the LPS chain (H7 portion of the *E.coli*), the LPS core, and the flagella of *E.coli* O157:H7. The 3 monoclonal antibodies have high specificity, detect the inoculum of 1 bacterium after 9 h growth at 37°C in TBS, and identify *E.coli* O157:H7.

Immuno-fluorescence coupled to a second antibody provides a simple, rapid, and easy indirect method for detection; it is best suited for the study of membrane antigens in addition to intra- and extracellular antigens, and may be applied to frozen tissue sections, to cells in suspension, and to cells attached to glass slides or coverslips [57]. Fluorescence-activated cell sorter (FACS) procedures may use this method for

studying cell populations and simultaneous detection of two different antigens (i.e., FITC and rhodamine-conjugated antibodies).

Compounds that give off light in the presence of an electric charge may be attached to an antibody that is specific for *E.coli* [13]. Measuring light from antibodies bound to bacteria may be used to determine the number of bacteria in the sample. One problem that results is that in addition to binding to *E.coli* O157 cells, the modified antibody also binds to a component the bacteria make and releases as it grows–thus it is difficult to make exact counts of the *E.coli* [13].

The binding analysis can be carried out by fixing or immobilizing whole cells of *E.coli* on the surface of a sensing instrument/biosensor followed by antibody binding onto the bacteria-sensor surface [43]. The biosensor detects the presence of the captured antibodies, assesses how fast and strong the antibodies were captured, and determines how fast they detached from the biosensor [43]. Thus, binding and dissociation constants can be determined and may shed light on how bacteria binds to meat and how the bacteria can be removed [43].

When deciding to recreate an physiological immune response on a silicon substrate, direct biomaterial application may not be all that is necessary. In normal physiological conditions, the interrelation of the B- and T-lymphocytes, the macrophages, and a host of other immunological components formulate the organism's immune response. Normal immunological cells have the ability to redistribute the antibodies for greater antibody-antigen binding configuration. The redistribution is called capping, aggregating, or patch forming. Macrophages, B- and T-lymphocytes, and other immunological cells interact and communicate in a dynamic process that may not be able to be simulated directly with patterned materials. This interaction matures the affinity and specificity of antibodies and the dynamics of the antibody-antigen binding.

Studies of the O157:H7 *E.coli* are confounded by the similarity of its surface epitopes with other non-EHEC *E.coli* and bacteria. Several of the similar epitopes include Shiga-like toxins, intimins, lipopolysaccharide (LPS), and enterohemolusins [39]. Therefore, one must ensure that the other toxins do not exist in the testing or that the antibodies have exclusive affinity for the desired antigen (O157:H7 *E.coli*).

Biosensor Review

The International Union for Pure and Applied Chemistry (IUPAC) defines a chemical sensor as "a device that transforms chemical information, ranging from concentration of a specified sample component to total composition analysis, into an analytically useful signal" [3]. An ideal sensor should have high selectivity and sensitivity, rapid recovery times with no histories, long lifetimes (if not single use), low drift, automated calibration, ability to self-diagnose, low cost, no required reagent additions or sample preparation [17]. Improvements to current sensor technology include better specificity, stability, ease of use, and decreased manufacturing costs. These improvements will enhance the devices currently found in medical/clinical diagnostics, bioprocess monitoring, food and beverage monitoring, and environmental monitoring markets [3].

Biosensors are chemical sensors that have a receptor (biocomponent), transducer (physical component), and, occasionally, a separator (membrane or coating, this is optional) [35]. The receptor often has a doped metal oxide or organic polymer capable of specifically interacting with the analyte or other receptors. Biocomponents include enzymes, antigens, antibodies, receptors, tissues, whole cells, cell organelles, bacteria and nucleic acids. The transducer converts the component into a measurable signal–electrical, mechanical or optical. Hardware components include electrochemical devices, optical devices, acoustic devices, ion sensitive field effect transistor (ISFET), and calorimetric devices. The separator screens out unwanted

materials and includes polymer membranes, electropolymerized coatings, and self-assembling monolayers.

There are four possible modes of physically coupling biomolecules to the basic sensor: membrane entrapment, physical adsorption, matrix entrapment, and covalent bonding, as detailed in Fig. 3.1 [13]. There are several factors that are unique to each immobilization device, including permanence of attachment to the biosensor, ability to produce by-products, and potential inactivation of the biomaterial [13].

Biosensors components fall into three primary categories: transducers, bioreceptors, and other supporting technologies [28]. Transducers include electrochemical (amperometric, potentiometric, and thermometric/calorimetric), opticals (surface plasma resonance (SPR), fluorescence, and holography), and piezoelectric (quartz crystal microbalance and surface acoustic wave) devices. Bioreceptors involve the use of antibodies, enzymes, microorganisms, and other bioreceptors. Supporting technologies include membranes (cellulose, polymers, and others), immobilization techniques (adsorption, covalent bonding, crosslinking, and entrapment), and mediators.

The following paragraph details many specific biosensor applications. Biosensor research is a rapidly expanding field with numerous interdisciplinary applications and designs. Several common fabrication methods for biosensor nanotechnology, and components involve photolithography, screen-printing, ink jet printing and microelectromechanical systems (MEMS) [28]. Resonant biosensors detect biomolecules bound to resonators [4], [34]. Optical-detection biosensors detect changes in optical patterns as a result of binding of biological molecules onto surfaces [26], [43], [50], [63]. The thermal-detection biosensor binds enzymes to temperature sensors [60]. In the presence of analyte, the heat of reaction for each enzyme is
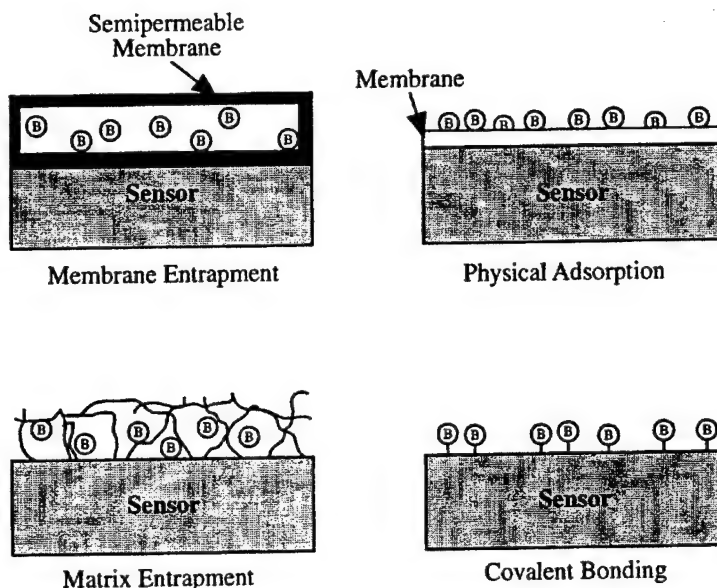
Figure 1.1. Four modes of physical coupling biomolecules to the sensor in a biosensor device (33).

measured, and is related to its concentration. ISFET biosensors (CHEMFETs) involve an immunoenzymatic assay utilizing covalent bonding of a molecule to which a specific receptor antibody could then be physically adsorbed [11], [47]. pH-based biosensors function by using variations in pH to perform quantification analysis of biomolecules [37], [41], [46]. Electrochemical-detection works through detection of electrochemical variations [24], [44]. Standard Complementary Metal-Oxide Semiconductor (CMOS) wafers may be post-processed into biosensors by using screen-printed polymer membranes containing the desired biomolecules [19]. Hybrid biosensors are a technology based on living, cultured cells grown on microelectrode array substrates [3], [6]. Additional research involves pharmacology testing [51], pressure sensors [5], patterned cell growth [33], [40], nanofluidic sieving [12], and DNA electrophoresis on silicon wafers [21], [59].

Conclusion

There is a wide range of biosensor technology currently being used in research and development laboratories. Avidin-biotin technologies are useful tools for controlling and analyzing the interactions taking place at the cellular and molecular levels. The technology offers a means to immobilize molecules to substrates or other particles. A stable bond arises from the strong avidin-biotin association constant, the covalent bonding of exposed photobiotin, and the avidin-biotin bond's ability to withstand harsh experimental conditions. Specificity is provided to these devices with antibody use and low nonspecific binding. Additional benefits of the technology are the ease of biotinylating molecules, versatility of light sources for photobiotin exposure, and low processing cost. Avidin-biotin patterning is preferred for molecules that must remain in solution, are not functionally affected by the biotinylation process, and are desired to form either a monolayer or only a few layers.

μCP technology uses lithographic methods to produce a mask with resolution that is below 1 μm. PDMS solidifies and forms a resilient stamp that can accurately and repeatedly transfer the pattern for protein stamping. SAMs provide well-defined surfaces for the PDMS patterning of biomolecules. Understanding the surface characteristics that promote (i.e. laminin) and deter cell growth/adhesion (i.e, PEG) are essential for precise patterning. μCP is preferred for molecules that are hydrophilic, not adversely affected by short periods of dryness, and can withstand compression pressure.

The immunological aspects of this study center on understanding the antibody-antigen interactions, current immunological testing technologies, and variations between the *in vivo* and *in vitro* environments of the research's chemical reactions.

Biosensors provide a means to detect biological molecules as an analyte interacts with a specific biomolecule or layer once the analyte is coupled to the sensor

surface, the transducer, bioreceptor, and other supporting technology (membrane, immobilization technique, or mediator). Although nanofabricated biosensor research lags behind macro-scale biomedical equipment research and development, significant advances are being made rapidly. As the biosensor market grows and the research techniques mature, biosensor technology will offer an increasing number of commercial products. Additionally, the biosensor market growth will help the nanofabrication field create a manufacturing revolution comparable to the personal computer revolution.

References

[1]   Pritchard, D. J., H. Morgan, and J. M. Cooper. 1995. Micro-scale patterning of biological molecules. *Agnew. Chem., Int. Ed. Engl.,* 34:91-93.

[2]   Achtnich, U. R., L.X. Tiefenauer, and R. Y. Andres. 1992. Covalent immobilization of avidin on glassy carbon electrodes as the basis for multivalent biosensors. *Biosens. Bioelectron.,* 7:279-290.

[3]   Advanced Technology Programs. 2000. Nano-and MEMS technologies for chemical biosensors. Found on the World Wide Web on 22 Aug 00 at http://www.atp.nist.gov/atp/focus/98wp-nan.htm.

[4]   Andle, J. C. and J. F. Vetelino. 1994. Acoustic wave biosensors. *Sensors and Actuators,* A44:167-176.

[5]   Axiom Company, Ltd. 2000. Biosensors. Found on the World Wide Web on 22 Aug 00 at http://www.axiom-jp.com/explanation.htm.

[6]   Borkholder, D. A., J. Bao, N. I. Maluf, E. R. Perl, and G. T. Kovacs. 1997. Microelectrode arrays for stimulation of neural slice preparations. *J. Neurosci. Methods,* 77:61-66.

[7]   Branch, D. W., B. C. Wheeler, G. J. Brewer, and D. E. Leckband. 2000. Long-term maintenance of patterns of hippocampal pyramidal cells on substrates of polyethylene glycol and microstamped polylysine. *IEEE Transactions on Biomedical Engineering* 47:290-300.

[8]   Branch, D. W., J. M. Corey, J. A. Weyhenmeyer, G. J. Brewer, and B. C. Wheeler. 1998. Microstamp patterns of biomolecules for high-resolution neuronal networks. *Med. Biol.Eng. Comput.,* 3:135-141.

[9]   Brooks, S. A., W. P. Ambrose, and W. G. Kuhn. 1999. Micrometer dimension derivatization of biosensor surfaces using confocal dynamic patterning. *Anal. Chem.,* 71:2558-2563.

[10] Chen, C. S., M. Mrksich, S. Huang, G. M. Whitesides, and D. E. Ingber. 1997. Geometric control of cell life and death. *Science* 276:1425-1428.

[11] Colapiccioni, C., A. Barbaro, F. Parcelli, and I. Giannini. Immunoenzymatic assay using CHEMFET devices. *Sensors and Actuators,* B4:245-250.

[12] Craighead, H. G., S. W. Turner, R. C. Davis, C. James, A. M. Perez, L. Kam, W. Shain, J. N. Turner, and G. Banker. 1998. Chemical and topographical surface

modification for control of central nervous system cell adhesion. *J. Biomed. Microdevices,* 1:49.

[13] Crawford C. G., J. D. Brewster, P. M. Fratamico, and H. Yu. Immunomagnetic-electrochemiluminescent detection of live *Escherichia coli* O157:H7. Found on the World Wide Web on 22 Aug 00 at http://www.nal.usda.gov/ttic/tektran/glimpse/data/000007/35/0000073551.html.

[14] Dewa, A. S. and W. H. Ko. 1994. Biosensors. Chapter 9 in "Semiconductor Sensors," Sze, S. M. [ed.], John Willey and Sons, New York, NY, 415-472.

[15] Dontha, N., W. B. Nowall, and W. G. Kuhr. 1997. Generation of biotin/avidin/enzyme nanostructures with maskless photolithography. *Anal. Chem.,* 69:2619-2625.

[16] Forster, A. C., J. L. McInns, D. C. Skingle, and R. Symons. 1985. Non-radioactive hybridization probes prepared by the chemical labeling of DNA and RNA with a novel reagent photobiotin. *Nucleic Acid Res.,* 13:745-761.

[17] Frost and Sullivan. 1996. *World Biosensor Market.* Report 5326-32, *Biosensor Technology.*

[18] Fuccillo, D. 1985. *Bio. Techniques,* 3:494-501.

[19] Goldberg, H. D., R. B. Brown, D. P. Liu, and M. E. Meryhoff. 1994. Screen printing: a technology for the batch fabrication of integrated chemical-sensor arrays. *Sensors and Actuators,* B21:171–183.

[20] Green, N. M. 1975. Avidin. *Advances in Protein Chemistry* 29:85-133.

[21] Han, J. and H. G. Craighead. 2000. Separation of Long DNA molecules in a microfabricated entropic trap array. *Science,* 288:1026.

[22] Harris, J. M. 1992. Poly(ethylene glycol) Chemistry--Biotechnical and Biomedical Applications, New York: Plenum.

[23] Hengsakul, M. and A. E. G. Cass. 1996. Protein patterning with photoactivatable derivative of biotin. *Bioconj. Chem.* 7:249-254.

[24] Hinkers, H., C. Dumschat, R. Steinkuhl, C. Sundermeier, K. Cammann, and M. Knoll. 1995. Microdialysis system for continuous glucose monitoring. *Proceedings of Transducers '95, the 8th International Conference on Solid-Sate Sensors and Actuators,* 1:470 – 473.

[25] Horbett, T. A. 1994. The role of adsorbed proteins in animal cell adhesion. *Colloids Surfaces B:Biointerfaces* 2:225-240.

[26] Hsueh, Y. T., R. L. Smith, and M. A. Northrup. 1991. A microfabricated, electrochemiluminescence cell for the detection of amplified DNA. *Sensors and Actuators,* 27:120-123.

[27] Iddon, B., O. Meth-Cohn, E. F.V. Scriven, H. Suschitzky, and P. T. Gallagher. 1979. *Agnew. Chem., Int. Ed. Engl.,* 18:900-917.

[28] Industrial Market Street and Analysis. Biosensors and chemical biosensors. Business Communications Co. Found on the World Wide Web on 29 Apr 00 at http://www.prgguide.com/reports/tocs/r2-287toc.html.

[29] Institute of Food Science & Technology. 1996. Verocytotoxin-producing *E.coli* food poisoning and its prevention. http://www.easynet.co.uk/ifst/hottop1.htm.

[30] James, C. D., R. C. Davis, L. Kam, H. G. Craighead, M. Issacson, J. N. Turner, and W. Shain. 1998. Patterned protein layers on solid substrate by thin stamp microcontact printing. *Langmuir,* 14:741-744.

[31] Keen, J., H. Yongheng, W. Laegreid, and R. Wilson. 2000. Rapid identification of *Escherichia coli* O157:H7 in broth using a panel of three monoclonal antibodies. Found on the World Wide Web on 22 Aug 00 at http://sun1.bham.ac.uk/bem4ght6/vtec/issue6/vtec141.htm.

[32] Kleinfeld, D., K. H. Kahler, and P. E. Hockberger. 1988. Controlled outgrowth of dissociated neurons on patterned substrates. *J. Neuroscience,* 8:4098-4120.

[33] Kossek, S., C. Padeste, and L. Tiefenauer. 1996. Immobilization of Streptavidin for immunosensors on nanostructured Surfaces. *J. of Molecular Recognition,* 9:485-487.

[34] Kovacs, G. 1998. Chemical and Biological Transducers. Chapter 8.2 in Micromachined Transducers Sourcebook, McGraw Hill, Boston, 719-777.

[35] Kovacs, J., G. L. Mayers, R. H. Johnson, R. E. Cover, and U. R. Ghatak. 1970. *J. Org. Chem,.* 35:1810-1815.

[36] Kumar, A., H. A. Biebuyck, and G. M. Whitesides. 1994. Patterning self-assembled monolayers: applications in materials science. *Langmuir,* 10:1498-1511.

[37] Kung, V. T., P. R. Panfili, E. L. Sheldon, R. S. King, P. A. Nagainis, B. Gomez, D. A. Ross, J. Griggs, and R. F. Zuk. 1990. Picogram quantitization of total DNA using DNA-binding proteins in a silicon sensor-based system. *Anal. Biochem.,* 187:220–227.

[38] Laegreid, W., J. Keen, and J. Kwang. 2000. Development of a competitive enzyme-linked immunosorbent assay (CELISA) for detection of serum antibodies to O157 antigen of *Escherichia coli*. Found on the World Wide Web on 22 Aug 00 at http://sun1.bham.ac.uk/bcm4ght6/vtec/issue6/vtecv142.htm.

[39] Laegreid, W., R. Westerman, R. Elder, J. Keen, J. Kwang, and R. Wilson. 2000. Enterohemorrhagic *Escherichia coli* share a common surface epitope. Found on the World Wide Web on 22 Aug 00 at http://sun1.bham.ac.uk/bem4ght6/vtec/issue6/vtec140.htm.

[40] Lahiri, J, L. Isaacs, J. Tien, and G. M. Whitesides. 1999. A strategy for the generation of surface presenting ligands for studies of binding based on an active ester as a common reactive intermediate: a surface plasmon resonance study. *Anal. Chem.*, 71:777-790.

[41] Lauks, I. R. 1979. pH measurements using polarizable electrodes. *IEEE Transactions on Electron Devices,* 26:1952-1959.

[42] Lopez, G. P., M. W. Albers, S. L. Schreiber, R. Carroll, E. Peralta, and G. M. Whitesides. 1993. Convenient methods for patterning the adhesion of mammalian cells on surfaces using self-assembled monolayers on alkanethiolates on gold. *J. Amer.Chem. Soc.,* 115:5877-5878.

[43] Mendelson, Y. 1995. Optical sensors. The Biomedical Engineering Handbook. CRC Press, Boca Raton.

[44] Millan, K. M. and S. R. Mikkelsen. 1993. Sequence-selective biosensor for DNA based on electroactive hybridization indicators. *Anal. Chem.* 65:2317–2323.

[45] Nuzzo, R. G. and D. L. Allara. 1983. Adsorption of Bifunctional Organic Disulfides on Gold Surfaces. *J. Am. Chem. Soc.,* 105:4481-4483.

[46] Olson, J. D., P. R. Panfili, R. F. Zuk, and E. L. Sheldon. 1991. Quantitation of DNA hybridization in a silicon sensor-based system: application to PCR. *Molecular and Cellular Probes,* 5:351-358.

[47] Peura, R. 1998. Medical Instrumentation: Application and Design, 3rd ed. Webster, ed. John Wiley & Sons, Inc, New York, p. 468.

[48] Pirrung, M. C. and C. Y. Huang. 1996. A general method for the spatially defined immobilization of biomolecules on glass surfaces using "caged" biotin. *Bioconj. Chem.,* 7:317-321.

[49] Pritchard, D. J., H. Morgan, and J. M. Cooper. 1995. Micro-scale patterning of biological molecules. *Agnew. Chem., Int. Ed. Engl.,* 34:91-93.

[50] Quantech. Biosensors. Found on the World Wide Web on 15 Apr 00 at http://www.biosensor.com/bio/intro.htm.

[51] Santini, J. T. Jr., M. J. Cima, and R. Langer. 1999. A controlled-release microchip. *Nature,* 397:335-338.

[52] Savage, D., G. Mattson, S. Desai, G. Niedlander, S. Morgensen, and E. Conklin. 1994. Avidin-Biotin Chemistry: A Handbook. Pierce Chemical Company, Rockford.

[53] Singhvi, R., A. Kumar, G. P. Lopez, G. N. Stephanopolous, D. I. C. Wang, G. M. Whitesides, and D. E. Ingber. 1994. Engineering cell shape and function. *Science,* 264:696-698.

[54] Smith, P. A. S. 1984. In azides and nitrenes. Reactivity and Utility. Academic Press, London, p. 95.

[55] Steward, M. W. and J. Steensgaard. 1983. Antibody Affinity: Thermodynamic aspects and biological significance. CRC Press, 1-131.

[56] Sundberg, S. A., R. W. Barrett, M. Pirrung, A. L. Lu, B. Kiangsoontra, and C. P. Holmes. 1995. Spatially-addressable immobilization of macromolecules on solid supports. *J. Am. Chem. Soc.,* 117:12050-12057.

[57] Tai, T. 1996. Immunohistochemistry using anti-ganglioside antibodies. Found on the World Wide Web on 22 Aug 00 at Http://www.glycotech.com/protocols/Proto2.html.

[58] Tsuchiya, T. 1995. In CRC Handbook of Organic Photochemistry and Photobiology. CRC Press, Boca Raton, 980-984.

[59] Turner, S. W., A. M. Perez, A. Lopez, and H. G. Craighead. Monolithic nanofluid sieving structures for DNA manipulation. *J. Vac. Sci. Technol. B.,* 6:3835.

[60] van Herwaarden, A. W., P. M. Sarro, J. W. Gardner, and P. Batailard. 1993. Microcalorimeters for (bio)chemical measurements in gases and liquids. *Proc. of Trans. '93, the 7th Intl. Conf. on Solid-State Sensors and Actuators, Yokohama* 10:411-414.

[61] Wilchek, M. and E. A. Bayer. 1988. The avidin-biotin complex in bioanalytical applications. *Anal. Biochem.,* 171:1-32.

[62] Wilchek, M. and E. A. Bayer. 1990. Avidin- and streptavidin-containing probes. *Methods in Enzymology,* 184:174-176.

[63] Wolfbeis, O. S. 1990. Fiber Optic Chemical Sensors and Biosensors, 1, CRC Press, Boca Raton.

[64] Yang, Zhongping, W. Frey, T. Oliver, and A. Chilkoti. 2000. Light activated affinity micropatterning of proteins on self-assembled monolayers on gold. *Launguir,* 15:1751-1758.

[65] Zhang, S., L. Yan, M. Altman, M. Lassle, H. Nugent, F. Frankel, D. A. Lauffenburger, G. M. Whitesides, and A. Rich. 1999. Biological surface engineering: a simple system for cell pattern formation. *Biomaterials,* 20:1213-1220.

CHAPTER 2

AVIDIN-BIOTIN PATTERNING ON SILICON SUBSTRATES AND INSIDE MICROFLUIDIC CHANNELS

Abstract

High-resolution micron-scale protein patterning methods have been developed to immobilize functional proteins on a silicon dioxide substrate for biosensor applications. Techniques to visualize the patterned proteins have been refined to provide precise images of properly patterned protein layers. The N-hydroxysuccinimide (NHS) ester of photoactivatable biotin was covalently bound to the 3-aminopropyltriethoxysilane (3-APTS) self-assembled monolayer after irradiation by 350 nm light from a 1000W Hg arc lamp. The subsequent patterned layers were evaluated using Alexa-488 conjugated NeutrAvidin, two fluorescence-conjugated antibodies, and heat-killed *Escherichia coli* (*E.coli*) O157:H7 cells. The advantages of these methods are the versatility of being able to bind any biotinylated protein and providing a reduction of exposure to the surface by harmful pH or chemicals.

Biological molecules were also immobilized on the inner surface of a silica glass capillary tube using silanes, NeutrAvidin, and photosensitive reagents. Photoactivatable biotin was linked to the inner surface of a glass tube by the amino terminal of silane molecules. This process produced the ideal template for a nanofluidic affinity chromatography system. The advantage of this procedure is that the inner surface of enclosed vessels may be patterned without the requirement of high temperature, anodically-bonded glass cover. Future applications include patterning biotinylated molecules, developing bioassays and immunoassays with patterned biomolecules, and incorporating this technology into pre-existing silicon, glass, and plastic micro- and nanofluidic systems.

Introduction

This chapter details how avidin and biotin molecules were immobilized on a silicon surface and how they coupled to other molecules to serve a foundation for biotinylated antibody adhesion. Fig. 2.1 illustrates the layer concept of the avidin-biotin technology applied to this biosensor application. This figure shows a fluorescently tagged secondary antibody bound to the primary antibody. This chapter will also detail how the primary antibodies specifically capture target antigen, either bacterial cells or protein A-covered spheres.

The process provided a stable method for adhering antibodies of choice to silicon and other substrates for biosensor use in spatially defined regions. This research improved upon previously performed avidin-biotin patterning by providing sharper feature resolution than documented in journal articles. This research has also provided the first successful patterning of cells and spheres on patterned antibodies using photobiotin, as well as the most extensive characterization of the patterned biomolecule levels with fluorescence.

Techniques to visualize the patterned proteins have been refined to provide precise images of properly patterned protein layers. Antibody gratings, as small as 5 µm in width, with intervening 5 µm spacings, were patterned on the silicon wafer by NeutrAvidin-biotin technology. The N-hydroxysuccinimide (NHS) ester of photoactivatable biotin covalently bound to the 3-aminopropyltriethoxysilane (3-APTS) self-assembled monolayer after irradiation by 350 nm light from a 1000W Hg arc lamp. The subsequent patterned layers were evaluated using Alexa 488 conjugated NeutrAvidin, two fluorescence-conjugated antibodies, and heat-killed *Escherichia coli* (*E.coli*) O157:H7 cells.

The advantages of these methods were the control and versatility of the materials. Avidin and biotin molecules are both below 10 nm in size and, therefore,
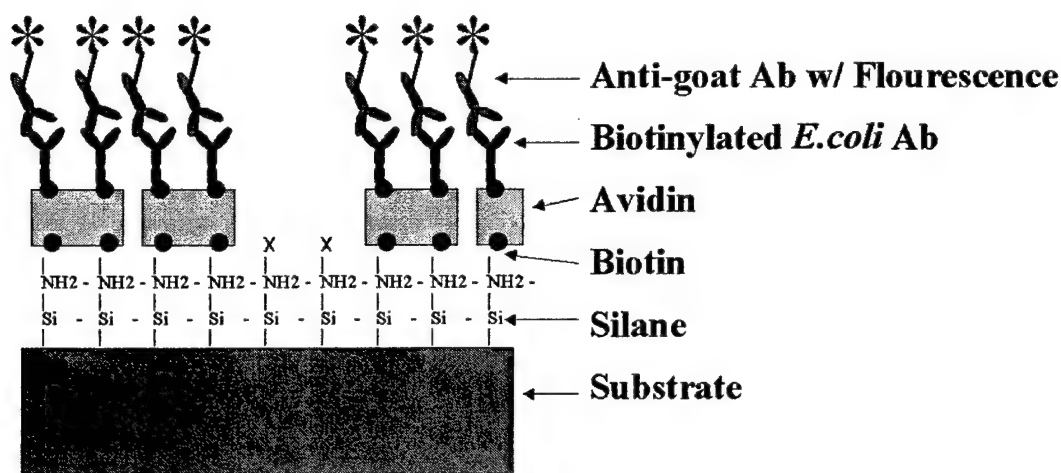
Figure 2.1. Illustration of avidin-biotin protein patterning layering with fluorescently-labeled antibody.
Illustration details the patterned layers of the biosensor chip with anti-*E.coli* antibodies are being tested with anti-goat IgG.

can easily match the patterning resolution of photolithography equipment, which is just below 1 μm [5]. The methods were versatile because they allowed binding of any biotinylated protein. Furthermore, the method helped ensure that the proteins and other patterned molecules maintained their functionality by avoiding exposure to harmful UV light, pH, chemicals, or salinity. Besides patterning lines as was done in this research, patterns may be made in any geometry that can be produced in a photolithography process. Future research involves applying patterning techniques to other biosensors, conducting multi-analyte tests, and quantifying patterned molecules using 40 nm FluoSpheres, radiolabled ions, and ELISA.

Avidin-biotin technology is an increasingly popular method for adhering substances to glass, silicon, independent molecules, and surfaces. Photoactivatable biotin has a 533.36 MW and is 3 nm in length [1]. Therefore, a patterning resolution below 10 nm could potentially be realized.

Biological molecules were immobilized on the inner surface of a glass capillary tube using 3-APTS, NeutrAvidin, and photosensitive reagents.

Photoactivatable biotin was linked to the inner surface of a glass tube by the amino terminal of silane molecules. Subsequent steps bound NeutrAvidin to the immobilized biotin molecules. The NeutrAvidin was bound to the patterned photobiotin and was evaluated by its conjugated Alexa 488 fluorescent dye.

Experimental Section

Reagents. The silane solution 3-aminopropyltriethoxysilane (3-APTS), NeutrAvidin, 0.5 mg EZ-Link™ Photoactivatable Biotin, sodium meta-periodate, 5 mL dextrose desalting columns, sodium acetate, and biocytin hydrazide were purchased from Pierce (Rockford, IL). Polyclonal, goat anti-mouse IgG antibodies and biotinylated goat anti-*E.coli* O157:H7 antibodies were purchased from Kirkegaard & Perry Laboratories (KPL, Gaithersburg, MD). The biotinylated, polyclonal goat anti-rabbit antibodies, NeutrAvidin conjugated with Alexa 488 fluorescent dye, and the protein A, FITC-labeled FluoSpheres® were purchased from Molecular Probes (Eugene, OR). The antibodies were diluted in phosphate-buffered saline with 0.1% Tween 20 (PBST). Tap water was filtered to a resistivity of 18.2 Mohm-cm using a Milli-Q Millipore filtration system. Tween 20 from Aldrich Chemical Company, Inc. (Milwaukee, WI) was used as a surfactant to decrease nonspecific binding. *E.coli* and *Salmonella* cells were cultured in a similar manner as described by St. John [1]. The wash solution contained PBST. CD26 developing solution and S1813 photoresist came from Shipley. Capillary tubes (0.2 mm diameter) were purchased from Fischer Chemical.

Development of Microfabricated Pattern. A 4" chrome-plated quartz mask was processed in the GCA PG3600F Optical Pattern Generator using a pattern designed with L-Edit software. This mask was developed in a chrome etchant for 2 min, washed with deionized water, and developed in Shipley CD26 solution for 2 min.

Silane Application on Silicon Wafer Surface. A 258 nm $\pm$ 5 nm oxide layer was grown on the surface of 3" n-type (100) silicon wafers from Silicon Quest International (San Jose, CA) by treating with pyrogenic steam + 4% Trans-PC (Dichloroethane) in a Thermco tube furnace for 45 min at 900°C.

The silane solution was prepared in a 50 mL amber bottle using 0.5 mL of 3-APTS and 24.0 mL of acetone in a nitrogen atmosphere glovebox to create a 2% silane solution. The silane application step began by cleaning 2 cm^2 silicon wafer chips or 1 mm diameter, 2 cm long capillary tubes (Fischer Chemicals). The chips/capillary tubes in the Harrick Plasma Cleaner/Sterilizer PDC 3-G for 10 min. The chips were removed and placed in 100°C Milli-Q filtered water for 30 min. The silicon chips/tubes were nitrogen dried and swiftly inserted into an air-tight amber bottle containing the silane (3-APTS) and incubated in a closed container of the solution under a fume hood for 30 min. The chips/tubes were removed, sonicated in acetone for 10 min, nitrogen dried, and baked on a hotplate at 120°C for 5 min.

Patterning of Silicon Surface. EZ-Link™ Photoactivatable Biotin was mixed with 0.5 mL Millipore water to produce a 1 mg/mL solution. All manipulations with photobiotin were carried out under a photographic safe light or in the dark. 20 μL of photobiotin was pipetted onto the silicon wafer chips (or capillary drawn into the tube) and dried in an oven for 2 h at 37°C.

Pattern Transfer. The photobiotin-coated chips/tubes were placed under the Hybrid Technology Group's (HTG) system 3HR contact/proximity mask aligner (the contact aligner was used in the flood exposure mode). The quartz mask was placed directly on the silicon chips/tubes and balanced evenly to ensure correct pattern transfer. The photobiotinylated chips were exposed with UV light at 365 nm for 90 seconds, with a15 mW/cm^2 intensity. The chips were rinsed in PBST for 30 seconds

to remove unreacted photobiotin. The samples were incubated in Pierce's Superblock blocking solution for 1 h and washed 3 times in PBST.

Avidin Application. NeutrAvidin or NeutrAvidin conjugated with Alexa 488 dye (with 495 nm/519 nm excitation/emission) was prepared by reconstituting with Millipore filtered water to10 mg/mL, followed by dilution to 1 mg/mL into PBST. The reconstituted product was stored at 4°C. Each sample was incubated with 35 µL of NeutrAvidin for 20 min. They were rinsed with PBST and dipped into Superblock solution. These two blocker steps were repeated two times. The samples were finally washed and stored in PBST bath until the beginning of the next step. When using the NeutrAvidin conjugated to Alexa 488 fluorescent dye, the chips were analyzed using the Zeiss microscope with an Omega Optical filter (450-490 nm/520 nm excitation/emission).

Labeling and Biotinylating Anti-*E.coli* Antibodies. Goat anti-*E.coli* O157:H7 antibodies were labeled using the Alexa 594 protein labeling kit from Molecular Probes (590 nm/619 nm excitation/emission). The labeled antibodies were biotinylated with biocytin hydrazide. 300 µL of 3 mM sodium *meta*-periodate solution was added to 600 µL of the antibody solution. The solution was incubated in the dark for 30 min at room temperature to produce aldehyde groups from the carbohydrates. Excess sodium periodate was removed with a 5 mL desalting column that had been pre-equilibrated with 100 mM sodium acetate, pH 5.5. The fractions were collected and the absorbance of the fractions was monitored in a spectrophotometer. The fractions containing high protein concentrations were pooled. 300 µl of 5 mM biocytin hydrazide solution was added to the pooled fractions and incubated for 1 h at room temperature. The reaction was terminated by adding 200 µL of 1 mM TRIS stop solution. Unreacted biocytin hydrazide was removed by a 5 mL dextrose desalting again and the sample was brought up to its original volume in stop solution. 35 µL of

the biotinylated antibody solution was pipetted onto the NeutrAvidin-coated silicon wafer chips. The antibodies were incubated for 20 min and were washed with PBST. The chips were analyzed using the Zeiss microscope with a XF 102 Omega Optical filter (590-640 nm/620 nm excitation/emission).

Secondary Antibody Analysis of Anti-*E.coli* Antibodies. Biotinylated, polyclonal goat anti-*E.coli* O157:H7 antibody and Texas Red (592 nm/618 nm excitation/emission) conjugated anti-goat antibodies were purchased from Pierce and reconstituted with PBST and diluted to a 50 μg/mL working solution using PBST. 35 μL of the biotinylated antibody solution was pipetted onto the NeutrAvidin-coated silicon wafer chips. The antibodies were incubated for 20 min and were washed with PBST. 35 μL of the Texas Red conjugated antibody solution was pipetted onto the antibody-coated silicon wafer chips. The antibodies were incubated for 20 min and were washed with PBST. The chips were analyzed using the Zeiss microscope with the XF 102 Omega Optical filter (590-640 nm/620 nm excitation/emission).

FluoSphere Application. Biotinylated goat anti-rabbit antibody came in solution and was diluted to 50 μg/mL. The biotinylated antibodies were added to the silicon chips by pipetting 35 μL of biotinylated antibody solution onto the NeutrAvidin-coated silicon wafer chips. The antibodies were incubated on the chips for 20 min. The chips were rinsed with PBST to remove unreacted biotin and left in PBST solution until the next step. The 0.4 mL stock solution of FluoSpheres protein A-labeled microspheres [40 nm, yellow-green fluorescent (505 nm/515 nm excitation/emission)] was diluted to produce working concentration of spheres ranging from 1×10^7 to 1×10^4 spheres/mL. 100 μL of sphere solution was pipetted onto each silicon chip, incubated for 20 min, washed with PBST, and dried with a low velocity nitrogen airstream. The chips were viewed in bright-field mode with a Zeiss

microscope and a fluorescence filter Omega Optical filter (450-490 nm/520 nm excitation/emission).

Fluorescence Intensity Measurement. A Hamamatsu photomultiplier tube (PMT) detection assembly, HC 124-02, was used to detect the light intensity of the fluorescence on substrates patterned with photobiotin and avidin. An Olympus IX70 inverted microscope with 20X and 40X objectives was used to visualize the samples. MCS-Plus software program and an IBM computer were used to interpret the data collected from the PMT detection assembly.

Results and Discussion

Avidin-biotin technology offered a useful method for producing a pattern of antibodies to an antigen of choice. In these experiments, each avidin and biotin layer was characterized with fluorescence: *E.coli* and Fluospheres were bound to the antibody-patterned surface.

Silicon wafers offered surfaces that were perfect for conducting reproducible experiments. Fig. 2.1 illustrates the layer concept of the avidin-biotin technology applied to this biosensor application. The silicon molecule of the silane binds to the silicon dioxide substrate. Additionally, the silicon molecules were cross-linked to one another. Collectively, these silane molecules formed a SAM with free amine terminals. The N-hydroxysuccinimide (NHS) ester of photoactivatable biotin contained an aromatic azide that reacted via nitrene intermediates when exposed to 350 nm wavelength light. The biotin bound to the amine terminal group of the silane after being exposed to light. The terminal amine groups in these areas were subsequently washed free of photobiotin and blocked by the Pierce Chemicals Superblock solution. Fig. 2.2 shows an optical micrograph of the patterning with biotin and Alexa 488-tagged NeutrAvidin. Alexa 488-conjugated NeutrAvidin was

used to verify successful pattern transfer from the photolithography mask to the photobiotin layer and to visualize the binding of NeutrAvidin to the bound photobiotin layer. The light bands are the Alexa 488-conjugated NeutrAvidin. The black bands are the silicon surface where the photoactivatable biotin was not exposed and was blocked by the blocker solution. A control chip was examined by first applying the silane followed by application of the Alexa 488-conjugated NeutrAvidin (photobiotin was not added). The fluorescence intensity was measured with a photomultiplier tube (PMT, data discussed later). The intensity of the control was 13.6% of the intensity of patterned Alexa 488-conjugated NeutrAvidin and 77% of the intensity of a chip where photobiotin was washed away and Alexa 488-conjugated NeutrAvidin was added.

The antibody layer application was characterized using two methods. The first method involved using Alexa 594 and biocytin hydrazide. First, the base layer of photobiotin and NeutrAvidin were patterned. Second, anti-*E.coli* O157:H7 antibodies were labeled at the lysine residues using Alexa 594 Protein Labeling Kit. Third, the hydrazide molecule of biocytin hydrazide preferentially bound to the -COOH on the F_c portion of the antibody. Consequently, the F_{ab} portion of antibodies was free to bind antigen. Fourth, Alexa 594-conjugated anti-goat antibodies were used to test the pattern viability of the bound goat anti-*E.coli* O157:H7 antibodies, as detailed in Fig. 2.3. In this figure, the light areas show where the antibodies are labeled with Alexa 594 dye and the black areas show where no avidin was present and, thus could not bind the fluorescently tagged antibody-biotin complex. A control chip was examined by first applying the silane followed by application of the Alexa 594-conjugated, biotinylated antibodies (photobiotin and NeutrAvidin were not added). The fluorescence intensity was measured with a photomultiplier tube (PMT, data discussed later). The intensity of the control was 9.7% of the intensity of patterned Alexa 594-conjugated antibodies and 82% of the intensity of a chip where photobiotin was
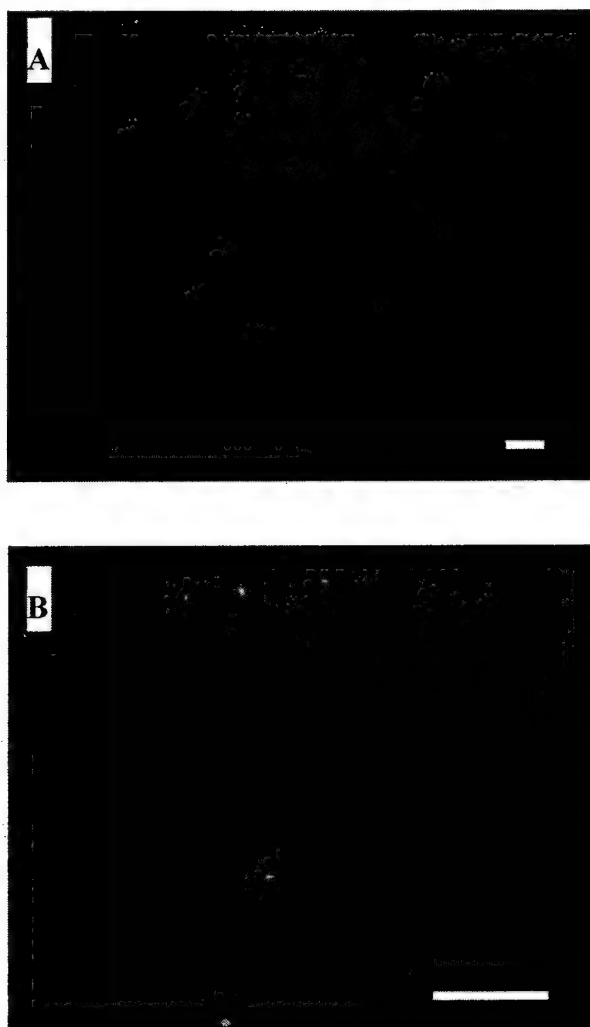
Figure 2.2. NeutrAvidin bound to patterned photobiotin.
Optical micrograph of Alexa 488 conjugated NeutrAvidin (green) bound to the patterned photobiotin on the silicon wafer surface (black): A) Image taken with 10X objective. The scalebar is 50 μm. B) Image taken with 100X objective. The scalebar is 25 μm.

washed away and NeutrAvidin and Alexa 594-conjugated, biotinylated antibodies were added.

The second method used to characterize the antibody application involved a fluorescently tagged secondary antibody, as illustrated in Fig. 2.4. Fig. 2.4 illustrates an optical micrograph of the Texas Red conjugated secondary antibodies that were bound to the primary biotinylated antibodies. In this figure, the light areas show the polyclonal, anti-goat, Texas Red-labeled antibodies bound to polyclonal, goat-derived,

biotinylated, anti-*E.coli* antibodies (which do not contain a fluorescent tag). These anti-*E.coli* antibodies were linked to the patterned avidin through the biotin link. The black areas show where no goat-derived antibodies were present and, thus, remained devoid of the Texas Red conjugated secondary antibodies. A control chip was examined by first applying the silane followed by application of the Texas Red-conjugated, biotinylated antibodies (photobiotin and NeutrAvidin were not added). The fluorescence intensity was measured with a photomultiplier tube (PMT, data discussed later). The intensity of the control was 10.5% of the intensity of patterned Alexa 594-conjugated antibodies and 79% of the intensity of a chip where photobiotin was washed away and NeutrAvidin and Texas Red-conjugated, biotinylated antibodies were added.

The effectiveness of the bound antibodies was also characterized using heat-killed *E.coli* cells. In the first characterization study, silicon wafer chips were processed using photoactivatable biotin, unlabeled NeutrAvidin, and biotinylated, polyclonal, goat anti-*E.coli* O157:H7 antibodies. *E.coli* cells were then pipetted onto these chips. Fig. 2.1 shows a conceptual illustration of bacterial cells binding to
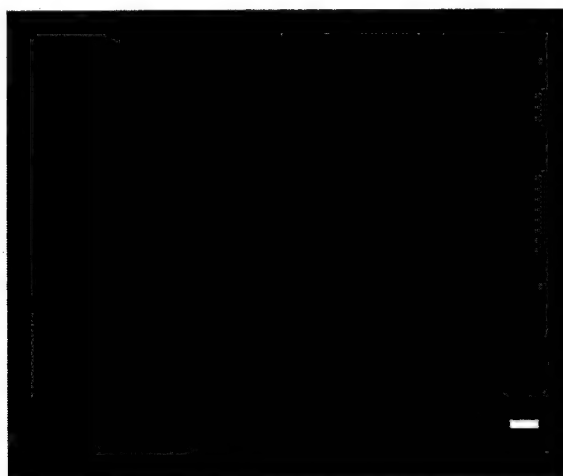
Figure 2.3. Optical micrograph of Alexa 594 labeled *E.coli* O157:H7 antibodies. Alexa 594 biotin-coupled *E.coli* O157:H7 antibodies (red) bound to NeutrAvidin on a silicon wafer surface (black), taken with 100X objective. The scalebar is 50 micrometers.

Figure 2.4. Optical micrograph of fluorescently-labeled secondary antibodies.
Optical micrograph of Texas Red conjugated anti-goat antibody (red) bound to goat anti-*E.coli* O157:H7 antibody on a silicon wafer surface (black), taken with 100X objective. The scalebar is 50 μm.

patterned antibodies. Fig. 2.6 shows an optical micrograph of the successful binding of *E.coli* cells to the anti-*E.coli* O157:H7 antibody pattern. The *E.coli* concentration in the solution for this sample was 10^6 cells/mL. For the cells to bind to the silicon wafer all the layers below the cells needed to be functional and the non-patterned areas needed to prevent nonspecific binding. This figure demonstrates the successful patterning and functionality of the photobiotin, avidin, and biotinylated anti-*E.coli* antibodies on top of the 3-APTS SAM. A control chip was examined with no biotinylated *E.coli* O157:H7 antibody added. The resulting pattern had no detectable *E.coli* patterned lines present. The chip had the same level of nonspecific binding that the normal chip had in the unpatterned areas. Further research will be required to reduce the nonspecific binding with applications of more blocking agents and/or more stringent washing.

Fig. 2.7 shows the conceptual binding of fluorescent microspheres to the patterned antibody pattern. Fig. 2.8 shows an optical micrograph of successful sphere binding to patterned polyclonal anti-rabbit antibodies. Like the patterning of the *E.coli*
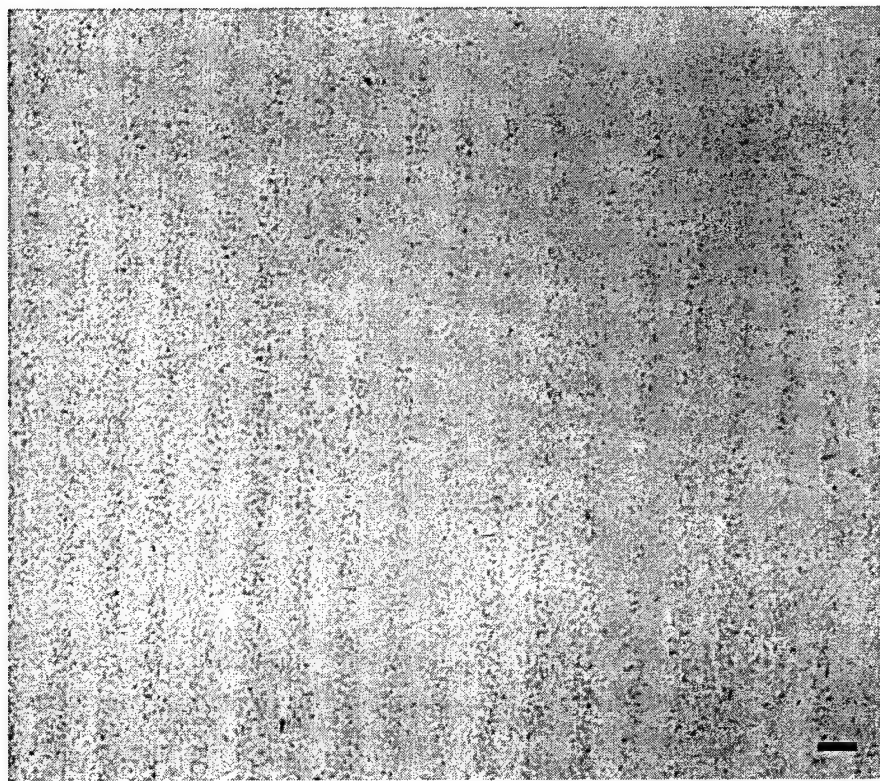
Figure 2.5. Optical micrograph of *E.coli* O157:H7 cells bound on patterned anti-*E.coli* O157:H7 antibodies array, taken with 100X objective. The scalebar is 50 μm.
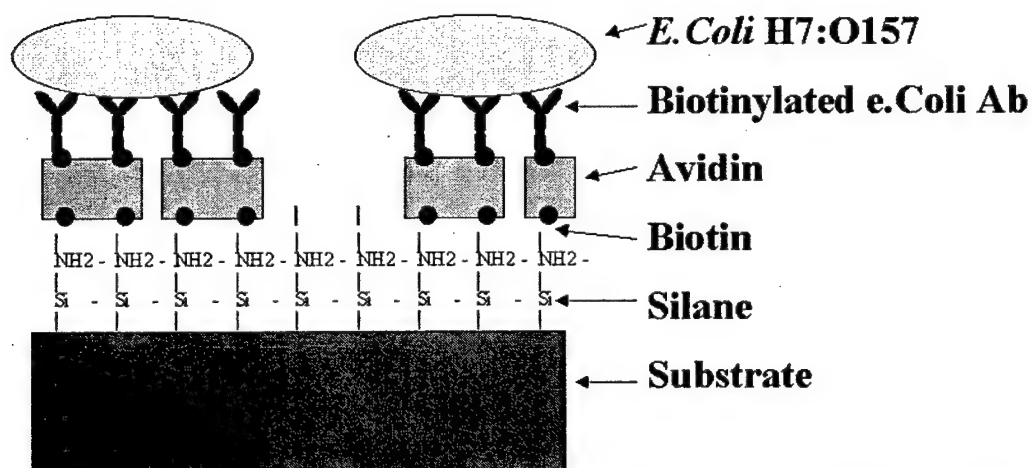
Figure 2.6. Bacterial binding to patterned antibodies. Illustration detailing the concept of the patterned layers of the biosensor chip with bound antigen.
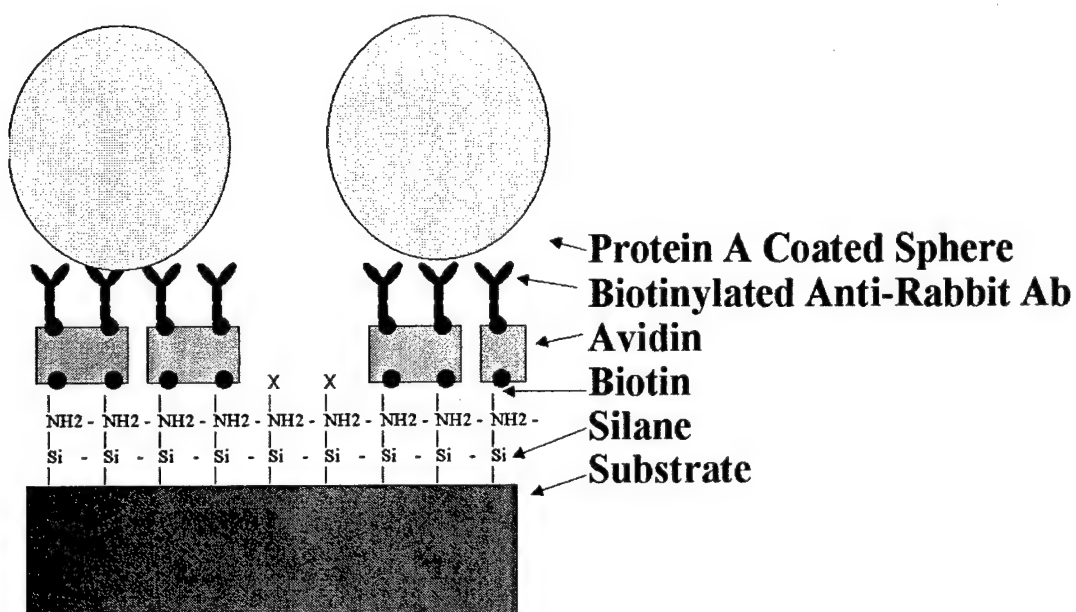
Figure 2.7. Illustration of fluorescent spheres binding to patterned antibody layer. Illustration detailing the patterned layers of the biosensor chip with anti-rabbit antibodies is used to bind protein A coated fluorescent spheres.

Figure 2.8. Optical micrograph of 40 nm fluorescent spheres bound to an avidin-biotin patterned antibody layer.

cells, this patterning demonstrates the successful patterning and functionality of the photobiotin, avidin, and biotinylated anti-rabbit antibodies on top of the 3-APTS SAM. Polyclonal anti-rabbit, anti-mouse, and anti-human antibodies bind successfully to protein A through their F_c region, with anti-rabbit having the highest binding affinity [2]. Rabbits, humans, and guinea pig antibodies have high affinity for Protein A [2], [3], [4]. This research will be used to calibrate the avidin-biotin technology to refine the technique for binding bacteria and other antigen.

Fig. 2.9 shows charts depicting the intensity of fluorescence on avidin-biotin chips as measured by the Hamamatsu PMT detection assembly. The chart illustrates the high signal to noise (S/N) ratio of the detection system, ranging from 5 to 13 arbitrary units (a.u.) for Alexa 488 NeutrAvidin samples and 6 to 22 a.u. for Rhodamine and Alexa 594 samples. The variability stemmed from the amount of bound fluorescent dye, amount of photobleaching by the microscope, gain setting of the PMT, and age of the samples being examined. Future experimentation will develop a standardized protocol to minimize this variation. This intensity measurement method provided a useful technique for detecting fluorescence in the micrometer scale and could potentially detect resolution in the mid hundred nanometer region, since the system was set to a very low gain and was capable of detecting amplifying individual photon signals.

Nanofluidic Affinity Chromatography with Patterned Biological Molecules on Inner Surface of Microfluidic Tubes

Work conducted in this laboratory prior to the this research involved stamping antibodies onto a silicon surface using microcontact printing antibodies and photolithographic patterning biotin, NeutrAvidin, antibodies, and bacteria cells on a silicon surface using biotin-avidin technology. Fig. 2.8 illustrates the concept of this
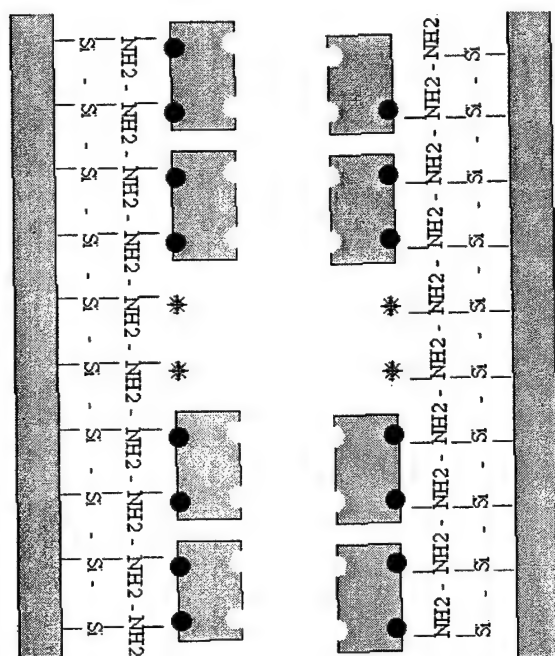
Figure 2.9. Illustration detailing the patterned layers of the patterned glass tube with biotin (purple circle) and NeutrAvidin (green tetramer).

work and Figs. 2.9-10 illustrate an epifluorescence image of the patterned surface. Photoactivatable biotin successfully transferred a pattern from a mask to the inner surface of a glass capillary tube. The 50 μm lighter bands are the Alexa 488-conjugated NeutrAvidin. The 25 μm black bands are the transparent portions of the glass that were not illuminated; thus, the photobiotin was removed from these areas during the subsequent washing step. The solid light band down the center of the figure is light artifact developed because of light being reflected orthogonally through the full expanse of the glass tube.

The patterning of the layers was identical to the method used in the previous section, except for the fact that a tube or microfluidic system was being used in place of a silicon dioxide surface. New methods had to be taken to ensure that fluid properly filled the capillary and, just as importantly, was fully removed from the capillary after

each processing step. If the fluid was not removed from a step, such as the photobiotin application stage, then the solution contained in the next layer to be patterned would not be able to displace the solution remaining in the tube or microfluidic channel.

As seen in Fig. 2.10 the areas that were not exposed have very low nonspecific binding of the Alexa-488 conjugated NeutrAvidin. The ease with which unexposed photoactivatable biotin was washed off contributes to the high patterning resolution possible with the photobiotin. The blocking agents in the Superblock solution bound to the newly exposed primary amine groups on the silane molecules. Blocking these amines minimized the nonspecific NeutrAvidin binding to these areas.

Multiple trials were conducted with the different exposure durations to determine the ideal amount of time required for activating the photoactivatable biotin using the HTG. Trials ranged from 30 seconds to 15 min. Ninety seconds appeared to be the ideal duration. The intensity of the Alexa-488 fluorescence was reduced for periods shorter than 60 seconds, indicating sub-optimal exposure of the photoactivatable biotin.

Typical high performance liquid chromatography (HPLC) devices use columns that are ten to several hundred millimeters in length and 3-5 mm in diameter; fast HPLC use microcolumns that are as small as 3 μm internal diameter and 3 mm long. Reduction of the diameter in a microfluidic system to 1 μm diameter and 1 mm long will create a 27-fold reduction in the required fluid volume, as compared to HPLC with the smallest microcolumn commercially available. Use of a nanofluidic device with a 500 nm-diameter internal diameter and 100 μm-long channel will lead to a ~1080 fold reduction.

Fig. 2.1 details the patterning of antibodies that could be used in a micro HPLC system. Fig. 2.11 details the patterning of microspheres that could be used in a micro HPLC system. Fig. 2.12 illustrates nanofluidic affinity chromatography that is possible by incorporating this protein patterning technique to existing nanofluidic
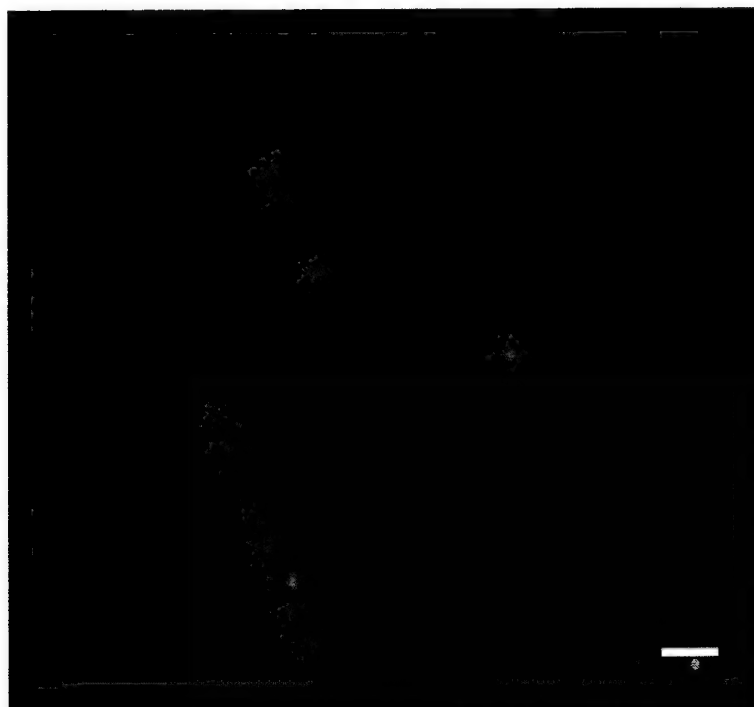
Figure 2.10. Optical micrograph of 50 μm band of Alexa 488 conjugated NeutrAvidin (green) bound to the patterned photobiotin on the inner surface of glass capillary tube. The bands are spaced 25 μm apart (black band), taken with 50X objective. The scalebar is 200 μm.

systems. The left column illustrates an antibody-based affinity column while the right side illustrates a porous bead-based affinity column. The highly specific antibody-based column will bind to the antigen's surface epitopes. The porous bead-based column will bind antigen by size of the antigen. The antibody of the target antigen can be adhered to the fluidic channel wall (Fig. 2.13A). When a mixed solution such as whole blood, serum, or contaminated solution, is added to the column, the antibodies (beads) will bind (trap) target antigen or particles (Fig. 2.13B). The adhered particulate will elute when rinsed with the proper pH buffer wash solution (Fig. 2.13C). The supernatant would be tested with standard ELISA protocols to calibrate the affinity chromatography system.

Avidin and biotin molecules were immobilized on the inner surface of capillary tubes and their coupling to other molecules serves a foundation for biotinylated

Figure 2.11. Optical micrograph of Alexa 488 conjugated NeutrAvidin (green) bound to the patterned photobiotin on the inner surface of glass capillary surface (black). Taken with 200X objective. The scalebar is 50 μm.
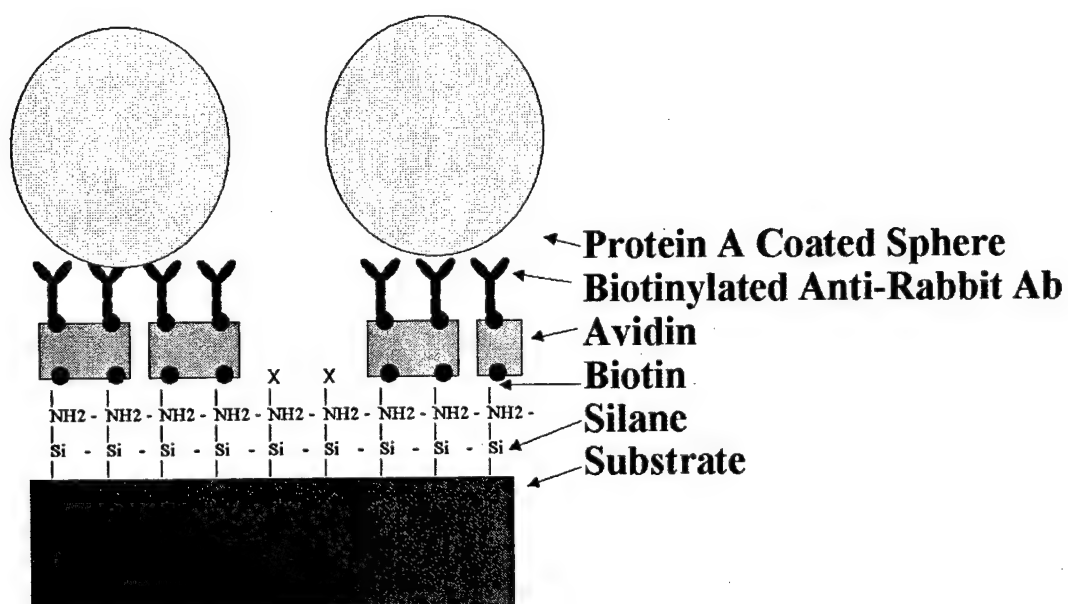
Figure 2.12. Illustration detailing the patterned layers of the biosensor chip with anti-rabbit antibodies is used to bind protein A coated fluorescent spheres.
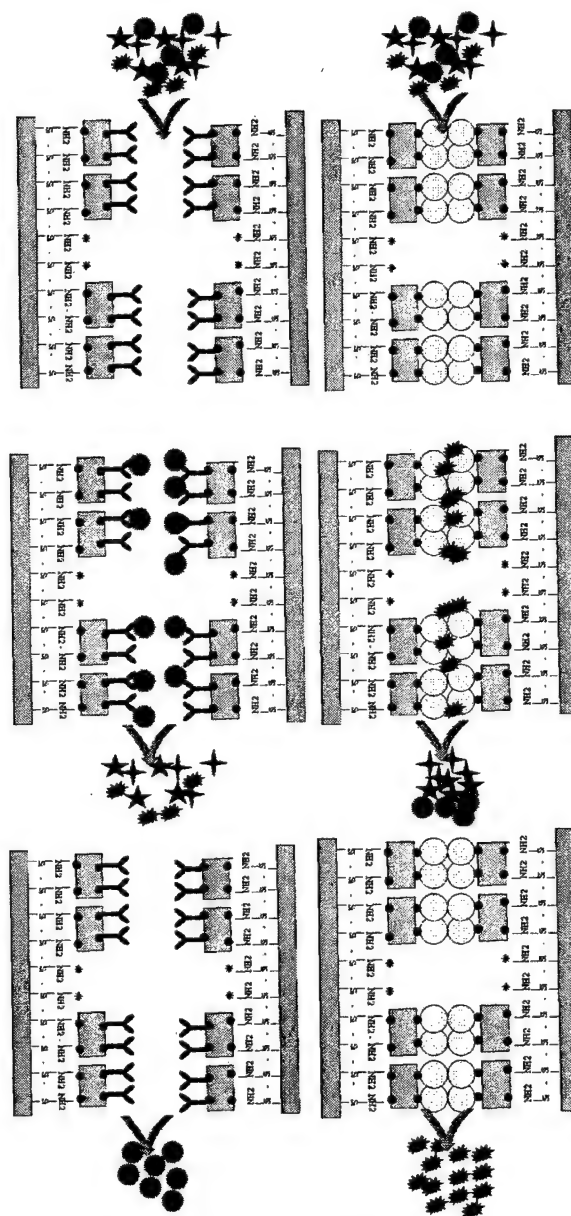
Figure 2.13. Illustration detailing the affinity chromatography possible with bound biotinylated antibodies (left) and porous spheres (right).
Step A illustrates the addition of a mixed serum. Step B illustrates the selective binding of one analyte per column. Step C illustrates the disassociation of the analyte from the column with addition of proper dissociation buffer.

antibody adhesion. This process shows how molecules were patterned to glass and other substrates for biosensor and affinity chromatography use. The use of photobiotin and avidin to pattern the inside of a capillary tube is a novel research technique that

offers the first photolithographic means to pattern biomolecules inside enclosed microfluidic systems.

This process produced a useful template for a nanofluidic affinity chromatography system. By patterning biotin and avidin layers to the inner surface of a glass capillary tube, biotinylated protein patterns could subsequently adhere to the capillary tube. The advantage of this procedure is that the inner surface of enclosed vessels may be patterned without the requirement of high temperature, anodic cover glass binding. Additionally, this process could reduce the required solution quantities ~1000 fold over current HPLC applications.

NeutrAvidin-biotin patterning involved applying a series of layering steps, including silane, photoactivatable biotin, NeutrAvidin, and biotinyated antibodies. This process used 3-aminopropylethoxysilane (3-APTS) that consequently formed a self-assembled monolayer (SAM). The SAM provided a uniform surface with exposed amine terminal groups to which the azide groups of NHS-ester conjugated biotin readily bind after UV irradiation. The NeutrAvidin-biotin bond was a very stable bond, $K_a = 1 \times 10^{15}$ M^{-1} [1] that withstands a wide range of chemical and pH range variations. Avidin was a tetrameric molecule that had four binding sites for biotin. NeutrAvidin was a 60 kD molecule that is a refined form of avidin and has less nonspecific binding to the substances than both avidin and streptavidin [1] Biotinylated molecules were subsequently bound to the avidin through the biotin link as antibodies were in this research.

The future work for this research includes the optimizing the multistep process, reducing nonspecific binding, and refining the photobiotin protocol. Since the process was performed over several steps to produce the different layers, each subsequent layer that was patterned was dependant on the one before it to offer a foundation to bind onto. Consequently, each new level offers the need for proper chemical nature,

position, size interaction, charge, and stereoisomerism [7]. Nonspecific binding was reduced with the use of blocking reagents. However, there was some background binding which makes quantitative analysis more difficult. Photobiotin was covalently bound to the surface after exposure to UV light at 365 nm. A representative at Pierce Chemicals specified the efficiency of this conversion on 4 Jul 99, although this was a generic efficiency–not necessarily linked to work performed on a silicon surface. Despite these limitations, the research proved that the process was viable and was an effective method for patterning biomolecules. Additionally, the incorporation into microfluidic channels will provide new barriers, including increased nonspecific binding of charged molecules, trapped air preventing fluid flow, and fluid dynamics affecting equal fluid flow through the microfluidic system.

Conclusion

Avidin-biotin patterning is a simple and effective way to transfer micrometer scale patterns to a surface and to the inner surface of a glass tube. Using ultraviolet light in conjunction with photolithographically patterned masks offers a method to derivitize biological molecules to a variety of surfaces. In these studies, each layer of the patterning process for the biotin-NeutrAvidin patterning process was confirmed with fluorescence. Once the surface is patterned with photobiotin, biotinylated molecules or other biological molecules and cells can also be captured on these surfaces. Affinity chromatography can be realized at much smaller features that are currently commercially available. Future research may prove this technology to be compatible with other surfaces, including glass, silicon, and plastic surfaces and microfluidic devices.

References

[1] Elgert, K. D. 1996. <u>Immunology: Understanding the Immune System</u> (Wiley-Liss, New York, p. 50).

[2] Harlow, E. and D. Lane. <u>Antibodies: A laboratory manual</u>. 1988. Cold Spring Harbor Laboratory, Cold Spring Harbor, p. 616.

[3] Krovall, G., U. S. Seal, J. Finstad, and R. C. Williams, Jr. 1970. Phylogenetic insight into eveolution of mammalian F_c fragment of γG globulin using straphylococcal protain A. *J. Immunol.,* 104:140-147.

[4] Richman, D. D., P. H. Cleveland, M. N. Ocman, and K. M. Johnson. 1982. The binding of staphylococcal protein A by the sera of different animal species. *J. Immunol.,* 128:2300-2305.

[5] Savage, D., G. Mattson, S. Desai, G. Niedlander, S. Morgensen, and E. Conklin. 1994. <u>Avidin-Biotin Chemistry: A Handbook</u> (Pierce Chemical Company), p. 76.

[6] St. John, P. M., R. Davis, N. Cady, J. Czajka, C. A. Batt, and H. G. Craighead. 1998. Diffraction-based cell detection using a microcontact printed antibody grating. *Anal. Chem.,* 70:1108-1111.

[7] Analytical Spectroscopy Research Group. 2000. History of HPLC. Found on the internet on 28 Dec 00 at http://kerouac.pharm.uky.edu/asrg/hplc/history.html.

CHAPTER 3

CREATING BIOLOGICAL MEMBRANES ON THE MICRON SCALE: FORMING PATTERNED LIPID BILAYERS USING THE WET POLYMER LIFT-OFF TECHNIQUE Ψ

This chapter reviews applications based upon a new method for patterning materials at micro- and nanometer resolution using a photolithographically patterned polymer lift-off technique [33]. Lipid bilayers were used as the initial biomaterial for these investigations. The functionality of these surfaces is verified with binding of antibodies and avidin on these uniform micron-scale platforms. A mask consisting of arrays of different sized features is used to pattern materials down to 1 μm resolution using a photolithographically patterned polymer lift-off technique. The polymer is used as a stencil for the patterning of the underlying surface. The patterns are realized as the polymer is mechanically peeled away in one contiguous piece in solution. Biomaterial features have been patterned from 700 nm to several millimeters in length. For the lipid bilayer patterning, small unilamellar lipid vesicles spread to form a supported fluid lipid bilayer on oxidized silicon surface as confirmed by fluorescence photobleaching recovery. Fluorescence photobleaching recovery measurements of DiI (1,1'-dioctadecyl-3,3,3',3'-tetramethylindocarbocyanine perchlorate $(DiIC_{18}(3))$) stained bilayer patches yielded an average diffusion coefficient of 7.54 ± 1.25 μm^2 s^{-1}, equal to or slightly faster than typically found in DiI stained cells. This diffusion rate is ~3x faster than previous values for bilayers on glass. This method provides a new means to form functionalized fluid lipid bilayers as micron-scale platforms to

---

immobilize biomaterials, capture antibodies and biotinylated reagents from solution, and form antigenic stimuli for cell stimulation. Metal is used to characterize the smallest features that can be attained by this procedure.

Introduction

Over the past decade, micron-scale patterning methods have been developed to immobilize functional biomolecules on silicon dioxide substrates for biosensor and bioassay applications. Many techniques use lithographic methods, borrowed from microelectronics fabrication technology, to produce patterned biomolecules on a surface [1]. Photopatterning has been used for enzymes, antibodies, and nucleic acids, in the development of biochips on silicon, glass, and plastic substrates [2].

There are several common technologies used to pattern materials on silicon and glass substrates including microarray patterning, ink jet printing, electron beam patterning, and microcontact printing. Microarray printing is commonly used to create biomaterial arrays on glass using a quill or flat headed pin to spot sizes ranging from 50-300 μm. However, pin damage as well as variations in glass substrates thickness, humidity, sample wetting properties, pin pressure can lead to differences in spot diameter and thickness. Ink jet printing is a noncontact printing technique with commercial applications offering 1440 dpi resolution (17.6 μm). Electron beam lithography involves striking a resist surface with a beam of electrons with patterning capabilities below 100 nm. Such methods allow spatial control for a wide range of patterned materials. Other PDMS limitations include elastomer shrinkage after curing, swelling in some solvents, and inherent elasticity that makes patterning over large areas a challenge.

Microcontact printing has been widely applied for rapid application of materials. While microcontact printing is a versatile and widely used method for patterning a variety of materials, it has the potential for surface fouling, nonspecific binding after primary layer application, and molecular denaturation of associated biomolecules due to drying. Furthermore, deformation of the polydimethyl siloxane elastomeric stamp has been shown to alter the expected size of the patterned material [35].

In our research we sought to develop a new method for patterning uniform and reproducible lipid bilayers. For this, we utilize photolithography in combination with a recently described polymer lift-off technique [33]. In comparison to the patterning techniques listed above, the polymer lift-off method can form uniform features down to 1 μm which is a significant size reduction over microarray and inkjet printing. The technique has been adapted to photolithography with use of steppers, which can pattern a whole wafer faster and at a lower cost than the serial process of electron beam lithography. Since the polymer is a temporary stencil that is removed in one piece, it circumvents the problems of PDMS contamination. Furthermore, the polymer lift-off technique avoids the PDMS pattern distortion and nonuniformity over large surface areas.

With the polymer lift-off approach, di-para-xylylene (Parylene C) is vapor deposited on a silicon substrate to produce a conformal polymer film that adheres weakly to the surface (Fig. 3.1). Following the addition of a photoresist, the film is patterned using conventional photolithography, and is then subjected to a controlled reactive ion etch (RIE) that removes exposed regions of Parylene down to the silicon dioxide substrate. The RIE also creates a more hydrophilic silicon dioxide surface in the exposed regions compared to the nonexposed regions of the substrate.
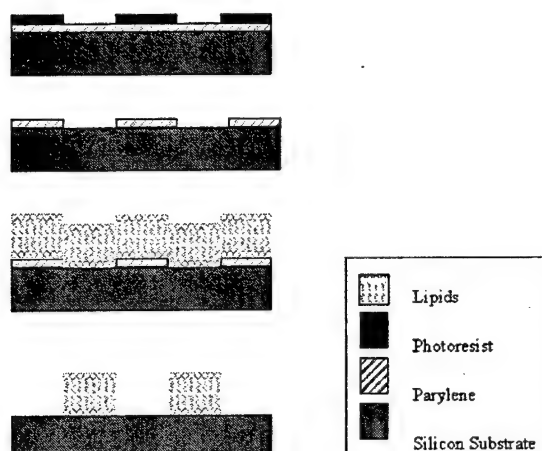
Figure 3.1. Schematic of the fabrication steps (adapted from Ilic and Craighead [33]).
(A) Photoresist patterning using optical lithography. (B) Reactive ion etching of
Parylene and removal of the top photoresist layer. (C) POPC lipid immobilization.
(D) Peeling of Parylene, resulting in a lipid bilayer.

Microfabrication methods have also been applied to the patterning of lipid
bilayers on solid substrates. Such methods allow precise spatial control over lipid
deposition and offer new possibilities for studies of lipid mobility kinetics,
diagnostics, and the study of cellular interactions with lipid-associated biomolecules.
Micropatterned lipids have been examined for their stability and sensitivity [4], [5],
[6], [7], [8], [9], [10], [11], as well as other parameters including lateral diffusion of
lipid molecules [12], and mobility of lipids within confined protein barriers [13]. To
date, the most widely used approach toward lipid patterning has been microcontact
printing using a polydimethyl siloxane elastomeric stamp [14], [15], [16], [17], [8],
[10]. This approach has allowed deposition of lipids down to feature sizes as small as
5 μm [18].

We hypothesized that lipid vesicles applied to the patterned oxidized silicon
substrate would adhere to regions of exposed silicon dioxide and form lipid bilayers.
The patterned lipids could then be submerged in aqueous solutions and the Parylene

removed leaving sharp boundaries between surface features. Since neither drying nor compressive force would be used with this technique, denaturation and attendant loss of functionality of more delicate molecules (viz. proteins) associated with the bilayers would be obviated. Fluorescence Photobleaching Recovery (FRP) [19], [20] has been used to study the mobility of lipid molecules in cellular lipid bilayers as well as supported lipid bilayers.

We describe the use of this method to pattern lipid bilayers of various feature sizes as small as 1 μm on a silicon substrate. The bilayers are fluid in nature, and model ligands incorporated into them retain their functionality and the potential applications of this technology. The use of avidin-biotin technology offers a powerful method for immobilizing biotinylated biomaterials from solution [21]. The strength and the versatility offered with binding biotinylated proteins or polysaccharide make avidin-biotin technology widely applicable to biomaterial patterning [22]. The avidin-biotin complex is a useful tool since it remains stable in conditions up to 132°C temperature, pH values between 2 and 13, and mild detergents [23]. Biotin-conjugated lipids are used in this study to as a means to pattern biotin molecules on a substrate for subsequent capture of avidin and biotinylated molecules. The lipid patterns are functionalized with dinitrophenol (DNP)-cap-POPC and biotin. The patterning of lipids with DNP serves as a model system for the patterning of chemicals for cell stimulation. This capability extends the patterning demonstrated by photobiotin in this laboratory [22].

Experimental Methods

Silicon Wafer Preparation and Parylene Deposition. 3-inch <100> type silicon wafers (Silicon Qwest, Int'l, Santa Clara, CA) were cleaned in base and acid baths to remove surface contaminants. Many patterned materials (e.g. lipids) require a freshly

oxidized surface for the formation of a hydrophilic substrate. This is achieved by initially growing 500 nm thermal oxide in the silicon wafers were baked at 1100°C for 50 min. After the initial batch is made, reactive ion etching the surface recreates the desirable hydrophilic surface. Patterned materials that could benefit from the hydrophobic properties of off-the-shelf silicon wafers (e.g. proteins) did not undergo thermal oxide treatment. A conformal layer of Parylene C was deposited using a PDS-2010 Labcoater 2 Parylene deposition system (Specialty Coating Systems, Indianapolis, IN). 1 g of Parylene dimer was used to deposit 1.5 μm thick Parylene film on five 3-inch silicon wafers.

Photolithography. OCG OiR 620-12i photoresist (OCG Chemical Company, West Patterson, NJ) was applied to the Parylene-coated silicon wafers at a thickness of 150% of the Parylene thickness. The optimized Parylene thickness for most biomaterial applications was 1.2 μm, so 1.8 μm was the optimal photoresist thickness. The samples were pre-baked for 1 min at 90°C and exposed using standard photolithographic techniques with a 10X stepper (Fig. 1A). After development in Microposit MIF 300 developing solution (Shipley, Marlboro, MA), the exposed portions of the Parylene film were subjected to an oxygen-based RIE etching step using a Plasma Therm 72 with an RF power density at 0.255 W/cm^2 (Fig. 3.1B). After etching, the samples were dipped into a beaker of acetone to remove residual resist, rinsed with isopropyl alcohol, and washed in deionized water. The samples were then dried with a nitrogen gas stream. Samples were immersed in Nanostrip (Cyantek Corp, Freemont, CA) for 1 min and then rinsed with deionized water and nitrogen dried.

Lipid Preparation and Patterning. Parylene is deposited on silicon substrates and photolithographically patterned as detailed in Chapter 3 using OCG OiR 897-12i photoresist (OCG Chemical Company, West Patterson, NJ) with a 1.3 μm Parylene

thickness. The lipids were purchased from Avanti Polar Lipids (Alabaster, AL). These lipids included DiI: 1,1'-dioctadecyl-3,3,3',3'-tetramethylindocarbocyanine perchlorate (DiIC18(3)), DNP-cap-DPPE: 1,2-Dipalmitoyl-sn-Glycero-3-Phosphoethanolamine-N-[6-[(2,4-dinitrophenyl) amino]hexanoyl] (Ammonium Salt), DOPC: 1,2-dioleoyl-*sn*-glycero-3-phosphocholine, DPPE-PEG(2000)Biotin: 1,2-dipalmitoyl-*sn*-glycero-3-phosphoethanolamine-N-[biotinyl(polyethylene glycerol) (2000), POPC, 1-Palmitoyl-2-Oleoyl-*sn*-Glycero-3-Phosphocholine, and Rh-PE: 1,2-dioleoyl-sn-glycero-3-phosphoethanolamine-N-lissamine rhodamine b sulfonyl. Lipids were dissolved separately and stored in chloroform at -20°C. Large unilamellar vesicles were prepared by extrusion [24] (Mayer *et al.*, 1986). Lipids were mixed at desired molar ratios and dried to a thin film under a stream of nitrogen gas. 5-10 μmol of total lipid was dried per 13x100mm glass test-tube. The resulting films were placed under vacuum for 1 h to remove residual organic solvent. Dried lipid films were hydrated in N-[2-Hydroxyethyl]piperazine-N'-[2-ethanesulfonic acid] (HEPES: 140 mM NaCl, 10 mM, pH 7.4, Aldrich, Milwaukee, WI), using vigorous vortex mixing to a final lipid concentration of 2 mM. Following hydration of the small lamellar vesicle (SLV) suspension was subjected to 5 freeze-thaw cycles (liquid nitrogen/room temperature water) to distribute the lipid mixture. The SLV suspension was then extruded 10 times through two stacked 0.1 μm Nucleopore polycarbonate filters (Whatman, Inc., Clifton, NJ) using a high pressure 10 mL Thermobarrel Extruder (Northern Lipids, Vancouver, BC) to obtain uniform 100 nm SLV. Lipid vesicles were diluted with phosphate buffered saline (PBS: 0.138 M NaCl, 0.0027 M KCl, pH 7.4). Functionalized lipids bound to the pattern on the silicon substrate were reacted with a target analyte as illustrated in Table 2.1.

Anti-DNP IgE and NeutrAvidin Preparation. Monoclonal, mouse anti-DNP IgE molecules were obtained from the Baird research group at Cornell University and

were stained with NHS-Alexa 488 dye (Molecular Probes, Eugene, OR). The stock solution was diluted to 0.5 µg/mL, 7.4 pH. Alexa 488-conjugated NeutrAvidin (Pierce Chemicals, Rockford, IL) solution was diluted to 50 µg/mL in PBS, 7.4 pH.

Target Analyte and Lipid Application. Parylene is deposited on silicon substrates and photolithographically patterned as detailed in Chapter 3. 20 µL drop of 2 mM DPPE-PEG(2000)Biotin lipids were pipetted onto the patterned polymer surface. The solution was placed on the Parylene-patterned substrate for 30 min, as illustrated in Fig. 3.1C. Samples were incubated in 35-mm plastic Petri dishes (Fisher Chemicals, Pittsburgh, PA) for 10 min and rinsed in Milli-Q water. The Parylene was removed by mechanically peeling it from the substrate with tweezers under Milli-Q water (Fig. 3.1D).

Microscopy and Fluorescence Photobleaching Recovery (FPR) Measurements. Epifluorescence microscopy was performed with a Zeiss Axitron upright microscope, water immersion objectives, and Omega Optical filter sets. Rhodamine and DiI fluorescent dyes were observed with a 510-590 nm excitation/590 nm emission filter set and an Alexa 488 fluorescent dye was observed with a 450-490 nm excitation/520 nm emission filter set. Images were captured using a Spot CCD camera (Diagnostic Instruments, Inc., Sterling Heights, MI).

Two photon laser scanning microscopy was carried out using a lab-built multiphoton system composed of a modified BioRad MRC600 scanner, Spectra-Physics Tsunami/Millennia (10W) Ti:S laser and a modified Olympus AX-70 upright microscope. FPR measurements of DiI stained bilayers were implemented on the same system using two-photon excitation. Fluorescence was detected by turret-mounted a GaAsP photomultiplier tube (Hamamatsu H7422). The output from the PMT was spilt into an amplified analog signal for imaging and pulsed (TTL) output available for photon counting applications such as FPR. In this manner we can image the specimen

Table 3.1. Functionalized lipid and target analyte association.

Functionalized Lipid	Target Analyte
DNP-PE	Alexa 488 Conjugated Monoclonal, mouse anti-DNP IgE
DPPE-PEG(2000)Biotin	Alexa 488 Conjugated NeutrAvidin

and then accurately park the laser any point in the sample to carry out the diffusion measurement. Using a 60x/0.9NA water immersion objective a spot (~300 nm $1/e^2$ radius) was bleached in the bilayer by a 100 μs duration bleaching pulse at 900 nm (~100 fs pulsewidth). Laser intensity was controlled by a resonance-dampened KD*P Pockels cell (Model 350-80BKLA , Conoptics, Inc, Danbury CT), which provided short, high intensity bleaching pulses followed by a low intensity monitoring level.

Fluorescence recovery was monitored for 80 ms using an 80 μs binsize by a lab-built acquisition system. Each FPR curve was averaged 50-100 times at the same location with a 250 ms delay between bleaching pulses. Data were fit to a model that assumes a single (Fickian) component, 2D diffusion and two photon bleaching [19], [25]:

$$\frac{F}{F_o} = \sum_{n=0}^{\infty} \frac{(-\beta)^n}{n!} \frac{1}{\left[1 + n\left(1 + \frac{8Dt}{\omega_{xy}^2}\right)\right]} \quad (1)$$

An immobile fraction was not needed to fit the data. The bleaching parameter (β)and the diffusion coefficient (D) are determined using the Marquardt-Levenburg algorithm. Summation to n = 8 in the non-linear fit is sufficient for convergence. The lateral two photon $1/e^2$ beam radius (ω_{xy}) for a 0.9 NA lens at 900 nm was calculated as [25]:

$$\omega_{xy} = \frac{0.325\lambda}{NA^{0.91}} \quad (2)$$

Equation 2 was determined from fits of the squared, diffraction limited illumination point spread function (calculated following Richards and Wolf [31]) for NA > 0.7.

Results

      The silicon substrates were photolithographically patterned using the technique outlined in Fig. 3.1. Following reactive ion etching, multilamellar vesicles of POPC-labeled with rhodamine-tagged phosphoethanolamine (PE) were added to the substrate in a 99:1 POPC:Rh-PR ratio, and the Parylene C film removed with a tweezers. Microscopic analysis revealed a uniform pattern of fluorescent squares of the expected size. The ratio of fluorescence in lipid-containing regions versus background was >150:1 (Fig. 3.2A). Indeed, because much of the observed fluorescence in the regions between squares was due to pixel "bleeding" in the CCD, the actual contrast was likely to be significantly higher.
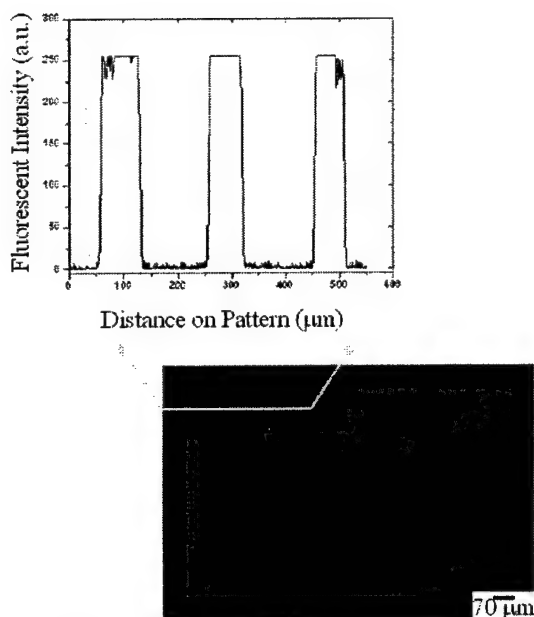
Figure 3.2. Fluorescence intensity image analysis of 3 squares of lipid in a 99:1 ratio of POPC:Rh-PE (2 mM).

The low end of this range is near the resolution limit of the 10X stepper, as confirmed with gold palladium patterned features of 700 nm dimension observed with SEM imaging (Fig. 3.3-4). Pattern distortions and lack of coating uniformity, which sometimes result from other methods, are eliminated since the features themselves are applied with photolithography and reactive ion etching. Finally, since the Parylene film covers unexposed areas, surfactant or blocking solutions are not required to prevent inappropriate binding in the unpatterned regions. Thus, Parylene can be used with either low or high concentration solutions and for long incubation times. With high concentration solutions, the application can be terminated after a short incubation period by rinsing without risk of redistributing the lipid to unpatterned regions. Blocking solutions can of course be added after Parylene removal to mask exposed areas of the substrate.

Homogenous patterns were routinely achieved. Several parameters affected the uniformity of the final lipid pattern. Patterns were reliably formed with a Parylene thickness of 1 μm, and a resist thickness of 1.2 μm. RIE needed to occur long enough to remove all the polymer in exposed regions. Biomaterial incubation time needed 10 min for the lipids and 30 min for the antibodies or avidin in the second layers. Finally, lipid vesicles were always used immediately upon preparation, and the resulting bilayers examined within 48 h to achieve uniform results. Fig. 3.5 shows an array of supported lipid bilayers created using this technique. The array is the fourth smallest array and can be located in Fig. 3.2 in the bottom row, third array from the left. This illustrates an example of the lipid bilayer patterns that can be attained using this technique.

Neutron scattering and NMR analysis of artificial membranes on glass beads [26], [27] have shown that lipid bilayers float on a thin film of water between the lipid and the solid substrate. We presumed that the same was true in this case. To examine
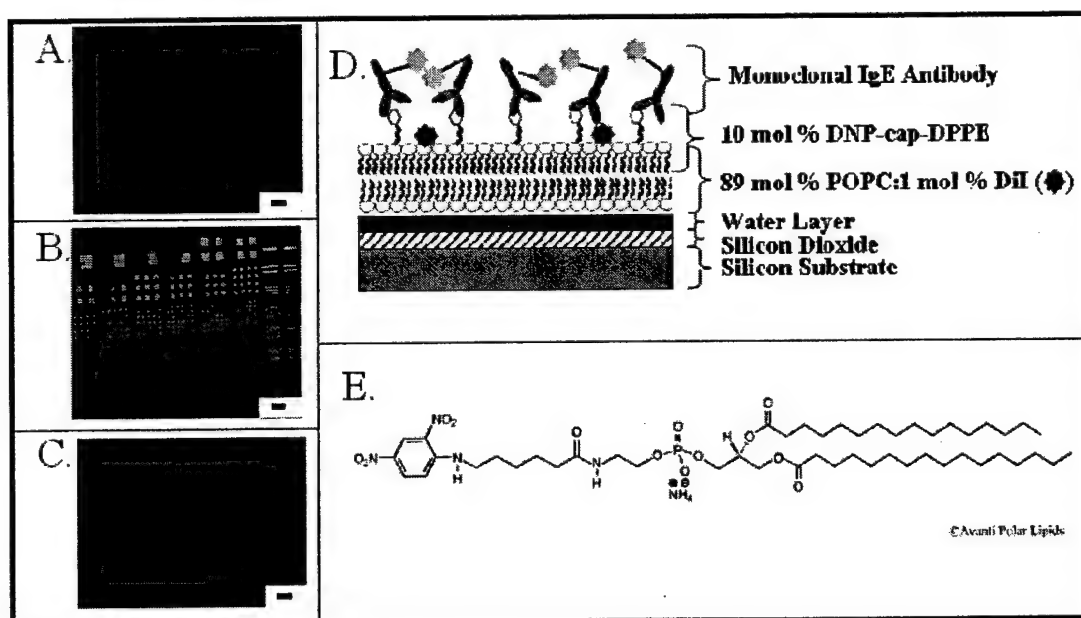
Figure 3.3. Fluorescence characterization of 1 μm to 76 μm wide squares and 1 μm to 20 μm wide lines of hapten-conjugated DOPC/Rh-PE supported lipid bilayer membrane.

(*A*) Membrane composed of 10 mol % DNP-cap-DPPE, 89% DOPC and 1 mol % DiI. Scalebar is 70 μm. (*B*) The same pattern from Fig. 3.2A with NHS-Alexa 488-conjugated monoclonal IgE. (*C*) Control using 99% POPC and 1 mol % Rh-PE and NHS Alexa 488-conjugated monoclonal IgE. (*D*) Schematic of the lipid layer is illustrated in Fig. 3A-B. (*E*) DNP-cap-DPPE structure [34].
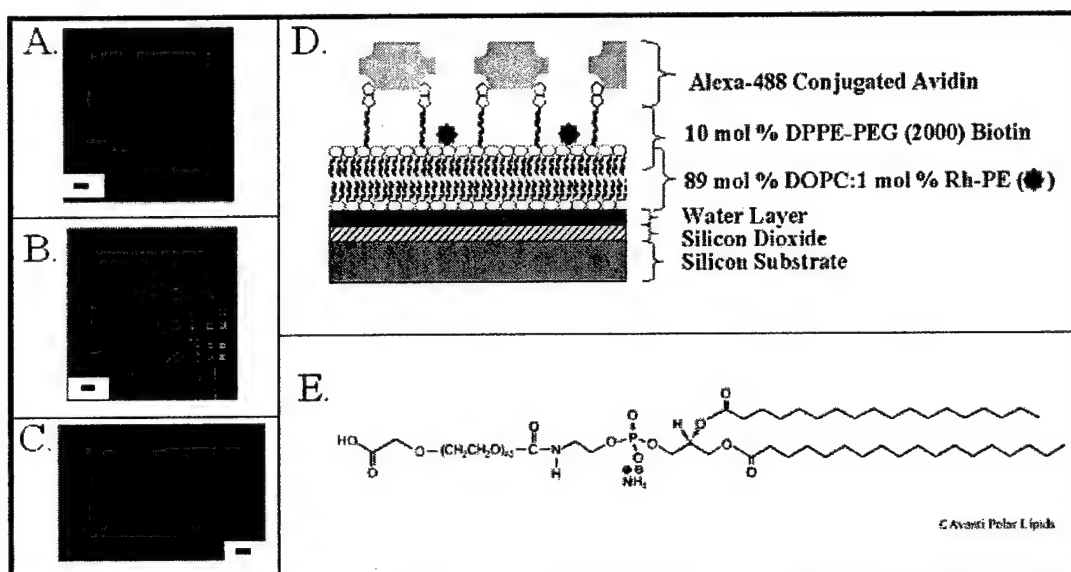
Figure 3.4. Fluorescence characterization of 1 μm to 76 μm wide squares and 1 μm to 20 μm wide lines of DPPE-PEG(2000)Biotin supported lipid bilayer membrane.
(*A*) Membrane composed of 10 mol % DPPE-PEG(2000)Biotin, 89 mol % DOPC and 1 mol % Rh-PE. Scalebar is 95 μm. (*B*) The same pattern from Fig. 3.3A with Alexa 488-conjugated avidin. Scalebar is 95 μm. (*C*) Control using 99% POPC and 1 mol % Rh-PE and Alexa 488-conjugated avidin. This image was taken with a 4x longer duration and an 8x greater gain than Fig. 3B to accentuate the contrast of the background to the patterned regions. Scalebar is 70 μm. (*D*) Schematic of the lipid layer illustrated in Fig. 3A-B. (*E*) DPPE-PEG(2000)Biotin structure [34].
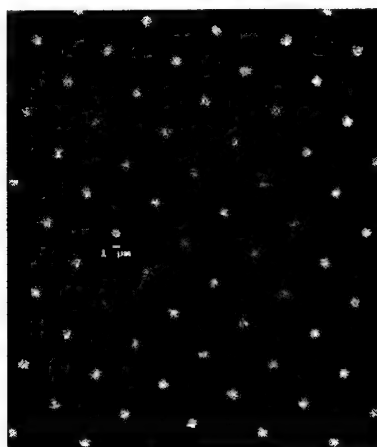
Figure 3.5. Confocal image showing the 1.3 μm patterns attained using the polymer lift-off method.

whether the patterned lipids described here behaved as normal supported bilayers, we measured their fluid properties by FPR. FPR was used to measure the lateral diffusion coefficient of the lipid probe DiI in supported bilayers as evidence of normal bilayer mobility. On properly prepared supported POPC bilayer samples, we found an average value of 7.5 ± 1.2 μm^2 s^{-1} (mean ± sd, n = 30) measured at 22°C (Fig. 3.6). This value was obtained from 30 measurements on bilayer patches in different areas (70 by 70, 20 by 20 and 3 by 3 μm). There was no significant difference between average values for each patch size: 6.6 ± 0.9, 8.2 ± 0.9 and 7.8 ± 1.3 μm^2 s^{-1} for the 70x70, 20x20 and 3x3 μm patches, respectively; 10 measurements on each patch size. Hovis and Boxer (2001) report values of 1-2 μm^2 s^{-1} (measurement temperature not given) for their supported bilayer system composed of egg PC and 1% Texas Red labeled DHPE, which is similar to other previous reports for bilayers on glass [28]. Literature values for the DiI diffusion coefficient in cell membranes range from 0.8-3 μm^2/s at 25°C, to 2-7 μm^2/s at 37°C [29], [30]. Measurements of DiI in polarized moving neutrophils at 24°C produced coefficients ranging from 1-7 μm^2/s, depending
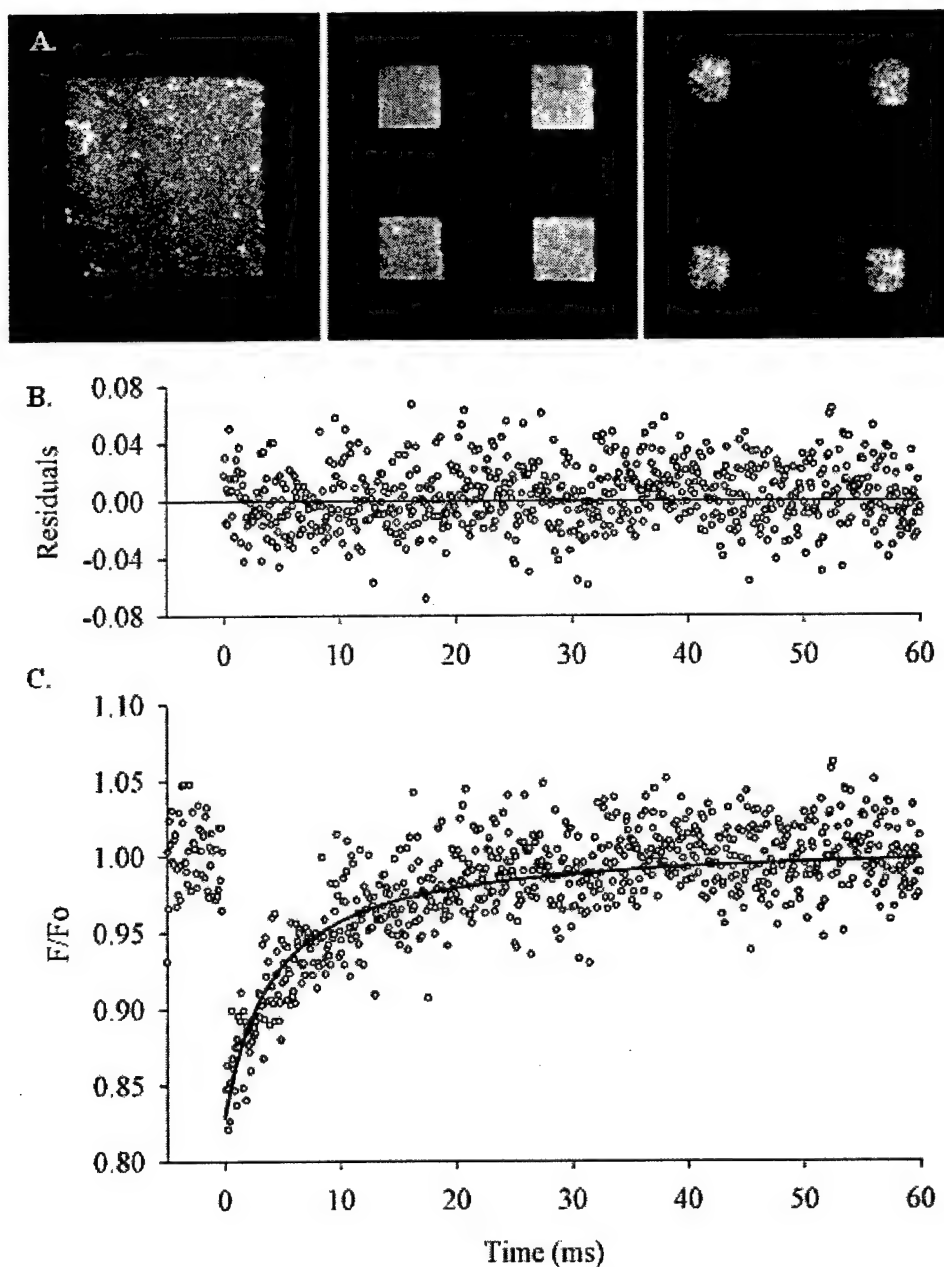
Figure 3.6. Multiphoton FPR measurements of DiI stained supported lipid bilayer patches composed of 10 mol % DNP-cap-DPPE, 89% DOPC and 1 mol % DiI.

(A) Representative DiI stained patches used in FPR measurements: 70 μm (*left*) and 20 μm (*center*), and 3 μm square (*right*). (B) Residuals from fit in C. (C) Data with fit. The excitation wavelength was 900 nm, bleaching pulse was 100 μs long at 5-8 mW average power during the pulse, and 0.5 mW while monitoring recovery. A 60x/0.9NA objective was used producing a $1/e^2$ radius of 0.32 μm at a 900 nm. Trace shown is an average of 120 bleaching pulses. Data was fit to a 2D-diffusion model and the returned diffusion coefficient was 6.8 μm^2 s^{-1} for this curve.

on the position of the measurement (leading vs. trailing edge) (Zipfel, unpublished results). In artificial systems such as black lipid membranes (BLM) and other types of multilaminar vesicles made of DPPC (measured at ~40°C), the DiI diffusion coefficient ranged from 1-32 μm^2/s, depending on the type of preparation and the amount of solvent trapped between the bilayers [32]. Our measurements in POPC supported lipid bilayers presented here yield an ~3x faster diffusion than found on an intact cell membrane, as might be expected due to the absence of dye/proteins interactions in the membrane. It is also ~3x faster than previous values for bilayers on glass, which we believe, indicates fewer interactions with the substrate.

Spatial patterning of lipid-soluble ligands and/or receptors on a micro- or nanoscale would be extremely useful in a number of potential bioassays. Nevertheless, such assays require that the respective molecules (either ligands or receptors) retain their binding properties following incorporation into the patterned lipid bilayer. To examine the functionality of ligand/receptor interactions in the lipid bilayers described here, we prepared bilayers that contained either a model antigenic determinant (namely, dinitrophenyl) or a model ligand (namely, biotin) and tested the ability of these substances to bind their cognate receptors (anti-DNP antibodies on the one hand, or avidin on the other). In the first instance, DPPE was covalently linked to DNP, and the resulting compound incorporated into DiI-labeled POPC vesicles (POPC:DNP-cap-DPPE:DiI; 89:10:1 mol %). Patterned lipid bilayers were then prepared from these vesicles using the polymer lift-off method. As in the case of the POPC lipid vesicles, these formed arrays that were clearly visible under the fluorescence microscope (Figure 3.3A). This platform was considered a model for a cell surface carrying a single antigen (that is DNP). After transfer to aqueous medium, samples were incubated for 30 min with DNP-specific mouse antibodies tagged with

Alexa-488, and then washed thoroughly. As shown in Fig. 3.3B, strong Alexa-488 (*green*) fluorescence was seen in a pattern that corresponded precisely to the DiI-containing squares. When lipid bilayers were formed without DNP-conjugated lipids, antibody binding to the lipid features was below the background level associated with the silicon substrate itself (Fig. 3.3C). In the case of biotin, DOPC vesicles (DOPC: DPPE-PEG(2000)Biotin:Rh-PE; 89:10:1 mol %) containing biotinylated PEG were patterned on silicon as above (the use of PEG with biotin, as opposed to PE, reduced non-specific binding in the subsequent step due to repulsive factors associated with the longer carbon chain). Resulting lipid bilayers were then reacted with Alexa 488-conjugated NeutrAvidin. As with DNP-antibody combinations, lipid bilayers containing biotin were labeled strongly with Alexa 488-conjugated NeutrAvidin (Fig. 3.4B). When lipid bilayers were formed with (POPC:Rh-PE;99:1) rather than the biotin-conjugated lipids, the NeutrAvidin bound at a lower level than the background binding level to the silicon substrate (Fig. 3.4C). Fig. 3.4D illustrates the layering of the molecules in this patterning process. These results clearly suggest that the lift-off process could serve as a model for patterning both lipids conjugated with antigens and biotin on a surface for subsequent binding of antibodies and biotinylated molecules, respectively.

Discussion

In this study, we demonstrate a new technique for creating precise, micron-scale lipid bilayers on silicon substrates. Lipids patterned with this technique had fluid properties comparable to those of biological membranes, and their associated ligands retained functionality, allowing capture of other biomaterials from solution.

The success of this technique can be attributed, in large part, to the properties of Parylene itself. Intramolecular forces in the chlorobenzene backbone of the polymer

create a strong film that is chemically inert to acid, base, and ketone exposure. At the same time, it binds weakly to the substrate and can be completely removed in a single, contiguous sheet. Its low permeability prevents binding to masked areas of the substrate, allows multiple reagents, such as biotin, avidin, and antibodies, to be applied to the patterned regions prior to removal of the film. Pattern distortions and lack of coating uniformity, which sometimes result from other methods, are less likely with this method since the features themselves are applied with photolithography and reactive ion etching. Bilayer patches do tend to become more rounded as the size decreases, presumably from deformation of the corners during the Parylene lift-off step as well as line tension effects due to the higher proportion of edge lipids in the smaller patches. Finally, since the Parylene film covers unexposed areas, surfactant or blocking solutions are not required to prevent inappropriate binding in the unpatterned regions. Thus, Parylene can be used with both low or high concentration solutions and for long incubation times. With high concentration solutions, the application can be terminated after a short incubation period by rinsing without risk of redistributing the lipid to unpatterned regions. Blocking solutions can of course be added after Parylene removal to mask exposed areas of the substrate.

We were able to produce uniform protein or metal arrays of ~700 nm wide features as verified by SEM imaging (Orth, unpublished). A line intensity profile through a confocal microscopic image of the patterned lipid showed the smallest feature was ~1 μm. Thus, this patterning technique was able to form patterns near the resolution limit of the photolithographic 10X stepper used in this experiment. While this is near the photolithographic resolution limit, electron-beam lithography should be able to pattern at smaller resolution, potentially at or below 100 nm. Even at 1 μm, the feature size attained with this method is well below the average spot size on chip arrays (produced by commercial print technologies), which are highly variable and

cover a diameter of roughly 100 μm. At the macro-scale, conventional 96-well plate analysis is conducted in wells with an average surface area of 45 mm^2.

Conclusion

This patterning technique provides an ideal platform for lipid bilayer mobility studies, cell surface receptor interrogation, and cell stimulation experimentation. The verification that soluble antibodies bound specifically to the patterned antigen suggests that membrane-bound receptors, such as antibodies, could bind to the patterned surface. The spatially controlled patterning to the 1 μm level offers the ability to target small domains on a cell surface. With the use of a small mol % of functional lipid molecules in the lipid composition, this technique may approach the level of single molecule binding and single ligand stimulation. Additionally, the demonstration that the biotin-conjugated lipid surface can bind avidin enables the patterning of biotinylated molecules to the surface. This extends this patterning technique to the extensive range of compounds that can be biotinylated, such as antibodies, DNA, other proteins, etc. Patterned lipids appear stable over several days to weeks of storage in solution. Standard FPR measurements confirm that our supported lipid bilayers have a lateral mobility equal to that expected from an independent bilayer undergoing minimal interactions with the substrate. Therefore, this can serve as a versatile model system for *in vitro* cell membrane experimentation where supported lipid bilayers can be tailored to consist of the functional molecules in patches down to 1 μm.

References

[1] Branch, D. W., B. C. Wheeler, G. J. Brewer, and D. E. Leckband. 2000. Long-term maintenance of patterns of hippocampal pyramidal cells on substrates of polyethylene glycol and microstamped polylysine. *IEEE Trans. Biomed. Eng.,* 47:290-300.

[2] Dontha, N., W. B. Nowall, and W. G. Kuhr. 1997. Generation of biotin/avidin/enzyme nanostructures with maskless photolithography. *Anal. Chem.,* 69:2619-2625.

[3] Fitzgerald, D. 2002. Microarrayers on the Spot. *The Scientist,* 16:42-45.

[4] Tien, H. T., and Z. Salamon. 1990. Self-assembling bilayer lipid membranes on solid support. *Biotechnol. Appl. Bioc.,* 12:478-484.

[5] Zviman, M. and H. T. Tien. 1991. Formation of a bilayer lipid membrane on rigid supports: an approach to BLM-based biosensors. *Biosens. Bioelectron.,* 6:37-42.

[6] Sackman, E. 1996. Supported membranes: scientific and practical applications. *Science,* 271:43-48.

[7] Groves, J. T. and S. G. Boxer. 1995. Electric field-induced concentration gradients in planar supported bilayers. *Biophys. J.,* 69:1972-1975.

[8] Groves, J. T., H. Ulman, and S. G. Boxer. 1997. Micropatterning fluid lipid bilayers on solid supports. *Science,* 275:651-653.

[9] Cremer, P. S. and S. G. Boxer. 1999a. Formation and spreading of lipid bilayers on planar glass supports. *J. Phys. Chem.,* 103:2554-2559.

[10] Cremer, P. S., J. T. Groves, L. A. Kung, and S. G. Boxer. 1999b. Writing and erasing barriers to lateral mobility into fluid phospholipid bilayers. *Langmuir,* 15:3893-3896.

[11] Groves, J. T. and Boxer, S. G. 2002. Micropattern formation in supported lipid membranes. *Acc. Chem. Res.,* 35:149-157.

[12] Hovis, J. S. and S. G. Boxer. 2000. Patterning barriers to lateral diffusion in supported lipid membranes by blotting and stamping. *Langmuir,* 16:894-897.

[13] Kung, L. A., L. Kam, J. S. Hovis, and S. G. Boxer. 2000. Patterning hybrid surfaces of proteins and supported lipid bilayers. *Langmuir,* 16:6773-6776.

[14] Biebuyck, H. A., N. B. Larsen, E. Delemarche, and B. Michel. 1997. Lithography beyond light: Microcontact printing with monolayer resists. *IBM J. Res. Develop.*, 41:159-170.

[15] Xia, Y. and G. M. Whitesides. 1998. Soft lithography. *Agnew. Chem. Int. Ed.*, 37:550-575.

[16] Yang, P., T. Deng, D. Zhao, P. Feng, D. Pine, D. F. Chmelka, G. M. Whitesides, and G. D. Stucky. 1998. Hierarchically ordered oxides. *Science*, 282:2244-2246.

[17] James, C. D., R. C. Davis, L. Kam, H. G. Craighead, M. Isaacson, J. N. Turner, and W. Shain. 1998. Patterned protein layers on solid substrates by thin stamp microcontact printing. *Langmuir*, 14:741-744.

[18] Kam, L. and S. G. Boxer. 2001. Cell adhesion to protein-micropatterned-supported lipid bilayer membranes. *J. Biomed. Mater. Res.*, 55:487-495.

[19] Axelrod, D., D. E. Koppel, J. Schlessinger, E. L. Elson, and W. W. Webb. 1976. Mobility measurement by analysis of fluorescence photobleaching recovery kinetics. *Biophys. J.*, 16:1055-1069.

[20] Brown, E. B., E. S. Wu, W. Zipfel, and W. W. Webb. 1999. Measurement of molecular diffusion in solution by multiphoton fluorescence photobleaching recovery. *Biophys. J.*, 77:2837-2849.

[21] Green, N. M. 1975. Avidin. *Adv. Protein Chem.*, 29:85-133.

[22] Orth, R. N., T. G. Clark, and H. G. Craighead. 2003. Microcontact printing and avidin-biotin patterning methods for biosensor applications. *Biomed. Microdevices*, 5:29-34.

[23] Savage, D., G. Mattson, S. Desai, G. Niedlander, S. Morgensen, and E. Conklin. 1994. Avidin-Biotin Chemistry: A Handbook. Pierce Chemical Company, Rockford.

[24] Mayer, L. D., M. J. Hope, and P. R. Cullis. 1986. Vesicles of various sizes produced by a rapid extrusion procedure. *Biochim. Biophys. Acta.*, 858:161-168.

[25] Zipfel, W. R. and W. W. Webb. 2001. <u>Methods in Cellular Imaging</u>, Ed(s) A. Periasamy, Oxford University Press, Oxford, 216-235.

[26] Johnson, S. G., T. M. Bayerl, D. C. McDermott, G. W. Adam, A. R. Rennie, R. K. Thomas, and E. Sachmann. 1991. Structure of an adsorbed dimyristoylphosphatidylcholine bilayer measured with specular reflection of neutrons. *Biophys. J.*, 59:289-294.

[27] Bayerl, T. M. and M. Bloom. 1990. Physical properties of single phospholipid bilayers adsorbed to micro glass beads. A new vesicular model system studied by H-2-nuclear magnetic resonance. *Biophys. J.*, 58:357-362.

[28] Hovis, J. S., and S. G. Boxer. 2001. Patterning and composition arrays of supported lipid bilayers by microcontact printing. *Langmuir,* 17:3400-3405.

[29] Bloom, J. A. and W. W. Webb. 1983. Lipid diffusibility in the intact erythrocyte membrane. *Biophys. J.,* 42:295-305.

[30] Fulbright, R. M., D. Axelrod, W. R. Dunham, and C. L. Marcelo. 1997. Fatty acid alteration and the lateral diffusion of lipids in the plasma membrane of keratinocytes. *Exp. Cell Res.,* 233:128-134.

[31] Richards, B. and E. Wolf. 1959. Electromagnetic diffraction in the optical systems II. Structure of the image field in aplanatic system. *Proc. R. Soc. London Ser. A.,* 253:358-379.

[32] Fahey, P. F. and W. W. Webb. 1978. Lateral diffusion in phospholipid bilayer membranes and multilamellar liquid crystals. *Biochemistry,* 17:3046-3053.

[33] Ilic, B. and H. G. Craighead. 2000. Topographical patterning of chemically sensitive biological materials using a polymer-based dry lift-off. *Biomed. Microdevices,* 2:317-322.

[34] Avanti Polar Lipid Catalogue. 2001. Avanti Polar Lipids, Inc. Alabaster.

[35] Hovis, J. S. and S. G. Boxer. 2000. Patterning barriers to lateral diffusion in supported lipid membranes by blotting and stamping. *Langmuir,* 16:894-897.

CHAPTER 4

PATTERNING ANTIBODIES FOR BIOSENSOR APPLICATIONS AND FOR USE AS A DIFFRACTION BIOSENSOR

We have developed a method for patterning antibodies with micrometer scale resolution on a silicon substrate. Lithography and reactive ion etching are used to pattern a polymer-coated surface. Biomaterials applied to the patterned substrate and removal of the polymer produces uniform micrometer scale patterns. This procedure is applied to immobilize antibodies to the substrate using protein A or avidin-biotin complexes. Protein A-coated microspheres were initially captured from solution mimicking the capture of analytes from solution. A specific application involves the use of the antibodies patterned in lines to capture virus and bacteria. One specific application investigated was the use of patterned antibodies for a diffraction biosensor device. When this pattern is illuminated with an incident laser beam, it creates a diffraction pattern from baculovirus captured on the spatially patterned surface. Amplification of the diffraction signal occurs through the preferential binding of anti-baculovirus IgG-coated microspheres to the IgG-immobilzed virus. This system provides the necessary elements for an economical, portable diffraction-based virus and bacteria biosensor.

Introduction

Antibodies are a critical component in the immune system for their ability to specifically target molecules. Antibodies are generated with a level of specificity that enables them to bind to whole classes of molecules (i.e. anti-mouse antibody) to an antibody that targets only a specific 8-15 peptide sequence. Once immobilized, the antibodies serve as markers for immune system cells and molecules.

The polymer lift-off method detailed in Chapter 3 has been used to pattern polymers for the specific application of antibodies in a manner similar to the binding of functionalized lipid molecules [9]. Avidin-biotin and protein A chemistries offer useful tools for selectively adhering antibodies on the substrate. Avidin-biotin chemistry is an effective method for binding molecules together through use of the high-affinity, non-covalent interactions between an avidin derivative (avidin, streptavidin, or NeutrAvidin) and biotin [10]. The tetrameric, patterned avidin can bind biotinylated antibodies from solution. Similarly, protein A has high affinity for the F_c segment of antibodies.

Biosensors provide a mechanism for detecting trace quantities of target molecules from a heterogeneous solution. A wide range of optical biosensors have been detailed in the literature, including antibody-conjugated fiber optics [2], enzyme-catalyzed systems [3], Fluorescent nano-PEBBLE (Probes Encapsulated By Biologically Localized Embedding) sensors [4], surface plasmon resonance [5], [6], and internally-referenced total internal reflection [7]. Patterning functional proteins is an important facet for the integration of proteomics and microfabrication technology for biosensor and biomimetic applications.

A diffraction biosensor is a specific application that has been pursued with the micropatterning antibodies. Diffraction-based biosensors provide an alternative to immunofluorescence biosensing. Diffraction-based biosensors use a technique explored earlier in this research group by St. John, *et al.* [8]. The theory behind this device involves shining a laser onto an array of lines containing either only antibodies or antibodies with a captured target analyte such as *E.coli.* Diffraction-based optical detection involves measurement of the first-order diffraction pattern of a laser focused on the immobilized virus-sphere complexes. Anti-baculovirus IgG, protein A conjugated microspheres were used to amplify the diffraction signal. Unlike viruses

on the patterned antibodies alone, these anti-baculovirus IgG conjugated microspheres are large enough to create a significant diffraction signal from an incident beam of light.

Experimental Section

Silicon Wafer Preparation and Antibody Patterning. Parylene is deposited on silicon substrates and photolithographically patterned as detailed in Chapter 3 using OCG OiR 897-12i photoresist (OCG Chemical Company, West Patterson, NJ) with a 1.3 μm Parylene thickness. Two different methods are used to adhere antibodies to the silicon substrate. The first method involves protein A incubated on the patterned polymer substrate. Subsequently, the samples are incubated in the desired antibodies solution. The second method involves incubating the samples in a series of solutions: 100 μg/mL biotin, 50 μg/mL NeutrAvidin, and 10 μg/mL biotinylated antibody solution. Subsequenlty, the polymer is removed revealing micro- and nanometer antibody patches.

Target Analyte Capture. A solution containing the desired target analyte is applied to the surface and incubated for up to 20 min. The samples are rinsed to remove unbound analyte. If the target analyte is smaller than 500 nm, 1 μm Alexa 594-conjugated polystyrene microspheres are incubated on the samples. This amplifies the signal from the samples and allows a detectable diffraction to take place.

Diffraction Measurement. The silicon chips are held in a clip that was mounted on a Newport x, y, z stage, and illuminated with a He-Ne laser (632.8 nm). The layout of the equipment is show in Fig. 4.1. The laser light was focused to a 1-mm diameter on the antibody grating area by using two Newport collimators. The Newport digital power meter model 815 detector with 5-mm × 5-mm active detection

A.

Antibody Only

He Ne
Laser

Low Signal

B.

**Antibody, Virus,
and Microspheres**

He Ne
Laser

High Signal
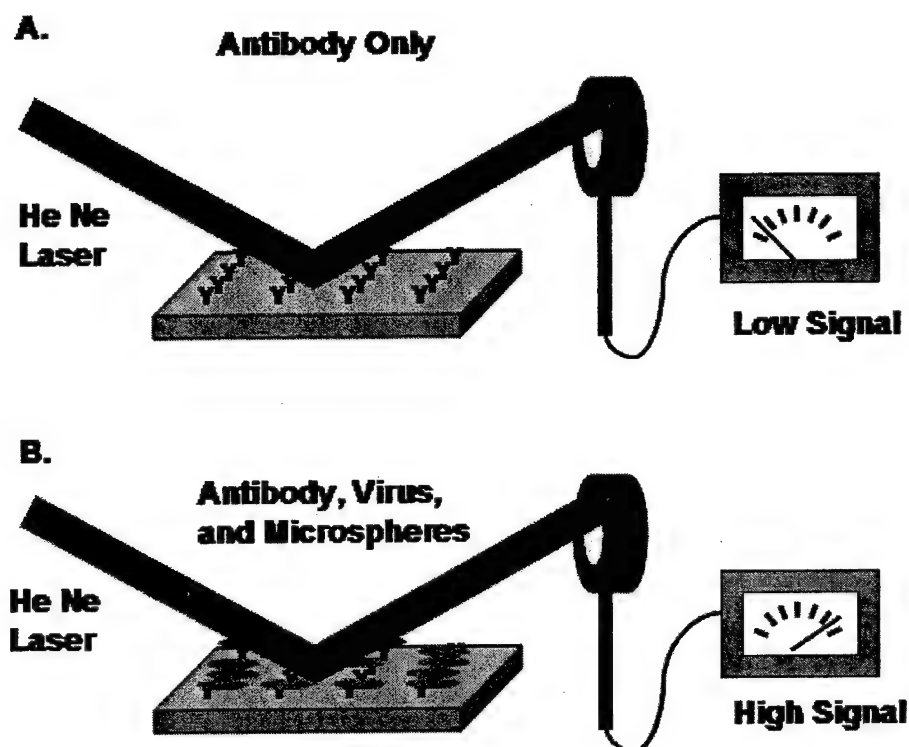
Figure 4.1. Schematic showing the equipment used in the diffraction-based biosensor as modified from St. John *et al.* [8].
(A) The left image shows He:Ne laser light reflecting off a surface containing only patterned antibodies. The right side show He:Ne light diffracting off the surface containing antibodies with captured analyte.

area was placed in the path of the diffracted light. The first order and zero order of diffraction light intensity are measured.

Results and Discussion

The initial objective was to create a method to pattern antibodies on the silicon substrate. Fig. 4.2 illustrates the sequential binding of biomaterials that takes place for the creation of functional biomimetic surfaces. This technique provides a method for patterning highly uniform patches of biomaterials on supported substrates. The polymer lift-off technique is the ideal solution for real-time biosensing in the field.
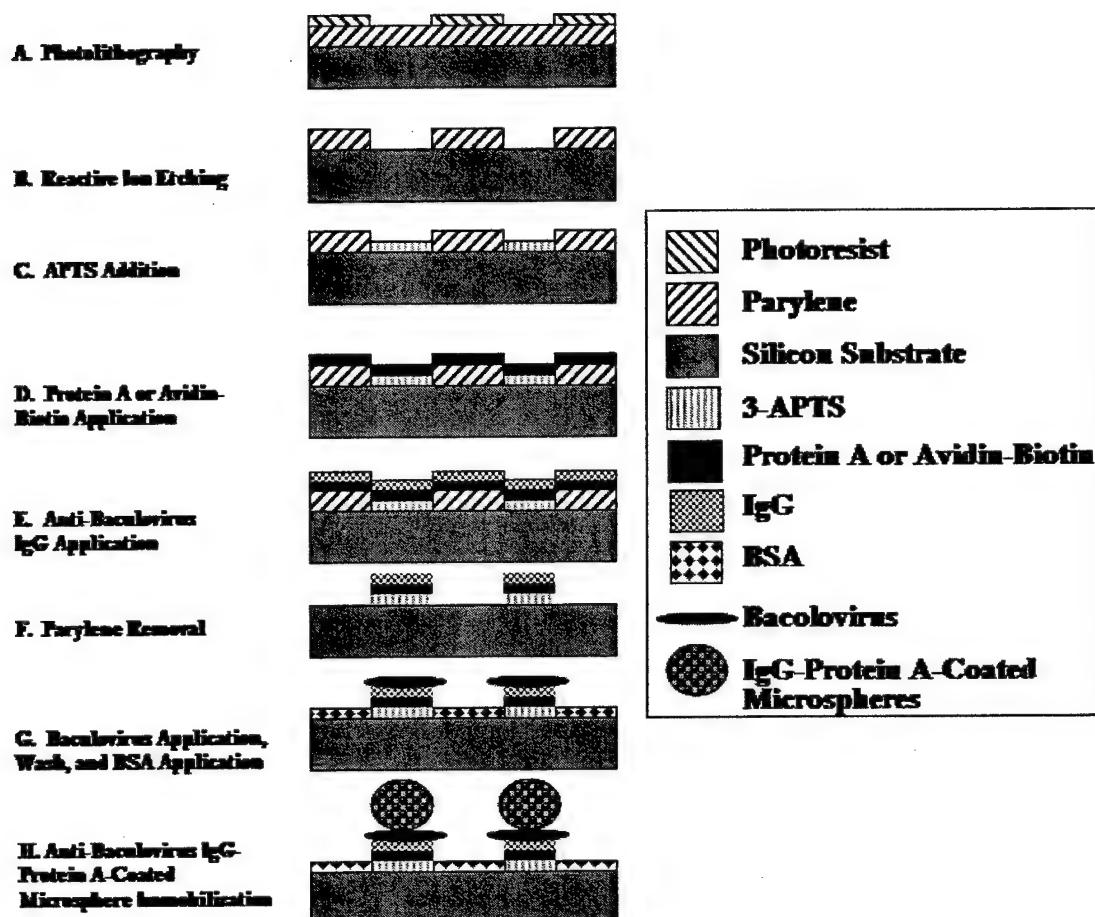
Figure 4.2. Schematic illustrating the fabrication process flow schematic modified from earlier research [8], [10] for application of functionalized biomaterials.

From top to bottom: (A) Photopatterning of photoresist that is 150% as thick as the polymer. (B) Reactive ion etching of the polymer to the silicon surface. (C) 3-APTS silane application. (D) Protein A or biotin-avidin covalent immobilization onto the silane surface. (E) Anti-baculovirus IgG binding to protein A or biotinylated anti-baculovirus IgG binding to patterned avidin. (F) Polymer removal revealing the patterned surface. (G) Baculovirus or other pathogen capture onto the patterned surface. Samples are washed and then incubated in BSA to reduce subsequent nonspecific binding. BSA application earlier could contribute to increases in viral nonspecific binding. (H) Application of anti-baculovirus IgG-Protein A-coated microspheres.

The substrate fabrication is inexpensive, easy to handle, and compact. Once the substrate is patterned with the polymer lift-off technique, it provides a stencil with micro- and nanometer scale features on a solid substrate that can be stored potentially indefinitely. Additionally, the samples do not require refrigeration and do not require additional equipment for the reproducible micrometer scale patterning. Application of antibodies and target reagents occurs in solution just as in an environment analogous to normal physiological conditions. Therefore, antibodies in this application do not lose their functionality since they are not dried, heated, or compressed onto a substrate (these things occur in other micropatterning techniques). Insect-derived baculovirus is the target pathogen in this experiment.

Fig. 4.3A illustrates Parylene with photopatterned photoresist. The thickness of the photoresist should be 150% as thick as the Parylene to ensure that it protects the Parylene during the whole subsequent reactive ion etching step. The desired Parylene thickness depends upon the aspect ratio of the polymer thickness to the feature size. 1.2-1.5 μm of Parylene was the standard thickness for the patterning in this experiment. Parylene thickness matters in the application and it can be too thin or too thick. For example, very thin Parylene (e.g. 500 nm thick) would be difficult to peel in one piece from the surface and while very thick Parylene (e.g. 4.0 μm) would resulted in poor pattern transfer from the photoresist during the reactive ion etching for the smallest features (e.g. the 1 μm features). The thicker the Parylene, the easier the polymer is to peel in one piece. A tradeoff is that as the polymer thickness increases, there is a decrease in accuracy of pattern transfer from the photoresist pattern to the Parylene layer as shown in Fig. 4.2B. As a side consideration, the cumulative exposure of the isotropic reactive ion etching causes the highest portion of the Parylene, the area exposed to the reactive ion etching first, to be etched away to a
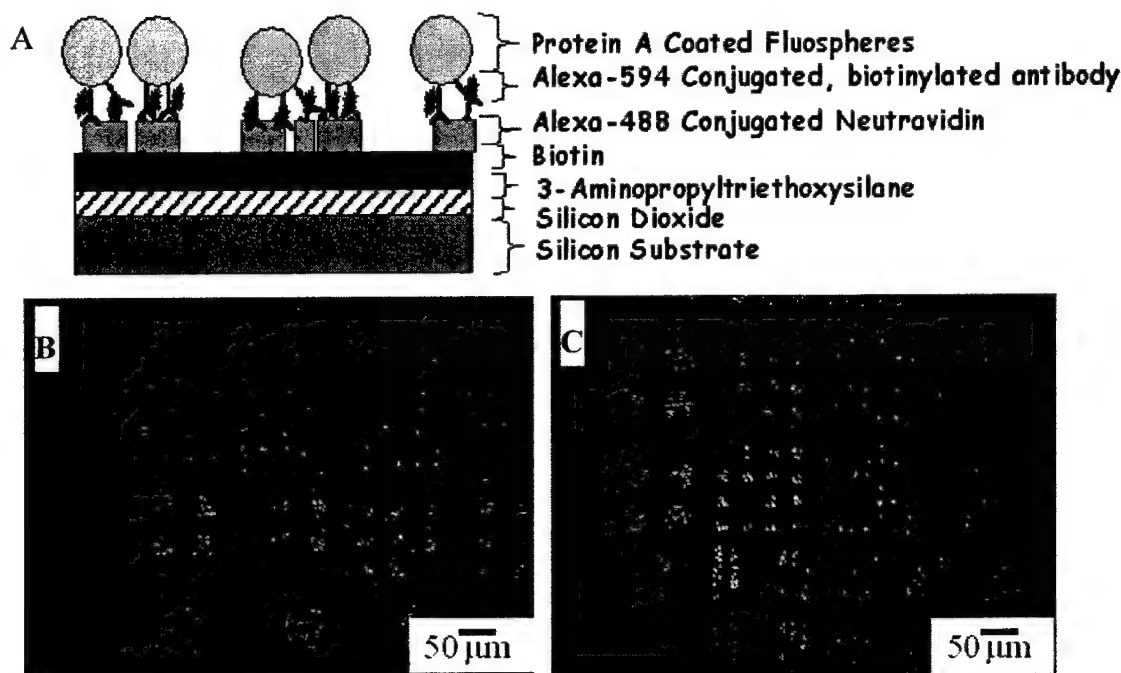
Figure 4.3. Optical fluorescence characterization using microspheres as model systems for bacteria captured from solution with avidin-biotin chemistry.
(A) Schematic illustrating the patterning of the biomolecules in this process. (B) Microspheres captured using avidin-biotin chemistry. The polymer was removed after microsphere addition. (C) Same as "B" except the microspheres are added after polymer removal and BSA application.

greater cumulative extent than the lower portions. Fig. 4.2C illustrates the application of 3-aminopropyltriethoxysilane (3-APTS) for the creation of amine-terminated self-assembled monolayers. These monolayers form covalent attachments to the molecules used to anchor antibodies, namely protein A or avidin-biotin as illustrated in Fig. 4.2D.

Protein A and avidin-biotin are robust molecules for adhering antibodies to the substrate. Protein A anchors mouse and human antibodies through their F_c regions. Protein G is also frequently used for this purpose. Biotin patterned using the Parylene lift-off method binds effectively to NeutrAvidin in solution. Subsequently, the tetrameric NeutrAvidin molecules can capture biotinylated antibodies from solution. Anti-baculovirus IgG adhere to the surface either through conjugation of the antibody

F_c receptor to protein A or by conjugation of biotinylated antibody to patterned avidin as illustrated in Fig. 4.2E. The bonding that takes place in either system occurs between molecules with high affinities for one another. Consequently, the molecules remain conjugated to one another and can withstand subsequent rinsing and application of other biomaterials. The removal of the Parylene takes place with tweezers and reveals patterned features as shown in Fig. 4.2F. The specificity of monoclonal antibodies enables the antibodies to selectively capture the desired target molecules from a heterogeneous solution. A solution containing the target molecule is added onto the samples as shown in Fig. 4.2G. After the sample is incubated in the solution, the sample is washed and then incubated in 1% BSA to reduce nonspecific binding during the following step. BSA is not added earlier since it had been found that baculovirus bound nonspeficically to the BSA.

Figs. 4.3-5 illustrate patterning of biotin or protein A. Figure 4.3 demonstrates a model system for the selective capture of bacteria-sized particles using avidin-biotin chemistry. In this system, Alexa 594-conjugated, biotinylated antibodies (red) are pattered as detailed in Fig. 4.2A-F. When antibodies are biotinylated, the biotin molecule usually adheres to lysine peptide along the length of the antibody. Therefore, it should not preclude the binding of the F_c tail to the protein A and only a small statistical quantity has the potential to end up binding in the variable region. As a result, the majority will have their variable regions and F_c regions open and available for intermolecular bonding. Since the F_c tail of mouse IgG bind to protein A, microspheres coated with protein A can be selectively captured onto the biotinylated antibody patches. A schematic of this interaction is illustrated in Fig. 4.3A and optical micrographs of the interaction are shown in Fig. 4.3B-C. The 1 μm microspheres contain Alexa 488 fluorescent dye (green). Microspheres at a 10^5 microspheres/mL
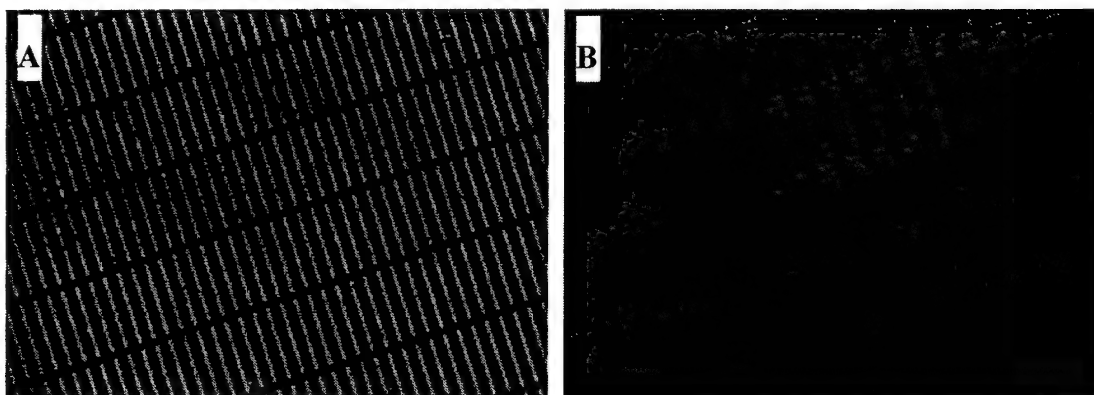
Figure 4.4. Epifluorescence micrographs showing protein A patterning using the polymer lift-off technique.
(A) 5 μm X 50 μm lines with 10 μm separation spacing. (B) 20 μm X 50 μm lines with 20 μm separation spacing.
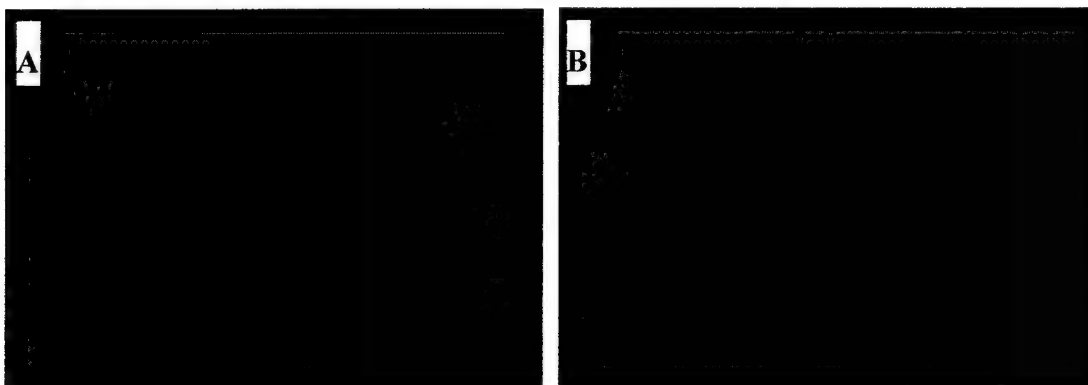
Figure 4.5. Anti-baculovirus IgG coated, 1 μm Alexa 594 fluorescent microspheres selectively captured on immobilized baculovirus that are selectively captured on 5 μm lines of micropatterned anti-baculovirus IgG.
The image on the left is a 200X magnification and the one of the right is a 500X magnification.

concentration are used for the experiments show in these images. The selectivity of the antibodies for the microspheres is demonstrated by their preferential adherence to the patterns and serves as a model system for the selective binding of the reagents from solution. Fig. 4.3B shows a sample where microspheres were added and incubated prior to Parylene removal. After Parylene removal there should be minimal to no

microspheres on the surface and this trial serves as a control for what the background would be with binding exclusively on the surface. Microspheres only go to the background if they rolled off the Parylene during the removal. Fig. 4.3C shows a sample where microspheres were added after the Parylene removal and BSA application. These images confirm that the cells prefer the patterned ligands to the background. In separate control samples consisting of (1) no biomolecules in the pattern region or (2) avidin only, there was consistently 50 to 100X fewer microspheres bound in the whole 5 mm x 5 mm area (whole area of all the grating lines).

In a related experimental set-up, antibodies are adhered to micropatterned protein A following the protocol detailed in Fig. 4.2A-F. A schematic of this interaction is illustrated in Fig. 4.4A and optical micrographs of the interaction are shown in Fig. 4.4B-D. The 1 μm, Alexa 488-conjugated microspheres are applied at a concentration of 10^6 microspheres/mL for the experiments show in these images. The selectivity of the antibodies for the microspheres was once again demonstrated by their preferential adherence to the patterns as well. Fig. 4.4B shows Parylene removal after the microsphere application and incubation. In comparison, Fig. 4.4C-E show samples where the Parylene was removed prior to microsphere application. This once again demonstrates the specific binding of the microspheres to the substrate with the target-ligand interaction. In a separate control samples consisting of (1) no biomolecules in the pattern region or (2) avidin only, there was consistently 50 to 70X fewer microspheres bound to the patterned region, corresponding to the background levels of the normally patterned samples.

Diffraction optical sensors [11], [12], [13] are well suited for portable field operations. The process shown in Fig. 4.1 is modified from the method of St. John *et al.* [11]. If the laser shines only on the 15 nm antibodies, a diffraction signal is created

that is negligible over the background level. However, if the laser shines on captured virus or bacteria that are 10-200X larger than antibodies, then a diffraction signal can be detected. The biosensor size is dependent upon the number of samples on one substrate and the focal spot of the laser. Therefore, a sample could be on the order of several cm^2 down to tens of μm^2.

For the optical biosensor detection system, monoclonal antibodies selectively capture baculovirus. Fig. 4.5A-B show two of the Protein A patterns used to immobilize antibodies. After a sufficient incubation, the Parylene was removed. The features are rectangular to allow for greater Parylene strength over the whole surface to ensure complete removal in one contiguous piece. Anti-baculovirus antibodies adhere to the surface through their F_c tail regions. Since the target molecules were smaller than the wavelength of the laser light, their diffraction signal was amplified by using 1 μm fluorescent microspheres conjugated with antibodies against the target molecule. Fig. 4.6 shows the successful capture of the microspheres onto the immobilized virus. Fig. 4.6A is oriented diagonally up to the right when Fig. 4.6B is oriented diagonally down to the left. Fig. 4.7 shows a diffraction signal off a surface containing patterned fluorescent microspheres on the selectively immobilized baculovirus on the patterned surface detailed in Fig. 4.6. No diffraction signals are observed when the surface contained only patterned antibodies. The experimental set-up is the same as shown in Fig. 4.1. The system creates a diffraction signal 1 meter from the sample. This would enable a field-operated diffraction biosensor attached to a wristwatch to shine a quantifiable signal onto a sheet of paper held an arm-length away from the sample.

This technique allows proteins to be pattered while still maintaining their functionality. The control experiments performed in the absence of antibodies demonstrated that the microspheres bound at low levels that corresponded with the
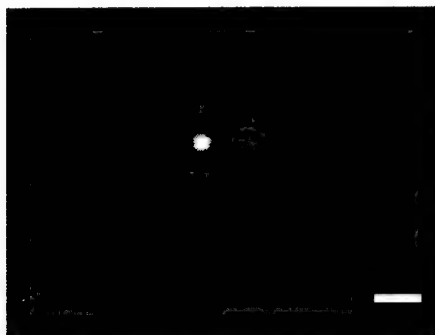
Figure 4.6. Digital photograph of a diffraction signal off a surface containing anti-baculovirus IgG-coated, 1 μm Alexa 594 fluorescent microspheres bound to captured baculovirus.
The lines in this example are 5 μm with 10 μm spacing. This diffraction signal was taken on a piece of paper placed 1 meter form the sample. Scale bar equals 3 cm.

low background level. These tests confirm the functionality of the patterned proteins and illustrate a method to selectively capture biomaterials from solution onto the micropatterned regions. The spheres serve as a model for selectively capturing bacteria and other biological cells from solution. The polymer protects the surface from specific and nonspecific binding until it is removed. This allows for long-during incubation times without concern for an increase in nonspecific binding. Parylene is biologically compatible so it does not interfere with the protein reactions. Parylene is easy to use, provides conformal coating, and is rapidly removed with a lift-off step.

Conclusions

The diffraction-based biosensor with biomaterials patterned using the Parylene lift-off methods offers a reliable biosensor with field operation capabilities. Parylene is easy to use, provides conformal coating, and is rapidly removed with a lift-off step revealing functional patterned biomaterials. This provides a spatially defined protein micropattern that can be used to selectively capture other biomaterials from solution for bioassay and biosensor applications.

References

[1] Vo-Dinh, T. 2002. *J. Cell Biochem. Suppl.*, 39:154-61.

[2] Anderson, G. P. and N. L. Nerurkar. 2002. *J. Immunol. Methods*, 271:17-24.

[3] Jenkins, D. M. and M. Delwiche. 2003. *J. Biosens. Bioelectron.*, 18:111-118.

[4] Hulme, J., C. Malins, K. Singh, P. R. Fielden, N. J. Goddard. 2002. *Analyst.* 127:1471-1477.

[5] Conway de Macario, E., U. H. Rudofsky, and A. J. Macario. 2002. *Biochem. Biophys. Res. Commun.*, 298:625-631.

[6] Hofmann, O., G. Voirin, P. Niedermann, and A. Manz. 2002. *Anal. Chem.* 74:5243-5250.

[7] Hulme, J., C. Malins, K. Singh, P. R. Fielden, and N. J. Goddard. 2002. *Analyst,* 127:1233-1236.

[8] St. John, P. M., R. Davis, N. Cady, J. Czajka, C. A. Batt, and H. G. Craighead. 1998. *Anal. Chem. 70*:1108-1111.

[9] Ilic, B. and H. G. Craighead. 2000. *Biomedical Microdevices*, 2:317-322.

[10] Orth, R. N., M. Wu, D. A. Holowka, H. G. Craighead, B. A. Baird. 2003. *Langmuir.* 19:1599-1605.

[11] Green, N. M. 1975. *Advances in Protein Chemistry,* 29:85-133.

[12] Kumar, A. and G. M. Whitesides. 1993. *Appl. Phys. Lett.*, 63:2002-2004.

[13] Kumar, A. and G. M. Whitesides. 1994. *Science*, 263:60-62.

CHAPTER 5

SPATIAL-CONTROLLED MICROPATTERNING IN MICROTRENCHES

We have developed a novel method for patterning biological material at the micrometer scale (smallest features ca. 2 μm) within microtrenches using a recently developed polymer liftoff technique. The trenches (with dimensions of 25 μm of depth, widths ranging from 50-200 μm, and 60 mm in length) contain micrometer scale patterned arrays of various shapes and sizes upon which biological material is deposited. These trenches, once a cover is put over them, simulate microfluidic channels. The microtrenches are fabricated on a silicon substrate via photolithography and reactive ion etching (RIE). Subsequently, a polymer coating is applied and the features are patterned using photolithography and RIE of the polymer. This reveals polymer templates inside the microtrenches. Either proteins or haptenated lipids are applied and bound to the exposed areas of the silicon substrate. Removal of the photolithographically modified polymer from the patterned surface reveals the biomaterial patches. This technique builds upon prior work where lipid bilayers containing dinitrophenyl (DNP)-capped lipids were used to stimulate immune cells. With the microtrenches, fluorescently-labeled cells, substrates and/or antigens can be spatially patterned to generate specific domains within the microfluidic channel. Thus this technique allows localized positioning of biological materials and control over the flow of ligands which will bind to the patterned material. Intake and concentration of substrates can be monitored, and at the same time, specifically bound cell types can be targeted for the study of ligand-ligand interactions.

Introduction

Microfluidic devices have become an attractive research tool and biomedical instrument because of their small volume and versatile capabilities. Microfluidic

devices are made in a wide range of materials including glass, silicon, plastics, and metal. They are formed using silicon micromachining reactive ion etching (RIE), hot embossing, micro injection molding, chemical etching, elastomer molding, eximer laser machining, UV lithography, and electron beam (e-beam) lithography. They offer the advantage that numerous procedures can be performed in parallel with the same starting solution. Additionally, the small volume allows the work to be highly reproducible from one trial to the next. Microfluidics can also be easily integrated into automated platforms. The fabrication methods permit a wide range of design flexibility (e.g. dimensions, interface with the macro world, complexity of design, incorporation of different analysis technologies, etc.) so the devices can be easily tailored to fit the needs of the experimental application. Microfluidic devices have considerable utility in biomedical experimentation. Their miniature nature of reduces reagent requirements, costs, and reaction times. They can also mimic many physiological environments including the blood circulatory system and tissue vasculature.

This research details a new capability which can supplement existing microfluidic devices: the patterning of materials within microtrenches using the polymer lift-off technique. The application of biomaterials follows a modified version [1] of the Parylene lift-off technique [3]. A silicon substrate patterned through reactive ion etching is covered with Parylene and patterned using the steps detailed in Chapter 3. This technique offers the patterning capabilities of photolithographic equipment, thereby enabling features to be patterned within microchannels with features sizes as small as 2 μm. In previous research, patterned materials have been introduced to a microenvironment where a polydimethylsiloxane microfluidic network has been inverted over a patterned surface. While this offers the introduction of

micropatterned materials to the system, alignment for features smaller than the channel width remains a challenge.

Experimental Section

Photolithography and Silicon Reactive Ion Etching. 5 μm of Shipley 1045 photoresist are applied to the silicon wafers. The samples are pre-baked for 1 min at 90°C and exposed using standard photolithographic techniques with a 5X stepper (Fig. 1). After development in Microposit MIF 300 developing solution (Shipley, Marlboro, MA), the exposed portions of the silicon are subjected to an RIE etching step using a Plasma Therm Reactive Ion Etcher. After etching, the photoresist is removed using the Aura 1000 Plasma Stripper. Parylene is deposited on silicon substrates, etched to a thickness of 1.5 μm and photolithographically patterned as detailed in Chapter 3. The samples are aligned to the next pattern in the 5X stepper using alignment marks that are applied to the first photoresist layer. The samples are then developed in MIF 300 and etched in the Plasma Therm 72 reactive ion etcher to expose patterns in the bottom of the microtrenches.

Biomaterial Patterning. Lipids, antibodies, and microspheres are prepared for application onto the patterned microfluidic device. The lipids purchased from Avanti Polar Lipids (Alabaster, AL) are prepared as detailed in Chapter 2. These lipids included DNP-cap-DPPE: 1,2-Dipalmitoyl-sn-Glycero-3-Phosphoethanolamine-N-[6-[(2,4-dinitrophenyl) amino]hexanoyl] (Ammonium Salt), POPC, 1-Palmitoyl-2-Oleoyl-*sn*-Glycero-3-Phosphocholine, and Rh-PE: 1,2-dioleoyl-sn-glycero-3-phosphoethanolamine-N-lissamine rhodamine b sulfonyl. IgG antibodies are stained using an Alexa 594 protein labeling kit (Molecular Probes (Eugene, OR) and diluted to 100 μg/mL. Alexa-488 containing microspheres (Molecular Probes, Eugene, OR) are diluted to 10^7 spheres/mL. For the lipid samples, the silicon microchannel pattern is

plasma cleaned prior to lipid application. 40 µl of biomaterial solution is applied to the microchannel inlet port. The patterning protocol for the different biomaterials had slight variations: (1) 50 µL of 2 mM 1:99 Rh-PE:POPC (10 min, room temperature (RT)), PBS wash. (2) 50 µL of 2 mM DNP-cap-DPPE (10 min, room temperature (RT)), PBS wash. (3) 50 µl of 100 µg/mL of Alexa-488-conjugated NeutrAvidin (1 h, 37°C), PBS wash. (4) 50 µL of 100 µg/mL protein A (Pierce Chemicals, Rockford, IL, 1 h, 37°C), PBS wash. (5) 50 µL of microspheres (1 h, 37°C), PBS wash. (6) 50 µL of 50 µg/mL fibronectin (1 h, 37°C), PBS wash. For each of the applications, the Parylene is mechanically peeled from the outer surface and from the inner surface starting at the inlet port revealing patterned biomaterials.

Biomaterial Characterization

Each of the biomaterial is characterized by the application of subsequent fluorescent molecule (except the microspheres that are already fluorescent): (1) No additional reagents were applied to the Rh-PE-POPC patterns. (2) 50 µL of 1 µg/mL of Alexa 488-conjugated monoclonal mouse anti-DNP IgE is applied to the surface patterned with DNP-cap-DPPE (1 h, 37°C), PBS wash. (3) 50 µL of 100 µg/mL biotinylated, Alexa 594-conjugated anti-baculovirus IgG is applied to the surface patterned with NeutrAvidin (1 h, 37°C), PBS wash. (4) 50 µL of 100 µg/mL Alexa 594-conjugated anti-baculovirus IgG is applied is applied to the surface patterned with protein A (1 h, 37°C), PBS wash. (5) No additional material is applied to the microspheres. (6) 50 µL of fibroblasts (10^5 cells/mL) are applied (24 h, 37°C), PBS wash. 50 µL of 10 µg/mL Alexa 594 phalloidin, DAPI, and Alexa 488 anti-fibronectin stains are applied (1 h, 37°C), PBS wash.

Results

The objective for this research was to develop a method to pattern materials at the base of existing microfluidic devices. Fig. 5.1F is a schematic of patterned biomaterial with molecules captured from solution. Fig. 5.2 shows a top view of the silicon substrate with Parylene patterned on the surface prior to the lift-off step. Fig. 5.2 A shows the open squares in the patterned channel. Fig. 5.2 B shows the inlet port to the microfluidic channel. Fig. 5.3 illustrates the patterning of RE-POPC. Fig. 5.4 illustrates Alexa 488-conjugated monoclonal mouse anti-DNP IgE adhering to the DNP-cap-DPPE. Fig. 5.5 illustrates biotinylated, Alexa 594-conjugated IgG bound to the Alexa-488 NeutrAvidin. Fig. 5.6 illustrates Alexa 594-conjugated IgG bound to protein A. Fig. 5.7 illustrates the patterned Alexa 488 containing microspheres. Fig. 5.8 illustrates Alexa 594 phalloidin, DAPI, and Alexa 488 anti-fibronectin stains bound to the fibroblast cells.

Discussion

The fabrication of the device relied on the careful alignment of the patterns in the 5X stepper. The standard alignment keys are used. The initial run produced a sample that is 40 μm off the desired location so subsequent exposures are performed accounting for this placement variation. Routine cleaning of the Parylene deposition machine is necessary to ensure the Parylene peels properly. After approximately the 15th run of 1-3 μm depositions, the Parylene becomes difficult to peel, potentially due to Parylene that builds up during the previous runs and degrades over numerous deposition cycles.

An example of a patterned silicon substrate is shown in Fig. 5.2. This shows the open regions onto which the biomaterials are applied. Additionally, it shows the inlet port with the multiple parallel inputs to the channels. Currently, the design can
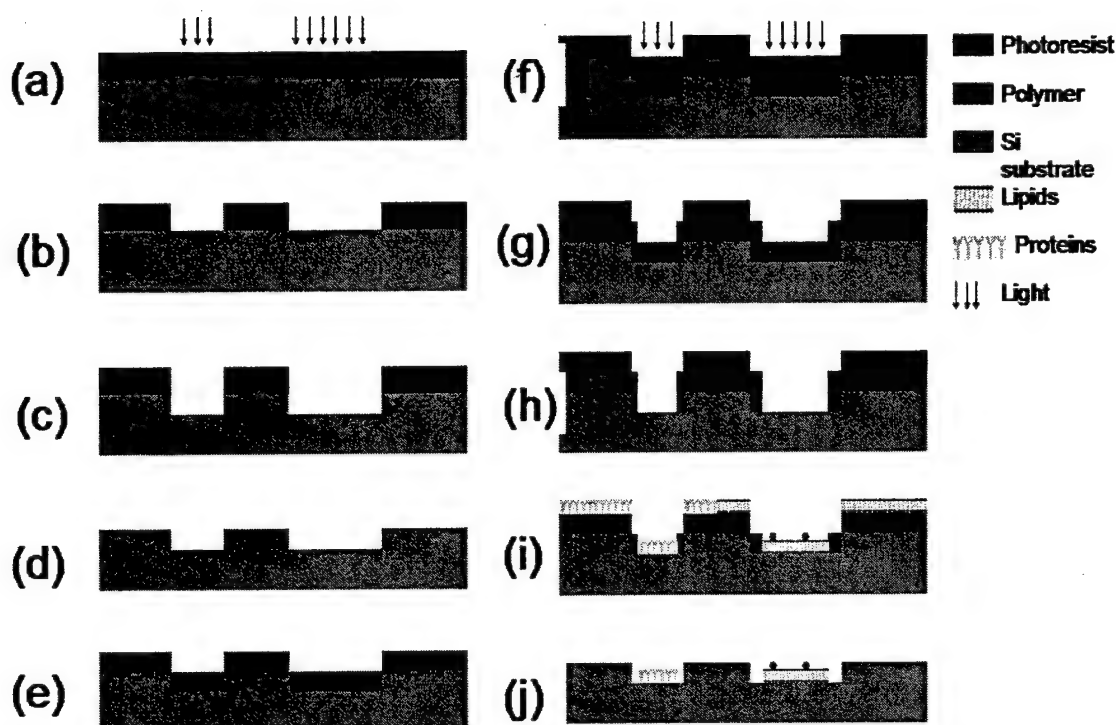
Figure 5.1. Microfabrication, patterning, biomaterial deposition and polymer liftoff. (a) Photoresist is spun on the Si substrate and irradiated. (b) Photoresist is developed and Si substrate is exposed. (c) Exposed silicon substrate is etched (RIE). (d) photoresist is removed. (e) Patterned Si substrate is coated with polymer. (f) Photoresist is spun on top of polymer and irradiated. (g) Photoresist is developed and polymer exposed. (h) Exposed polymer is etched (RIE). (i) Photoresist is removed and biological material is applied. (j) Polymer is lifted off, biomaterial is left as well defined patterns inside microtrenches. All microfabrication is done by standard photolithographic techniques. Preparation of biological samples is as described by Orth *et al.* [1]
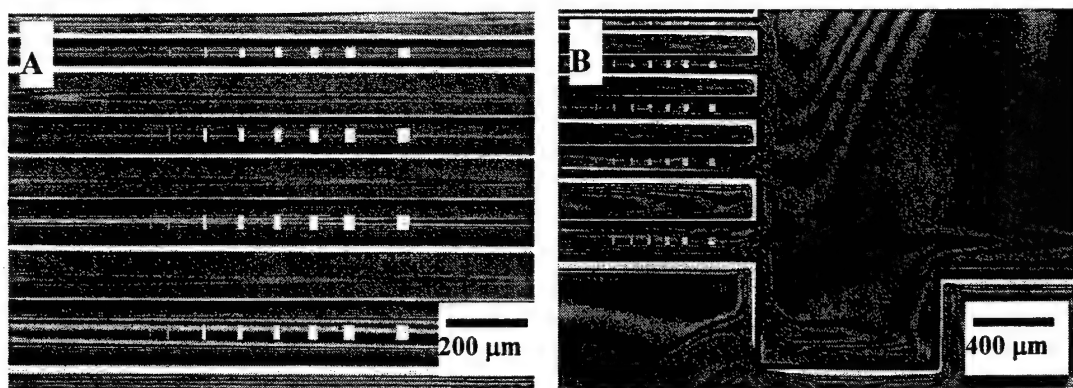
Figure 5.2. Top view of patterned channels with exposed Si substrate before polymer liftoff.
(a) Features patterned on the polymer are squares (2 – 40 μm, not shown) and lines (40 μm height, 2 – 30 μm width); (b) Input well where solution is loaded after the initial biomolecules are patterned.

be used to input one sample solution to the channels in a parallel fashion. Modifications of the design can be performed to create multiple parallel input ports for sampling of multiple different analytes in parallel.

. Excellent patterning is observed with the RhPE:POPC and DNP-cap-DPPE lipids. Fig. 5.3 shows the uniform binding of Rh-PE:POPC to the patterned surface. This lipid was an ideal reagent to initial sample the surface since it adheres strongly and the concentration for use was optimized during the research detailed in Chapter 2. Specific binding of the IgE antibody to the DNP-cap-DPPE is observed in Fig. 5.4. The patterning technique optimized by Orth *et al.* creates a supported lipid bilayer on an unetched silicon wafers. The application of the lipids in the microchannels may also form supported lipid bilayers. This has yet to be determined, for the reactive ion etching could roughen the surface enough to preclude lipid bilayer formation. Regardless, the top layer of the patterned lipids still presents the DNP hapten as verified in Fig. 5.4. This demonstrates that lipids containing hapten and antigen can
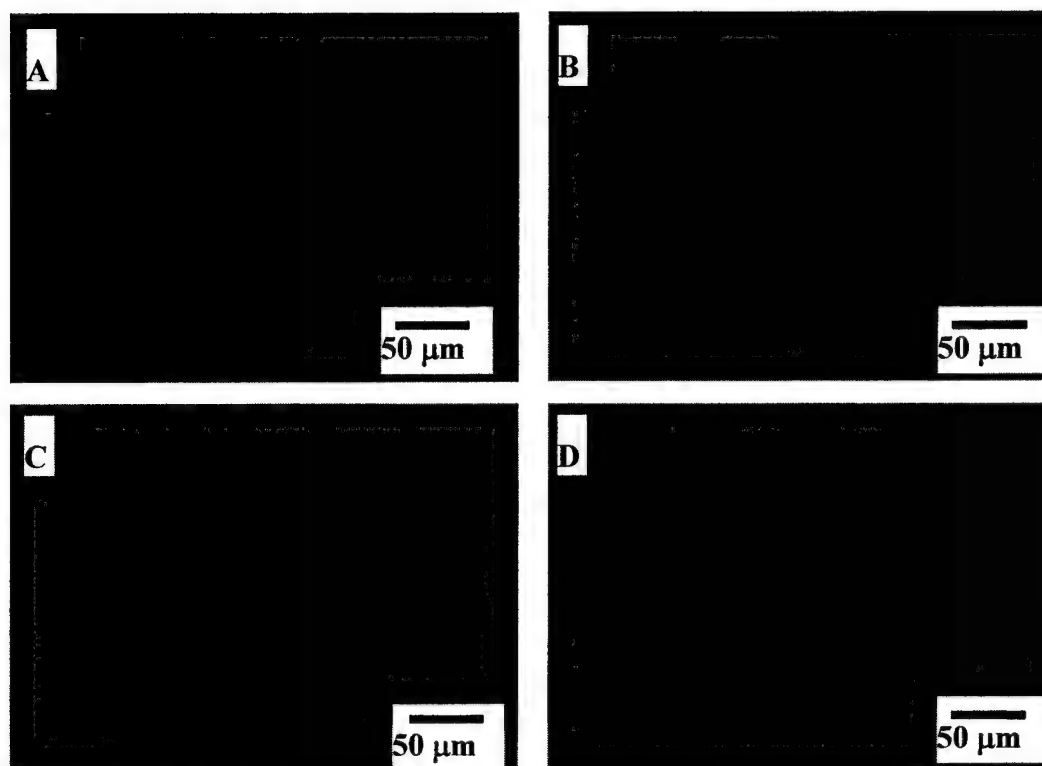
Figure 5.3. Fluorescently-labeled lipid patterns on the bottom of microchannels. 1:99 RE-PE:POPC lipids incubated and bound to patterns of exposed Si substrate. Solid bright red areas denote the channel separations where the polymer was not removed. (A) Square patterns of 2, 5 and 10 µm side length. (B) Square lipid patterns of 15, 20 and 25 µm side length. (C) Line lipid patterns of 2, 5 and 10 µm width. (D) Line lipid patterns of 10, 15, 20 and 25 µm width. be patterned at the base of the channel for interaction with solutions in the microfluidic device.

Biotinylated antibodies have been successfully immobilized in micropatterns in the channels as illustrated in Fig. 5.5. Avidin-biotin technologies are useful tools for controlling and analyzing the interactions taking place at the cellular and molecular levels. The technology offers a means to immobilize biotinylated molecules to a substrate through the avidin-biotin complex. A stable bond arises from the strong avidin-biotin association constant. Specificity is provided to these devices with the biotinylated, monoclonal antibodies. Avidin-biotin patterning is preferred for molecules that must remain in solution, are not functionally affected by the
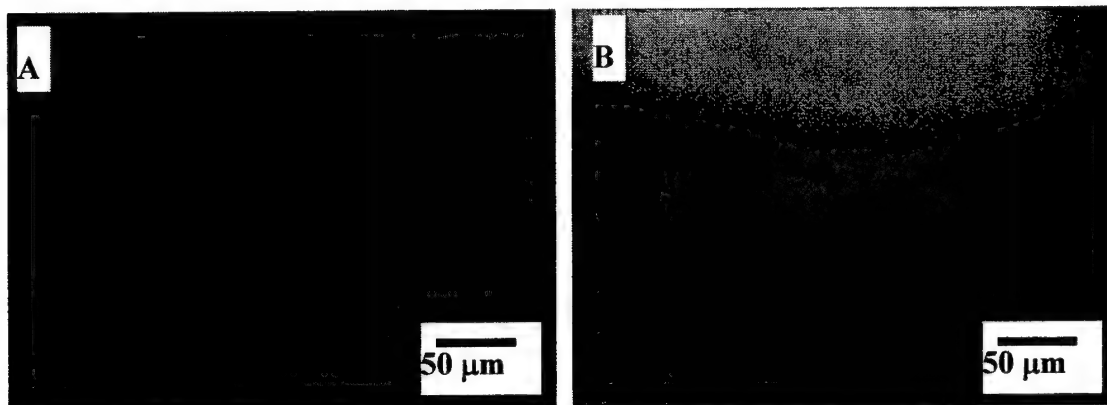
Figure 5.4. Micrographs of fluorescently-labeled lipid patterns and IgE antibodies bound to DNP capped lipids.
A) Patterns of artificial lipid bilayers composed of 89 mol % of DPPC, 10 mol % of DNP-cap-DPPE, 1 mol % of fluorescent lipid probe (DPPC-DiI). (B) Same features as Fig. 5.4A with IgE-FITC (100 nmol/mL) antibody bound to DNP capped lipids.
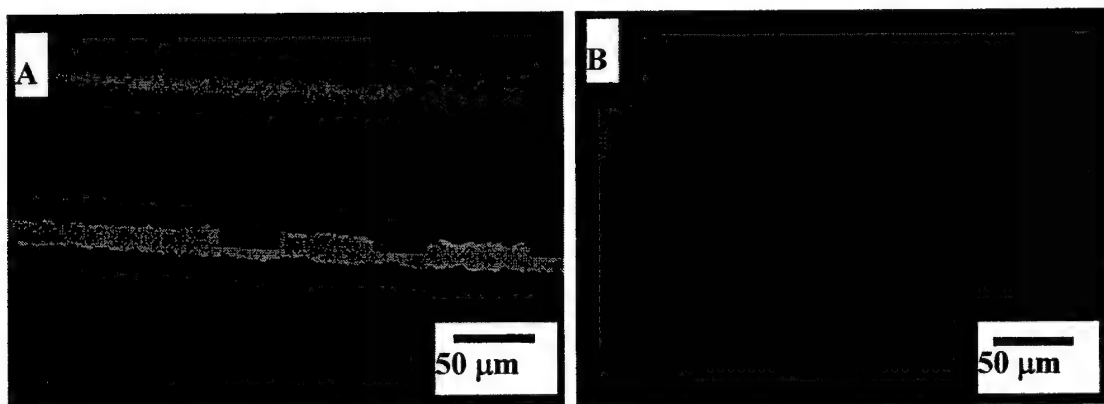
Figure 5.5. Fluorescence micrographs of patterned NeutrAvidin and binding of biotinylated IgG.
Patterned green fluorescently-labeled NeutrAvidin binds red labeled biotinylated IgG. Strips of unremoved polymer are left in the channels to show how the polymer leaves behind the desired patterns of biomaterials. (A) Green fluorescently-labeled NeutrAvidin (100 µg/mL) bound to the exposed patterns of Si substrate. (B) Red fluorescently-labeled IgG (100 µg/mL) binds to the patterned NeutrAvidin.

biotinylation process, and are desired to form either a monolayer or only a few layers. In this application, antibodies can either be applied directly or flowed into the device from the microchannel inlet port for specific capture on the patterns.

Protein A is a bacterial protein that specifically interacts with the F_c tail of antibodies. Fig. 5.6 illustrates antibodies capture on the patterned protein A. This demonstrates how protein A can serve as a versatile platform to bind antibodies that, in turn, specifically can capture materials from a solution in the microfluidic channel. In this application, antibodies can either be applied directly or flowed into the device for specific capture on the patterns.

An extensive variety of microspheres are commercially available that are conjugated to or contain nearly any ligand or reagent desired for a biomedical or research application. Fig. 5.7 illustrates the immobilization of microspheres within the patterned regions. Such a capability enables the full range of the microsphere technology to be incorporated effectively into a spatially patterned location within the microfluidic device.

Living cells have numerous cell surface molecules. Many of these molecules have adhesion properties that help the cell localize to specific tissues in the host organism. Cells respond to the microenvironment in which they reside. Consequently, the microfluidic channel is an excellent synthetic environment in which the cells can exist and mimic their native surroundings. Of particular importance is the volume into which the cell releases its cytokines. If the volume is too large, then the chemical message becomes diluted and cannot be detected by neighboring cells at the proper quantitative level or at all. The microchannel, however, has a nanofluidic volume that is analogous to a blood capillary. As a result, it provides an environment conducive for cellular experimentation. Fig. 5.8 illustrates the specific immobilization of fibroblasts onto the fibronectin micropatterns. The cells can be
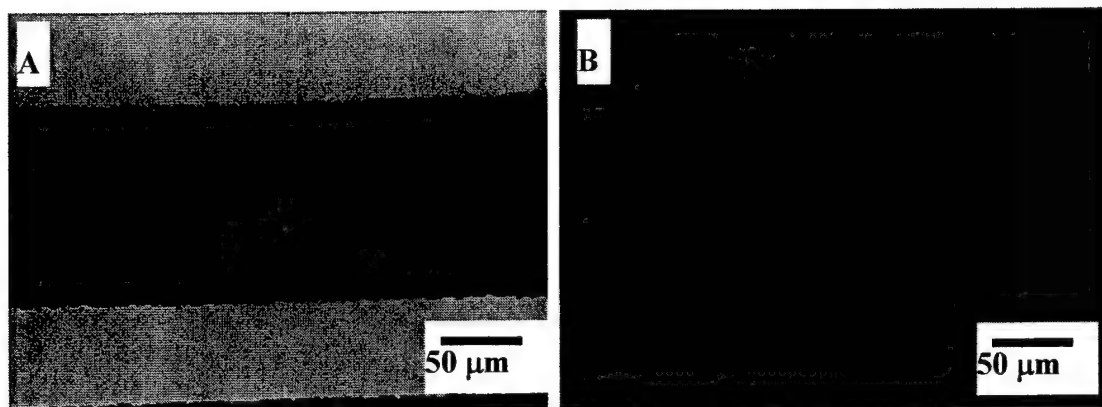
Figure 5.6. Fluorescence micrographs of patterned Protein A and binding of labeled anti-baculovirus IgG.
Patterned protein A binds fluorescently-labeled antibodies (anti-baculovirus). (A) Fluorescently-labeled protein A (100 µg/mL) bound to the exposed patterns of Si substrate. (B) Red fluorescently-labeled anti-baculovirus IgG (100 µg/mL) binds to the patterned protein A.
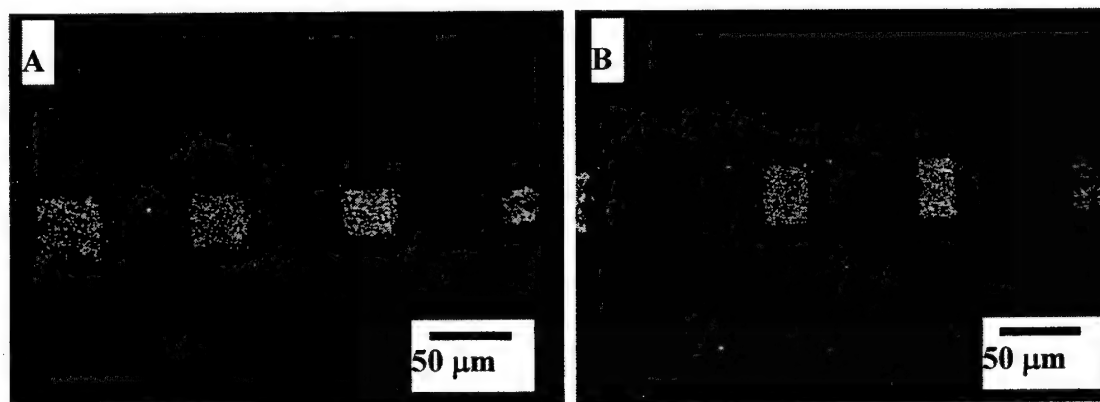
Figure 5.7. Fluorescence micrographs of Protein A covered fluorescent microspheres simulating selective binding of bacteria.
The protein A covering the fluorescent spheres (10^7 spheres/mL) binds down to the exposed patterns of silicon substrate. (A) Square patterns (25, 30 and 40 µm) of fluorescent spheres. (B) Line patterns (20 and 25 µm width) of fluorescent spheres.

distinguished by the DAPI stain that adheres to nuclear proteins. These results demonstrate that the cells prefer the patterned fibronectin regions to the bare silicon surface. This serves as a model system for the capture and immobilization of cells from solution.
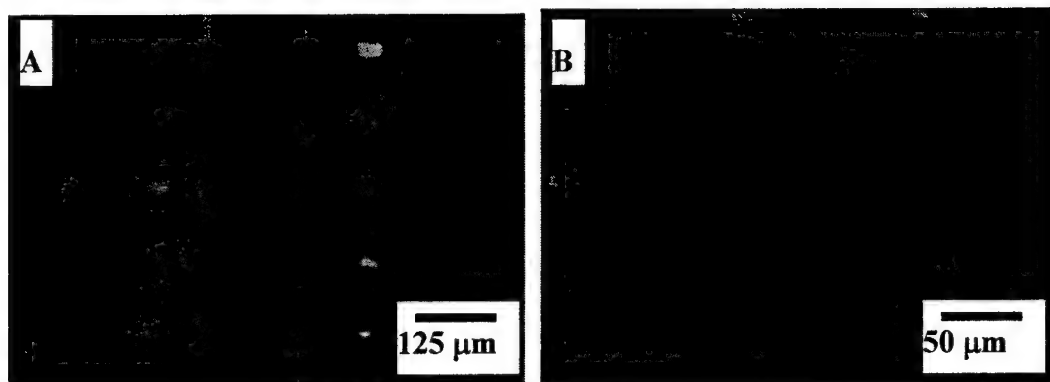
Figure 5.8. Fluorescence micrographs of fibroblast adhered to fibronectin in a microchannel.
(A) Alexa 488 conjugated anti-fibronectin IgG (green) binds to the fibronectin patterned at the base of a 25 μm deep microchannel. The cell nuclei are stained with DAPI dye. The image was taken with a 20X objective. (B) Fibronectin cells with the same conditions as Fig. 9.3A taken with a 50X objective.

Conclusion

We have developed a new method for patterning biomaterial within microtrenches. Experiments show that proteins, functionalized lipids, and microspheres can be patterned in specific regions and are capable of binding secondary ligands. These ligands can in turn bind cells or other antigens. Previous reported experiments with patterning of biomaterial have made use of PDMS channels [2]. The method here presented gives the advantage of smaller patterned features and volumes in the channels. This opens the possibility of incorporating the patterning of biomaterials with microfluidic networks for the study of cell response to various stimuli, biosensing, and the study of binding events under specific flow conditions.

References

[1] Orth R. N., Wu M., Holowka D. A., Craighead H. G., Baird B. A. 2003. *Langmuir.* 19:1599-1605.

[2] Hellstrom S. The 2001 NNUN REU Research Accomplishments. 2001. 62-63.

[3] B. Ilic and H. G. Craighead. 2000. B*iomedical Microdevices*, 2:317-322.

CHAPTER 6

MAST CELL ACTIVATION ON PATTERNED LIPID BILAYERS OF SUBCELLULAR DIMENSIONS[Ψ]

Abstract

T cells, B cells, and other specialized cells in the immune system are activated by clustering of antigenic receptors on their plasma membrane surfaces; RBL mast cells that express cell surface immunoglobulin E (IgE) receptors and operate in the allergic response serve as a prototypic model. To investigate signaling pathways of the cellular response, a versatile system is being developed for presenting antigens on micron scale patterns of lipid bilayers that are prepared with a polymer-based wet lift-off method. A supported lipid bilayer is formed on silicon substrate after photolithographic patterning polymer and before the polymer is mechanically peeled away in solution. This forms well-defined bilayer patterns that can contain haptenated and fluorescent lipids and can be used to simulate a biological substrate for cellular receptor engagement and response. For this model system DNP-cap-DPPE was used for specific binding of anti-DNP IgE. IgE bound to mast cell surface receptors (FcεRI) aggregate and cluster over the patterned features if they are significantly smaller than the cells. For patterned features that are cell-sized or larger, cells adhere to the silicon surface with receptors polarizing toward the edge of the patterned lipid. RBL cells with specifically engaged IgE-receptors are activated to undergo striking morphological changes that can be analyzed with fluorescence or scanning electron

microscopy. This novel method for patterning antigen-functionalized lipids provides spatial control down to micron resolution for the antigenic stimulus while retaining the features of a plasma membrane substrate, including dynamics and variable composition. This method offers an alternative to microcontact printing with some enhanced capabilities for cellular immunological studies.

Introduction

Cellular responses resulting from surface receptors binding to their specific ligands on the plasma membrane of other cells are common throughout physiology and especially among the immune responses. An important example is the interaction between the antigenic receptors on T cells (TCR) and major histocompatibility complexes (MHC) on antigen-presenting cells that occurs during the generation of almost all immune responses. This multivalent coupling and consequent plasma membrane interactions take place in interfacial regions called "immunological synapses," which have received considerable attention over the past few years [1]. The spatial-temporal evolution of membrane protein interactions may be as critical as the individual association/dissociation events between ligands and receptors [2], [3]. Immunoglobulin E (IgE) receptors (FcɛRI) on mast cells are in the same multi-subunit immune recognition receptor (MIRR) family as TCR, [4], [5] and serve as a simpler model. Cross-linking of IgE- FcɛRI by multivalent antigens initiates transmembrane signaling that ultimately leads to the exocytosis of chemical mediators of allergic reactions [6]. Recent research on immunoreceptor signaling has begun to focus on the participation of plasma membrane domains, commonly called lipid rafts [19], [35], and this has been most clearly demonstrated for IgE-receptors [9], [10]. A large amount of evidence supports the view that antigen crosslinking of IgE-receptors causes coalescence of lipid rafts and consequently phosphorylation of receptors by active Lyn

kinases that preferentially locate in this environment. Downstream signaling leads to morphological changes and exocytosis in mast cells [10]. Similar plasma membrane involvement in T cell signaling has been demonstrated [1], [11]. An additional factor operating in cells is the interplay between the membrane and the actin cytoskeleton which can alter structural features and thereby localization of signaling [12]. Clustering of receptors and consequent compartmentalization of biochemical reactions allows a rapid, regulated cellular response to specific stimuli with a limited number of targeted signaling components. Although this view is supported by a large accumulation of data, essential details of the structural coordination and dynamical process remain to be elucidated. Systematic examination of localized signaling could greatly benefit from spatially controlled stimuli.

Supported lipid bilayers offer the means for creating a plasma membrane template to interact with a responsive cell and address receptor binding and signaling questions [13], [14], [15]. An alternative is functionalized beads, but these have limitations for many studies, including cellular internalization that occurs under some conditions. The geometry of planar surfaces eliminates questions of curvature and is attractive for use with optical microscopy and other detection methods. For supported lipid bilayers an ultrathin film of water between the bilayer and substrate [16], allows the lipids in both leaflets to retain mobility similar to native plasma membranes. A major advantage of beads for some studies is the localization that is provided at the interface between the cell and the bead of selected size that bears the ligand for the cellular receptors. However, a limited interface can be displayed on a planar surface if its functional features are patterned with microfabrication. Microcontact printing is a versatile method that has become popular for patterning proteins [25] and mobile lipids [22], [23] on solid substrates. Patterning with this method has been reported for lipids down to 5 µm [27]. Researchers have started to use these patterning techniques to

analyze cell-substrate interactions and have primarily focused on cell adhesion [27] and control of neuron growth [26], [28].

Here we present a novel and easy method for spatially patterning a haptenated supported lipid bilayers using a recently developed polymer lift-off technique [24]. Uniform arrays of haptenated lipids with feature sizes down to ~1μm width are revealed after the polymer is peeled away in one contiguous piece under water, ready for controlled engagement of cellular receptors and monitoring of subsequent cellular responses.

Experimental Section

Materials. The OCG OiR 897-7i photoresist (OCG Chemical Company, West Patterson, NJ) was developed in Microposit MIF 300 solution (Shipley, Marlboro, MA). The lipids used include DPPC (1,2-Dipalmitoyl-*sn*-Glycero-3-Phosphocholine,$T_M=$ 41°C), POPC (1-Palmitoyl-2-Oleoyl-*sn*-Glycero-3-Phosphocholine, $T_M=$ -2°C), DNP-cap-DPPE (1,2-Dipalmitoyl-*sn*-Glycero-3-Phosphoethanolamine-N-[6-[(2,4-dinitrophenyl)amino]hexanoyl] (Ammonium Salt)) (Avanti Polar Lipids, Alabaster, AL), and fluorescent DiI (1,1'-dioctadecyl-3,3,3',3'-tetramethylindocarbocyanine perchlorate (DiIC18(3))) (Molecular Probes, Eugene, OR). POPC was used for fluorescence recovery after photobleaching (FRAP) so that the DiI probe would experience the fluid phase at room temperature. Lipid and cell mixtures were suspended in buffered saline solution (BSS; 140 mM NaCl, 6 mM KCl, 1 mM $MgCl_2$, 2 mM $CaCl_2$, 10 mM glucose, and 10 mM HEPES (4-(2-hydroxyethyl)-1-piperazineethane sulfonic acid pH 7.4). Milli-Q water (18.2 Mohm-cm) was used for rinses of the silicon wafers during preparation.

Lipid Preparation. The POPC/DPPC: DNP-cap-DPPE: DiI (99:0.5:0.5 or 99.5:0:0.5, molar ratio) solution was mixed in chloroform. 2 μmoles of total lipid was

transferred to 13x100 mm glass test tubes and dried with nitrogen gas. The solution was rehydrated with BSS to a final lipid content of 1 mM. The solutions were then vortexed for 30 sec to suspend multilamellar liposomes and probe sonicated to clarity (typically 0.5-1 h) using a Vibra Cell model ASI untrasonic disruptor. This was tuned at maximum setting to a temperature 10°C higher than phase transition temperature of the major lipid. The resulting suspension of small unilamellar vesicles (SUV) was sterilized by filtration through a 0.2 μm syringe filter (Acrodisc) and used on the same day.

Patterned Bilayer Formation. Parylene is deposited on silicon substrates and photolithographically patterned as detailed in Chapter 3. The Parylene-patterned substrate was plasma treated by PDC-32G Plasma Cleaner (Harrick Scientific Corp, Ossining, NY) just before use. 25 μl of SUV suspension (1 mM lipid) was added for 10 min, then the sample was thoroughly rinsed with 200 mL deionized water four times. The Parylene was mechanically peeled from the surface, revealing patterned lipids.

IgE and Cells. Monoclonal IgE specific for 2,4-dinitrophenyl (DNP) [30]was fluorescently modified with Alexa 488 according to the instructions of the labeling kit (Molecular Probes, Eugene OR). RBL-2H3 cells [17] were incubated with this IgE overnight and harvested from culture as previously reported [33]. (Pierini) IgE binds with high affinity and low dissociation rate to its cell surface receptor (FcεRI) such that the IgE-FcεRI complex is essentially irreversible within the timeframe of our experiments [29]. Solutions containing soluble IgE (100 ng/mL; room temperature) or sensitized cell suspensions (10^6 cell/mL; 37°C) were incubated with the lipid-patterned surface for 30 min or 1 h in BSS containing bovine serum albumin (BSA, 1mg/mL). All experiments were carried out in 35 mm Petri dishes with coverglass bottom (0.16-

0.19 mm; MatTek Corp, Ashland, MA). Samples were washed in BSS with BSA after the incubation periods and before microscopy.

Fluorescence Microscopy. Optical microscopy of all samples was carried out at room temperature. Epifluorescence microscopy was performed with an Olympus AX 70 upright microscope, with water immersion objectives, Omega Optical filter sets, and Spot CCD camera. DiI was observed with a 510-590-nm excitation/590-nm emission filter set, and Alexa 488 was observed with a 450-490-nm excitation/520-nm emission filter set.

A BioRad confocal head stage and an Olympus AX 70 inverted microscope were used for confocal microscopy and to measure fluorescence recovery after photobleaching (FRAP). DiI was observed with a 568-nm/585-nm filter set, and Alexa 488 was observed with a 488-nm/520-nm filter set. For FRAP measurements, one tenth of the field of view was photobleached for 10-15 sec under 100% laser power exposure by a 10X digital zoom. Using 3% laser power the intensity of bleached area, or a non-bleached area on the same patch, was plotted against time with a 3 sec interval.

Sample Critical Point Drying and Scanning Electron Microscopy (SEM). Specimens were fixed in a formaldehyde/PBS solution (3.7% w/v) for 10-15 min at room temperature. The fixation was quenched by adding PBS containing BSA (10 mg/mL) and rinsed with deionized water. The specimen was then dehydrated by gradually displacing the water with ethanol. The solution volume was returned to 100% by adding ethanol after removing 25% three times, 50% three times and 75% three times, then critical point dried with liquid carbon dioxide. Critical point dried specimens were attached to aluminum posts using double stick carbon tape and were sputter coated with gold palladium. SEM imaging was performed with a Hitachi 4500 scanning electron microscope.

Results and Discussion

The purpose of this investigation was to establish a micron scale array of patterned, haptenated lipids for localized engagement of IgE-receptors on RBL mast cells and evaluation of cellular responses that are stimulated. The patterned bilayers were created with a polymer-based wet lift-off method that we recently developed [24]. For our application of this method (Fig. 6.1), the Parylene C (di-para-xylylene) dimer is conformally vapor deposited on the silicon substrate and coated with photoresist. The polymer is then patterned with conventional photolithography and RIE. SUVs of defined lipid composition are applied, and they adsorb on the surface as clustered vesicles or self-assemble into a lipid bilayer, depending on lipid composition, lipid concentration, vesicle size, and presence or absence of Ca^{2+} [34]. Parylene is removed with a one-step mechanical lift-off, leaving a pre-determined pattern of lipid bilayers. Fluorescent DiI is included in the lipid mix to visualize the pattern, and the haptenated lipid DNP-PE can be included to enable specific binding of anti-DNP IgE.

Fig. 6.2A shows a patterned array of DPPC/DiI/DNP-cap-DPPE bilayer patches over ~1 - 76 μm square edge widths. The low end of this range is near the resolution limit of the 10X stepper, as confirmed with gold palladium patterned features of 700 nm dimension observed with SEM imaging as detailed in Chapter 3. The diffraction limit of optical microscopy does not allow the size of the smallest fluorescent features of the patterned lipids to be measured ~1 μm. The fluorescent probe shows that nonspecific lipid adsorption between the patches is negligible, demonstrating the tight adhesion of the Parylene prior to lift-off. The clear pattern revealed is also consistent with previous findings that adsorption of lipids on silicon is irreversible, although the patches undergo a small amount of lateral expansion that is self-limiting, characterized previously to be approximately 106% of the original size. Pattern uniformity with this method relies upon wafer cleaning, an optimized photoresist thickness of 1.0 μm,
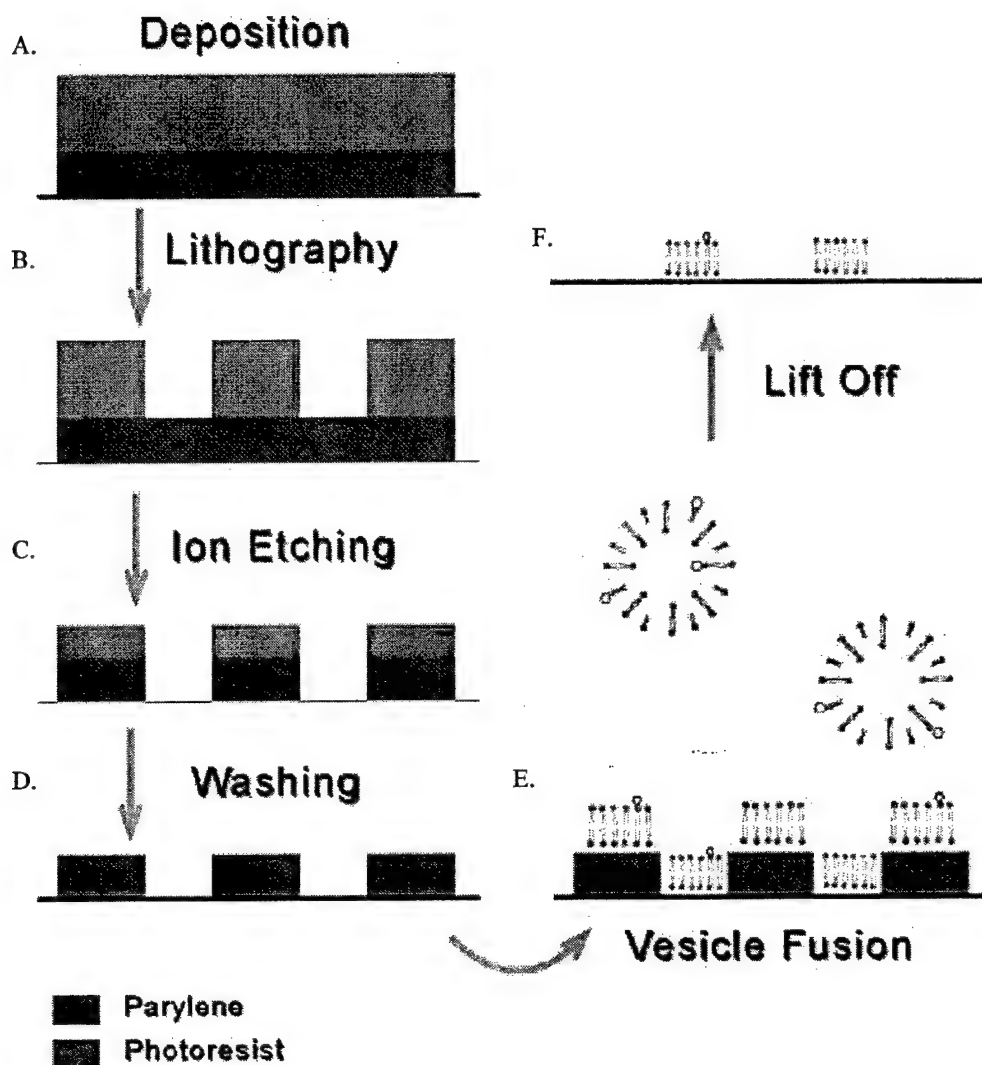
Figure 6.1. Process flow schematic of the fabrication steps, adapted from Ilic *et al*. [22]
(A) Deposition of photoresist on substrate. (B) Photoresist patterning using optical lithography. (C) Reactive ion etching of Parylene. (D) Removal of the top photoresist layer with acetone. (E) Lipid immobilization. (F) Peeling of polymer, resulting in a lipid bilayer.
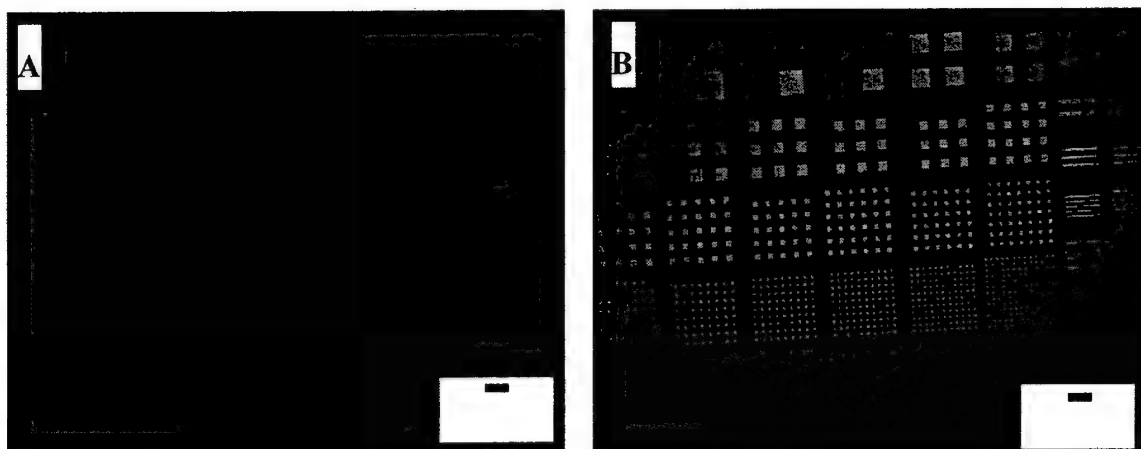
Figure 6.2. Patterning of hapten-conjugated supported lipid bilayer membrane with bound antibody.
(A) Fluorescent micrograph of 5% DNP-cap-DPPE in a membrane also composed of 94.5% DPPC and 0.5% DiI (red). (B) Fluorescent micrograph of the same sample as Fig. 6.2A with Alexa 488-conjugated anti-DNP IgE (green).

a Parylene thickness of 1.3 µm, photolithography precision and optimized RIE duration.

For our initial evaluation of localized cell activation, spatially restricting the receptor stimuli (DNP in our case) is sufficient and can be accomplished with immobile presentations such as adherent DNP-labeled proteins or clusters of SUV. In this regard, high magnification of pattern features made from DPPC/DiI-SUV suggested they contained clustered vesicles in some preparations. This may be related to the gel phase of the primary lipid at room temperature. Because later applications will test effects of hapten mobility and variable lipid composition, we also prepared lipid bilayers with POPC that is fluid at room temperature and more likely to form continuous bilayers. FRAP measurements of patterned bilayers made from POPC/DiI-SUV were used to evaluate this aspect. These studies examined $10 - 6000$ µm^2 in the confocal microscope field. After bleaching 10% of the area, we observe return to complete homogeneity of the entire bilayer patch within a min. We found that

consistent bilayer formation and lipid mobility, as observed by FRAP, requires rigorous cleaning with Nanostrip of the silicon surfaces exposed through the patterned Parylene prior to addition of the SUV suspension. Over exposure to the Nanostrip (greater than 1 min) can result in undercutting of the Parylene, thereby increased accessibility of the lipids and expansion of the feature size.

The pattern shown in Fig. 6.2A had been incubated with soluble IgE that is specific for DNP, and the Alexa-488 fluorescence conjugated to that antibody is shown by the micrograph with the green fluorescence filter (Fig. 6.2B). Clear coincidence of the red (DiI) and green (Alexa-488) patches demonstrates that IgE binds to DNP-cap-DPPE with a high degree of specificity. A small amount of nonspecific IgE binding to the plain silicon surface is observed; under our conditions the ratio of fluorescence on and off the patch is typically ~15. Interestingly, we found that anti-DNP IgE shows less nonspecific binding to patterned bilayers containing no DNP-cap-DPPE than to the silicon surface (data not shown). Some nonspecific binding of proteins to hydrophilic silicon surfaces is commonly observed, despite efforts to block it completely by pre-incubation with carrier proteins such as BSA. We found that pre-incubation with buffers containing as much as 10 mg/mL BSA blocks nonspecific IgE binding no better than our normal IgE incubation buffer that contains 1mg/mL BSA. For our experiments with cells described in this paper, IgE is pre-bound to its high affinity FcεRI receptor on the cell surface and the washed cells are added to the patterned surface. Thus, nonspecific binding of soluble IgE to lipid or silicon surfaces is not an issue in the cell experiments. However, nonspecific binding of cell surface components likely plays a role in the adherence of cells and the influence of this adherence on cell signaling remains to be determined.

Suspended RBL cells with Alexa-488 labeled anti-DNP IgE bound to cell surface receptors (FcεRI) were incubated at 37°C with the silicon wafer containing

patterned lipid bilayers. We obtained similar results with bilayers made with DPPC or POPC as the primary lipids in these experiments. Cells settled onto the wafer and became adherent within 30 min. In regions of the wafer with patches and periodic spacing larger than the cell diameter (~10μm for a rounded cell) the cells preferentially localized on the silicon surface between the bilayer features (Fig. 6.3). This preferred localization is likely due to the nonspecific protein binding to silicon that does not occur with the lipids as described above. Confocal microscopy shows striking differences between patterned lipids containing DNP-cap-DPPE and those that do not. With no haptenated lipid present the cells remain rounded and mostly detached from the patched features; these cells show homogenous IgE stain around the periphery (Fig. 6.3A). When the bilayers contain DNP-cap-DPPE, the cells near or on lipid patches flatten and spread out. When periodic spacing is larger than ~10 μm, the labeled IgE-receptors are distinctly polarized toward the edges of the features (Fig. 6.3B). When the periodic spacing is smaller than ~10 μm and cells settle over several patches in these areas, then the IgE-receptors concentrate and coincide with the haptenated patches (Fig. 6.3C). When the periodic spacing is similar to ~10μm, cells may settle between the patches or on top of one or more, and the IgE-receptors polarize toward the edge or cluster on top, respectively (Fig. 6.3D).

Clustering IgE receptors on mast cells initiates signal transduction that leads to degranulation and release of chemical mediators [31]. This process is accompanied by polymerization of cytoskeletal actin leading to spread of the rounded cell and ruffling caused extensions of lamellipodia [32]. This clear morphological change allowed us to establish that receptors clustered by the haptenated lipid patches stimulate a cellular response. As shown in Fig. 6.3, cells that contact the haptenated patches, either from

Figure 6.3. Interaction between RBL cells and patterned lipid bilayer.
(A-D) BioRad Confocal images of RBL cells sensitized with Alexa-488 anti-DNP IgE (green) on either (A) DPPC/DiI (red) with molar ratio 99.5:0.5 or (B-D) DPPC/DNP-cap-DPPC/DiI (red) with molar ratio 94.5:5:0.5. (A) 16X objective, 5, 30, 60 μm pattern. (B) 40X objective, 10 μm pattern, 20 μm period. (C) 40X objective, 1.5 μm pattern, 5 μm period (D) 40X objective, 6 μm pattern, 16 μm period.

the top or on the edge are enlarged and ruffled, corresponding to the activated state. The observed spreading and ruffling is similar to that occurring with adherent cells after addition of soluble antigen (DNP-BSA; data not shown) except that no receptor polarization occurs with soluble antigen. Clustering of Alexa 488-stained IgE and cellular ruffling occurs only when the patterned supported lipid bilayers contain DNP-cap-DPPE as illustrated by the comparison of panels A, C, and E to B, D, and F in Fig. 6.4. This series of images also compares cellular responses to a range of feature sizes: Fig. 6.4A-B are 6-8 µm, Fig. 6.4C-D are 2-3 µm, and Fig. 6.4E-F are ~1 µm.

A complementary and higher resolution view of morphological changes accompanying activation of cells by the haptenated lipid patches is provided by scanning electron microscopy (SEM). The lipid bilayers are poorly detected with this instrument, but the effects of haptenated lipids on cells are clear. Whereas adherent cells not associated with a pattern feature stay rounded or extend small protrusions isotropically (Fig. 6.5A), cells stimulated by contact with the haptenated lipid pattern (Fig. 6.5B-D) spread anisotropically. Most cells extend processes along the edge of the patterned, haptenated lipid. For example, Fig. 7.5B shows an image of a cell adherent on the silicon surface between four squares of haptenated lipids. Fig. 6.5C-D are images of stimulated RBL cells over patterned lines of lipids. As indicated in the fluorescence micrographs (Fig. 6.3-6.4), the cell bodies prefer to localize on the silicon surface but the cellular processes tend to align with the edges of the patterned lipids. Moreover, this IgE-receptor driven alignment is accompanied by cellular activation that causes lamellar spreading of the plasma membrane.

Figures 6.6-6.14 are SEM and epifluorescent images of mast cells on the micropatterned substrate. The cells are placed either on patterned vescicles or supported lipid bilayers, designated in the images with a "V" and "SLB", respectively.

	Green Channel	Red Channel	Combined Channels
A.			
B.			
C.			

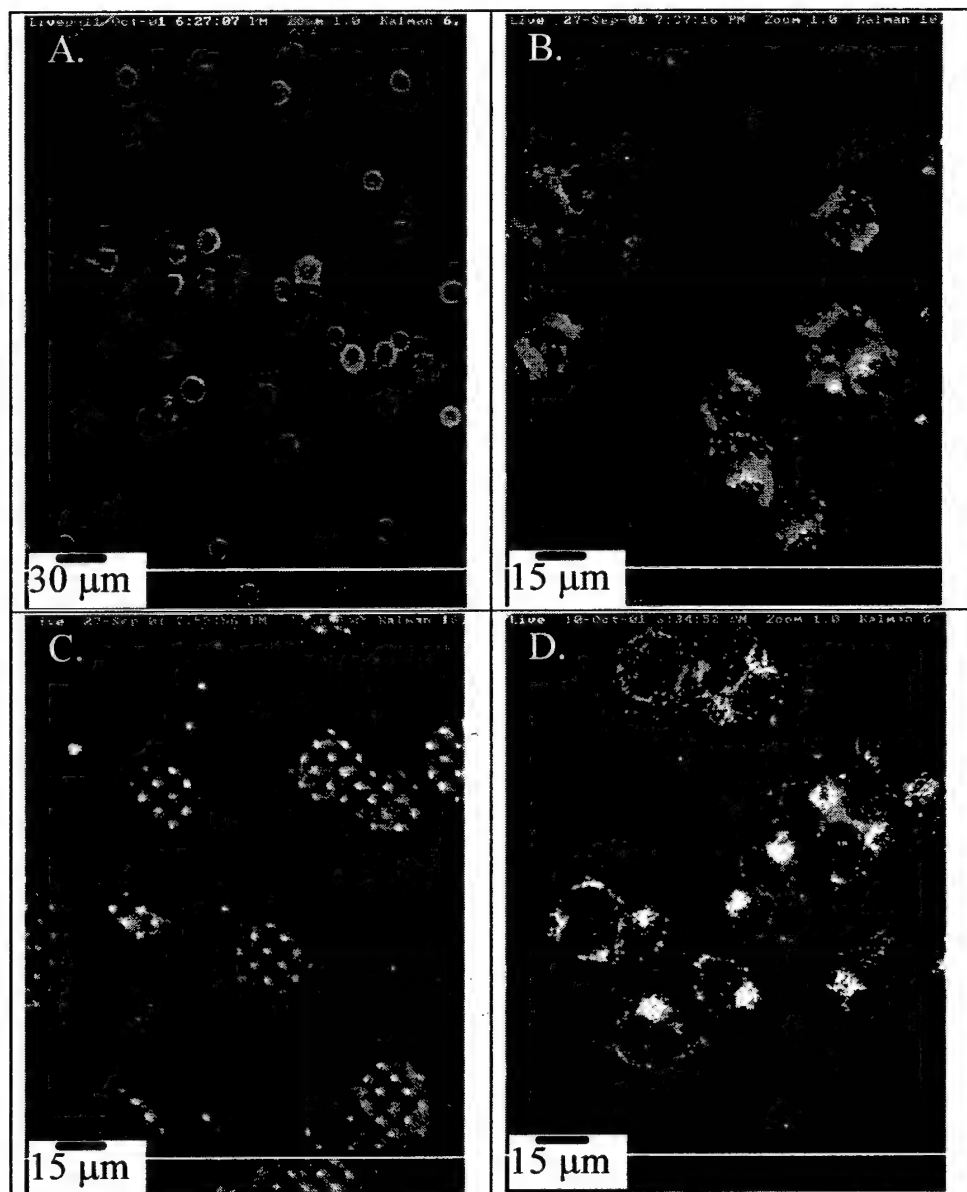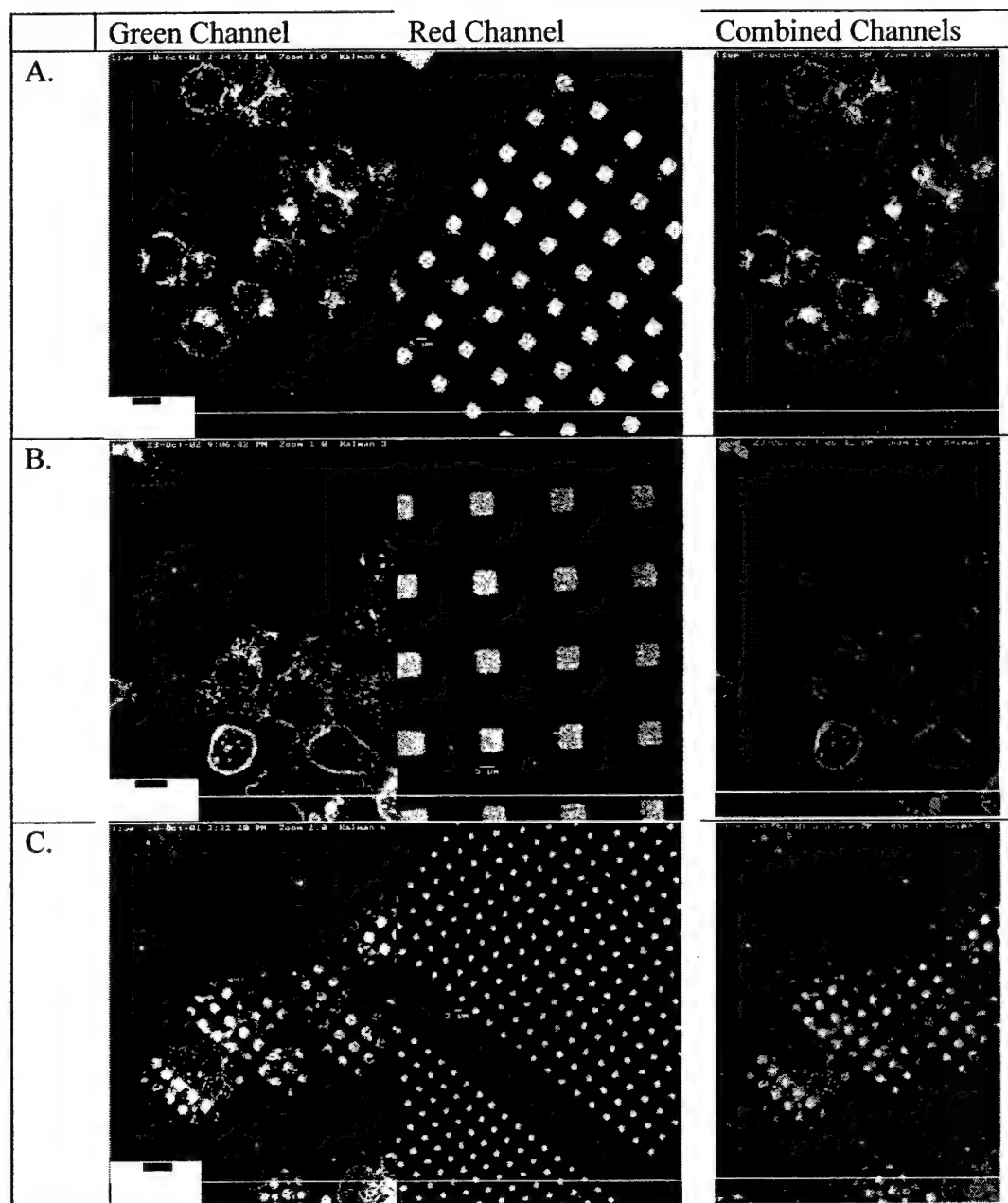|	Green Channel	Red Channel	Combined Channels
D.			
E.			
F.			
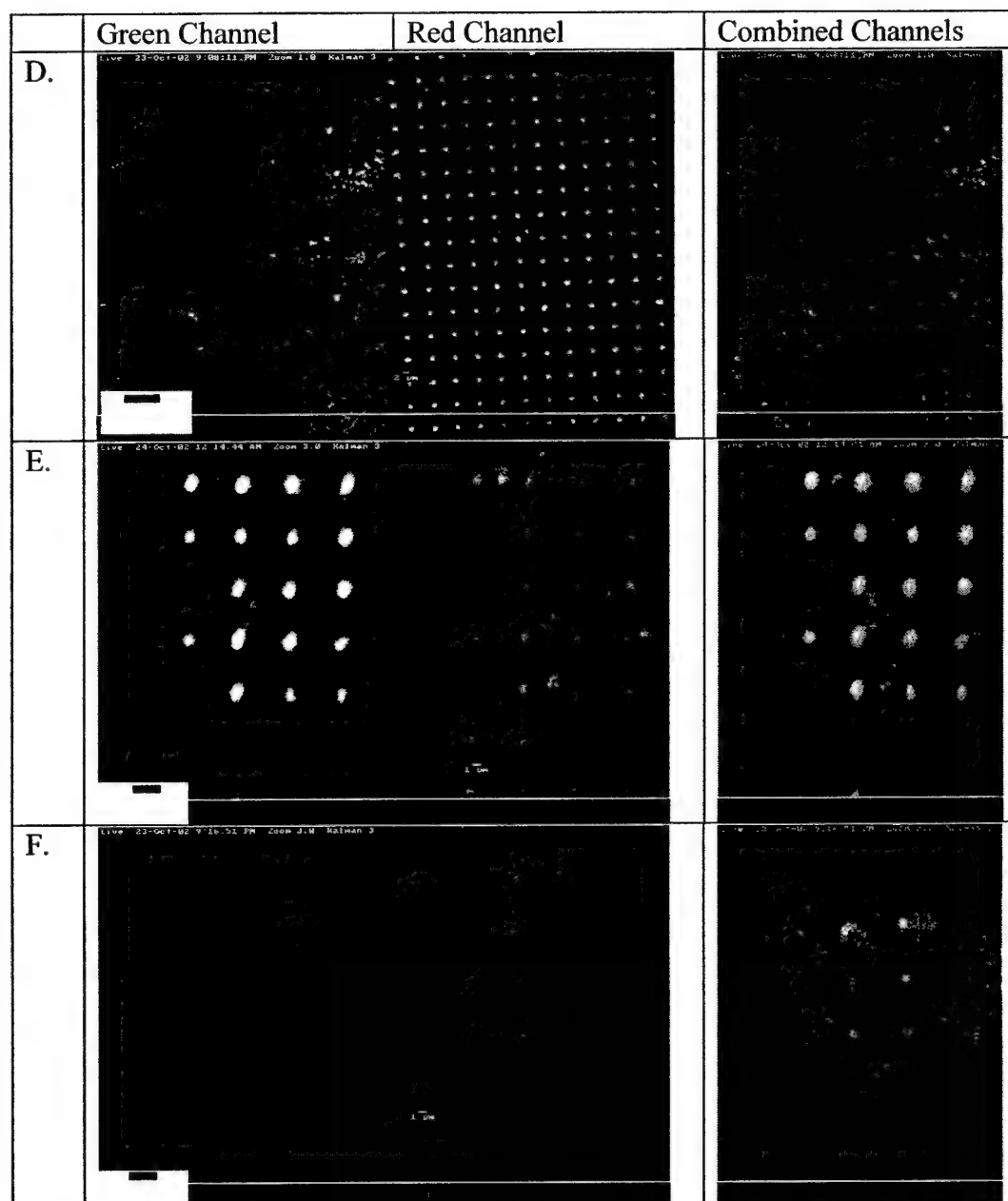
Figure 6. 4. Interaction between RBL cells and patterned lipid bilayer.
(A-F) BioRad Confocal images of RBL cells sensitized with Alexa-488 anti-DNP IgE (green) on DPPC/DiI (red). (A), (C), and (E) are haptenated supported lipid bilayers (DPPC/DNP-cap-DPPC/DiI) with molar ratio 94.5:5:0.5 and with 6 μm, 3 μm, and ~1 μm-patterned features, respectively. Fig. (B), (D), and (F) are control supported lipid bilayer samples (DPPC/DiI) with molar ratio 99.5:0.5 and with 8 μm, 2 μm, and ~1 μm-patterned features, respectively.
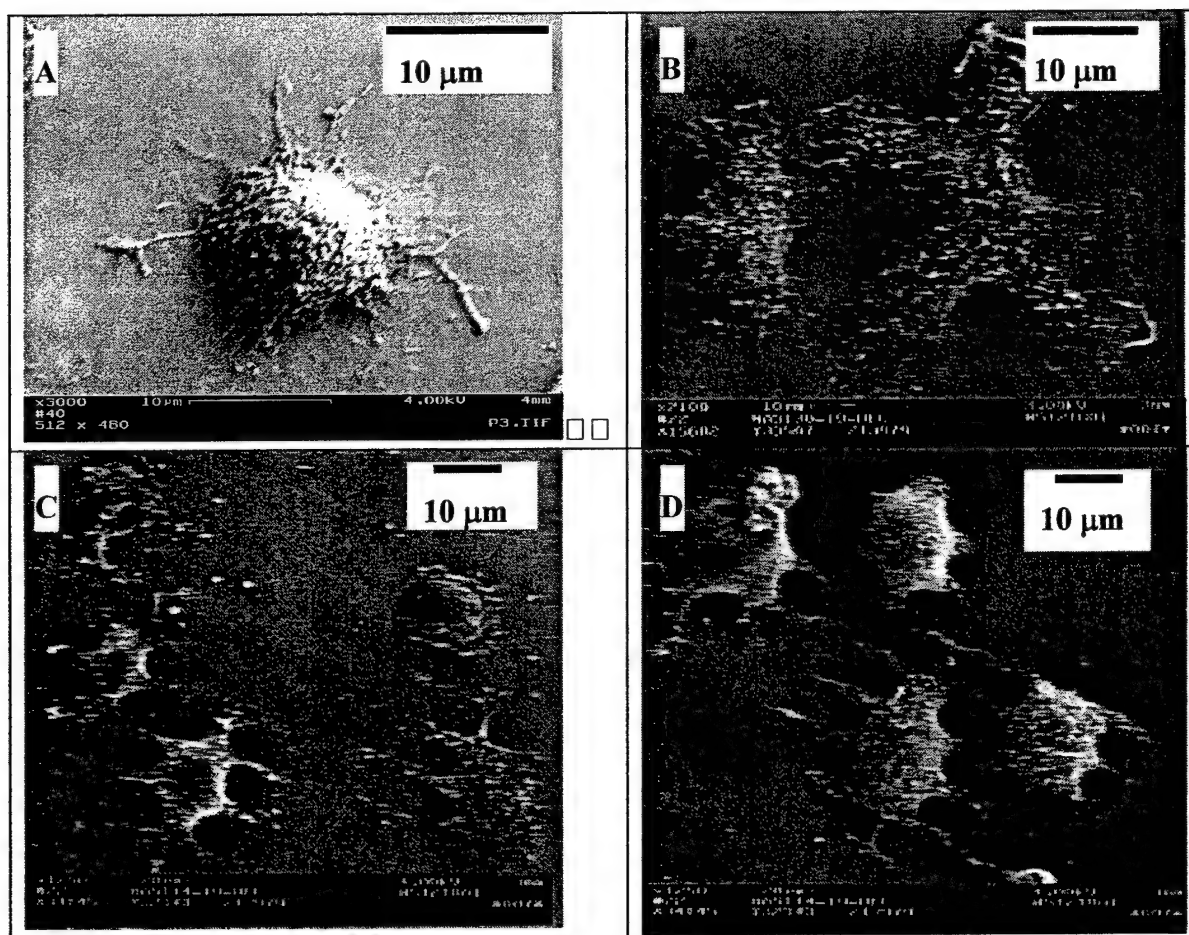
Figure 6.5. SEM images of RBL cells.
(A) Resting RBL on plain silicon surface with lamellipodia randomly spreading on the oxidized silicon substrate. Magnification: X3000. (B) Stimulated RBL at the corner of four patterned squares of lipids. Magnification: X2100. (C-D) Stimulated RBL over patterned lines of lipids. Magnification: X1250, X1250. Fig. C shows gray lines where the haptenated lipids were patterned.

Fig. 6.6 illustrates RBL cells patterned on micropatterned lines of haptenated lipids. Of particular interest are the distinct filopodia protruding from the cell in Fig. 6.6A and 6.6C. Filapodia and cellular extensions have been recently gain greater interest in the research community [36], [37], [38], [39], [40], [41]. The distinct number of filopodia from the cells, in my belief, result from a higher concentration of the DNP hapten from the vesicles than is found in the supported lipid bilayers. Aggregation of the FcεRI-Alexa 488-IgE can be observed over the patterned surfaces.

Figure 6.6. SEM and epifluorescence images of anti-DNP, Alexa 488-conjugated IgE sensitized RBL cells interacting with 10% DNP micropatterned lipid vesicles (SEM images) and supported lipid bilayers (epifluorescence images) on a silicon substrate. Each of these images illustrate cellular extensions. These different surfaces are annotated as vesicle "V" or supported lipid bilayer "SLB". The following images display unique morphology: (A,C) RBL cell with extensive filopodia extensions off the top of the cell and lamellapodia at the cell's base. The pattern are 2 and 3 μm, respectively. (B,D) Epifluorescence image of RBL cells with aggregated IgE-FceRI (green) on the micropatterned supported lipid bilayer lines (red). The lines are 4.5 and 3 μm, respectively.

Fig. 6.7 illustrates cells patterned on micropatterned squares of haptenated lipids. Again, filopodia and lamellapodia can be observed in these images. The filopodia shown in Fig. 6.7 B and 6.7D were shown by increasing the green intensity in these images so that these faint lines could be more easily distinguished. Fig. 6.8 through 6.10 show more images of RBL cells patterned on the vesicle features. The filopodia in these images appear to be oriented toward the patterned surfaces, either chemotactically or being stabilized by the topography. Fig 6.11 through 6.13 show more images of the cellular responses to the micropatterned, haptenated lipids. Fig. 6. 14 shows sensitized cells patterned on a surface lacking the DNP hapten. These images show a distinct reduction in the amount of cellular morphological changes.

Conclusion

This polymer lift-off procedure provides a direct and precise method for spatially restricting the presentation of membrane ligands that bind to soluble and cell surface receptors. In our experience, the main advantage over microcontact printing is reliable pattern uniformity and capacity for features as small as one micron or less. Beyond spatial localization, the patterned lipid bilayer system provides the means for critical evaluation of current hypotheses about cell interactions within an anisotropic environment. In these initial studies we showed that localized stimulation of mast cells causes targeted plasma membrane spreading and ruffling corresponding to cellular activation. Future studies will examine the targeting of signal transduction pathways leading to exocytosis that may or may not be spatially related to the original location of stimulus. By simulating a target cell membrane the patterned bilayers enable systematic investigation of lipid composition and hapten mobility in cell-cell interactions such as occurs in the immunological synapses of T cells. These studies lay the groundwork for future of cellular receptors and responses at interfaces.
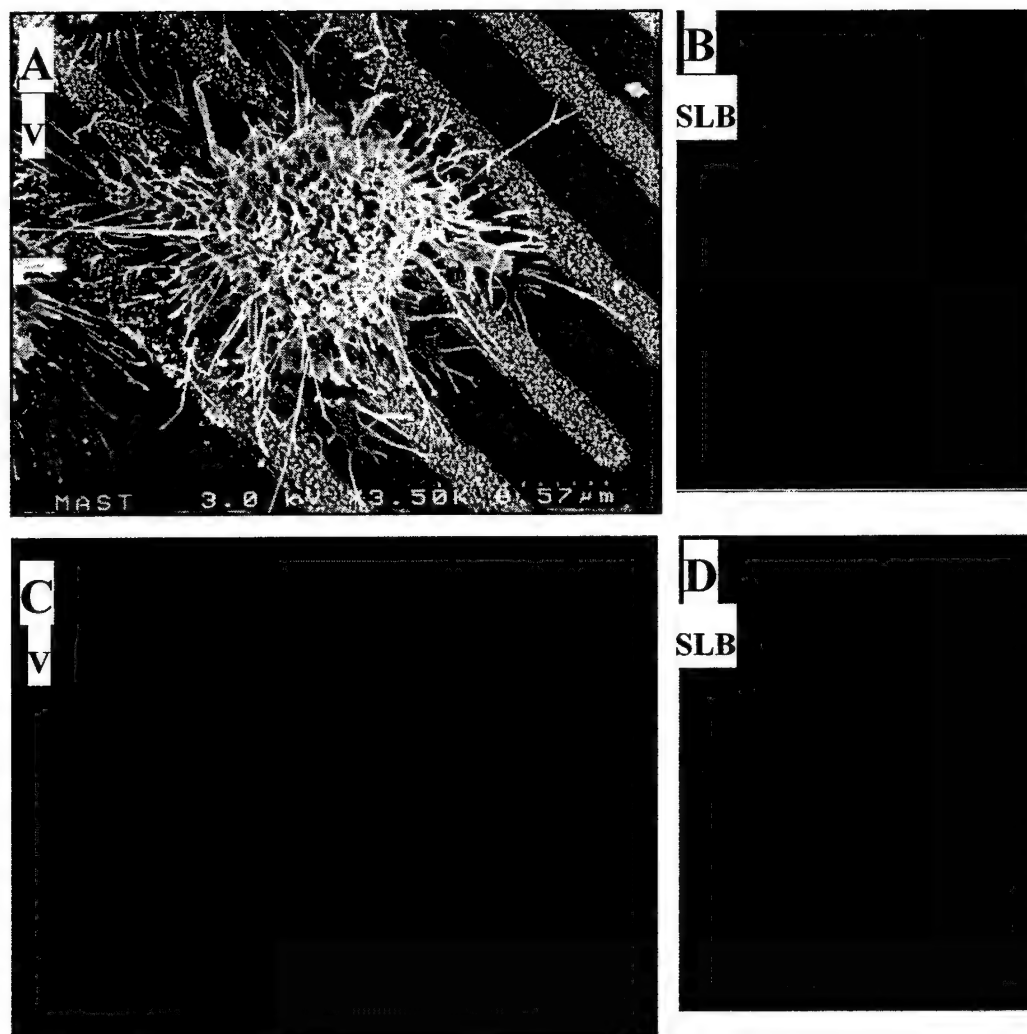
Figure 6.7. SEM and epifluorescent images of anti-DNP, Alexa 488-conjugated IgE (green) sensitized RBL cells interacting with 10% DNP micropatterned lipid vesicles (red) on a silicon substrate.

The following images display unique morphology: (A,C) RBL cell with extensive filopodia extensions off the top of the cell and lamellapodia at the cell's base. The pattern are 2.8 and 2.5 μm, respectively. (B,D) RBL cells with aggregated IgE-FceRI on the micropatterned vesicle lines. The pattern are 2.5 and 6.5 μm, respectively. The "V" represents patterned vesicles.
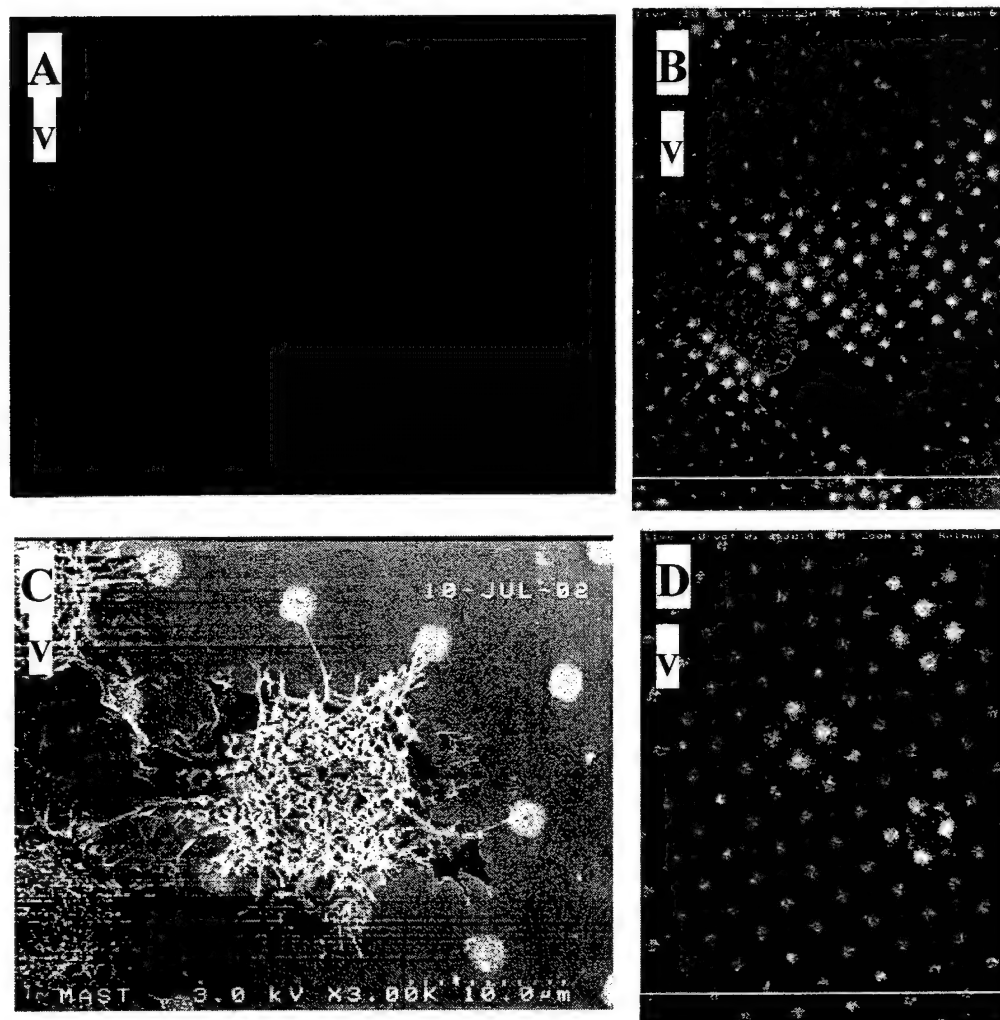
Figure 6.8. SEM and epifluorescent images of anti-DNP, Alexa 488-conjugated IgE sensitized RBL cells interacting with 10% DNP micropatterned lipid vesicles on a silicon substrate.

(A) RBL cell with extensive filopodia extensions. Note the thin filopodia with orientation toward or onto the patterns. The white arrows represent oriented fibers that are oriented toward but not touching the pattern. The red dashed arrow represents fibers touching the patterns. The patterns are 1.1 μm. (B) RBL cell with filopodia oriented to and in contact with the pattern. The white arrows represent oriented fibers that are oriented toward but not touching the pattern. The red dashed arrow represents fibers touching the patterns. The patterns are 2.2 μm.

Figure 6.9. SEM images of anti-DNP, Alexa 488-conjugated IgE sensitized RBL cells interacting with 10% DNP micropatterned supported lipid bilayers on a silicon substrate.

RBL cell with extensive filopodia extensions. Note the thin filopodia with orientation toward or onto the patterns. (A) The features are 1.15 μm. The features are 8.2 μm. The "V" represents patterned vesicles.
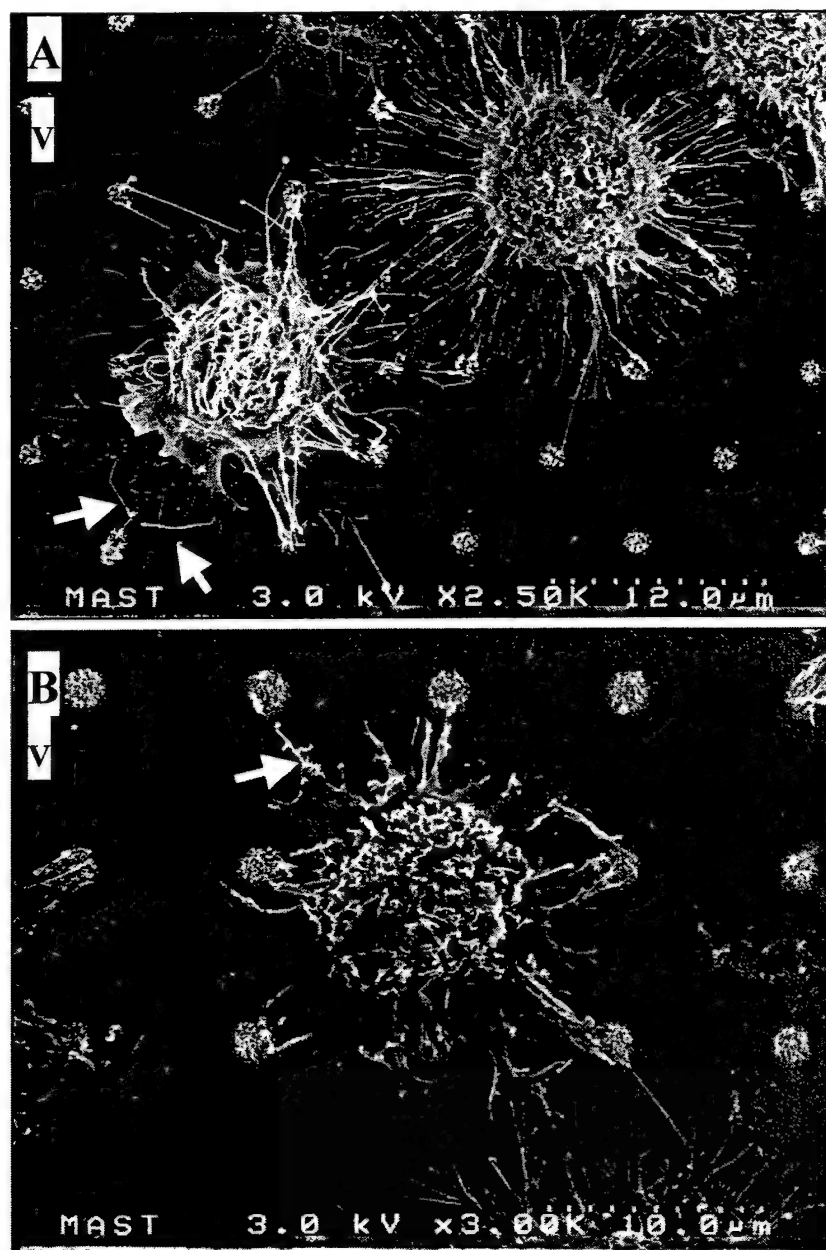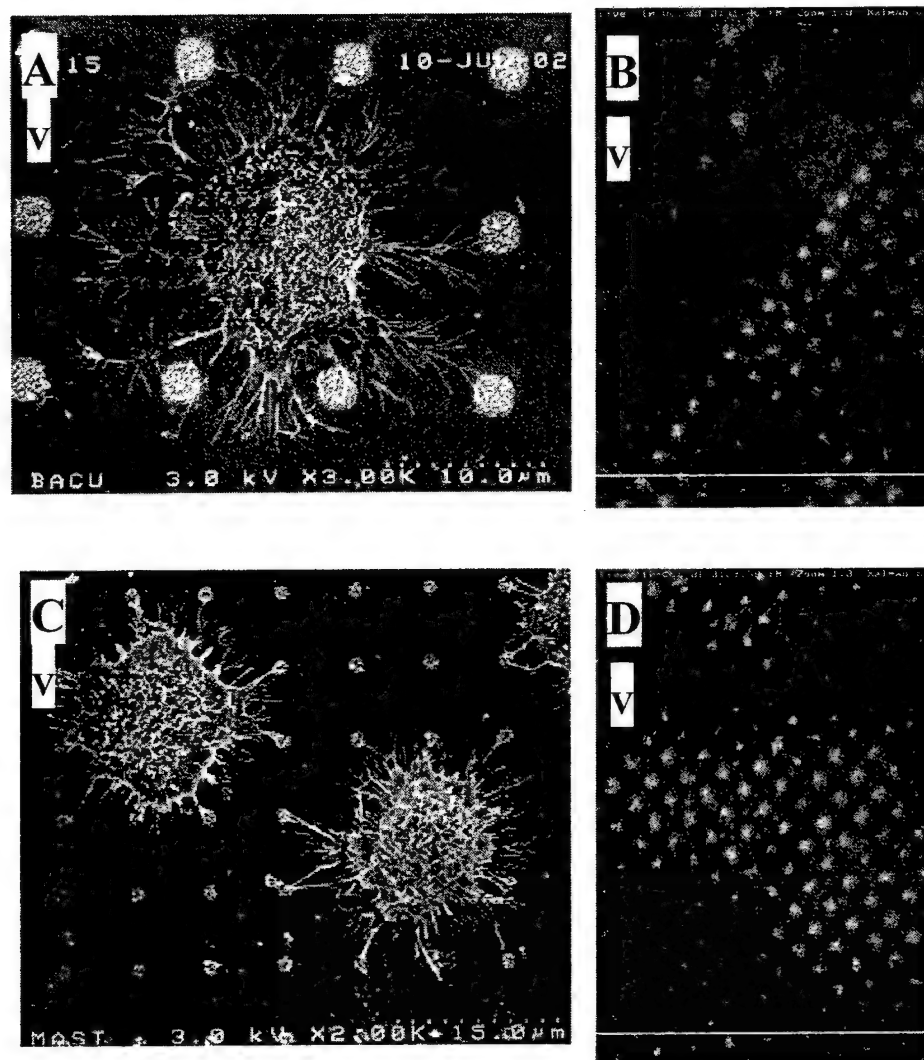
Figure 6.10. SEM and epifluorescent images of anti-DNP, Alexa 488-conjugated IgE (green) sensitized RBL cells interacting with 10% DNP micropatterned lipid vesicles (red) on a silicon substrate.

Each of these images illustrate cellular extensions. The following images display unique morphology: (A) The patterns are 2.5 μm. (B) The patterns are 5 μm (left) and 2.5 μm (right). (C) The patterns are 1.6 μm. (D) The patterns are 2.0 μm. The "V" represents patterned vesicles.
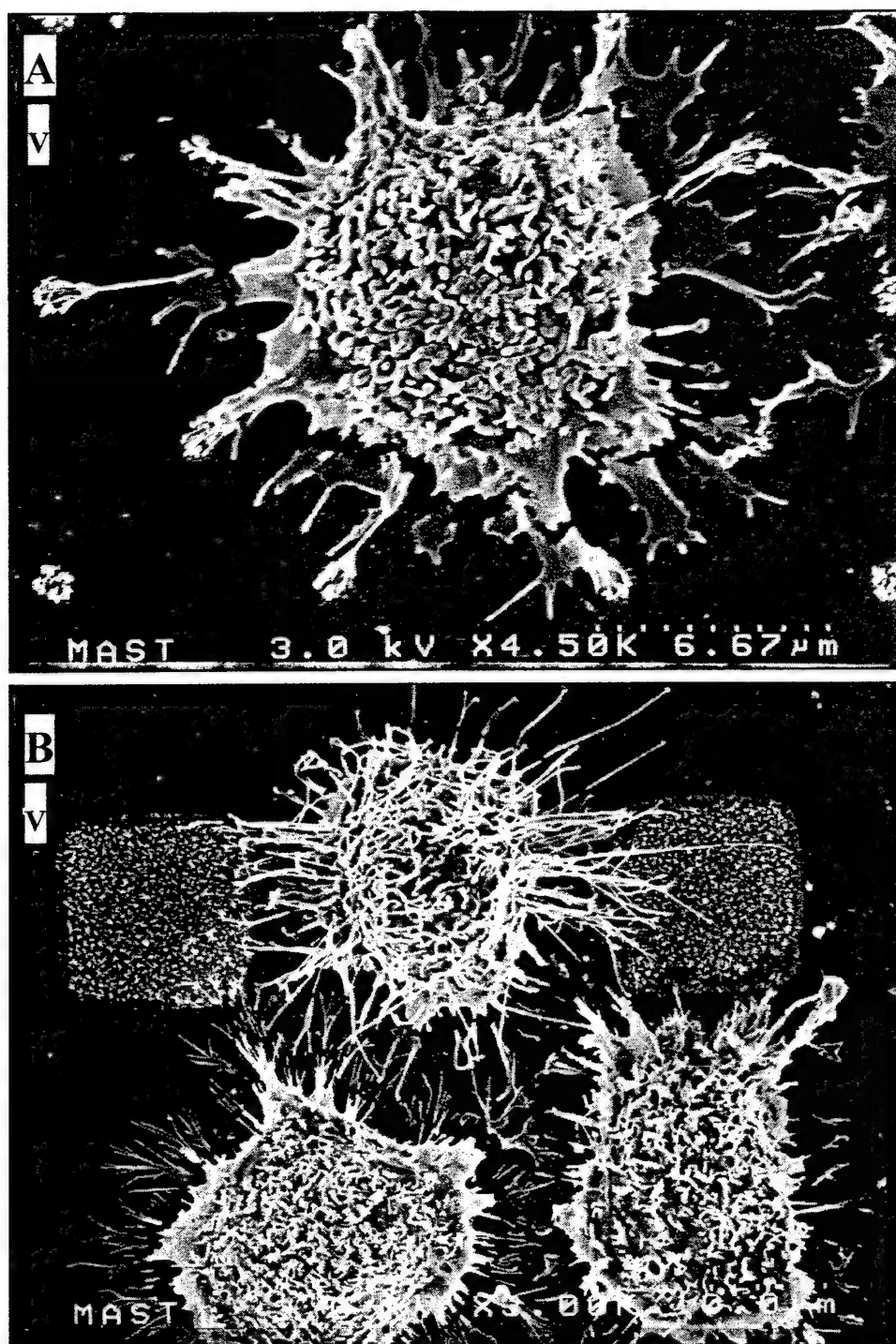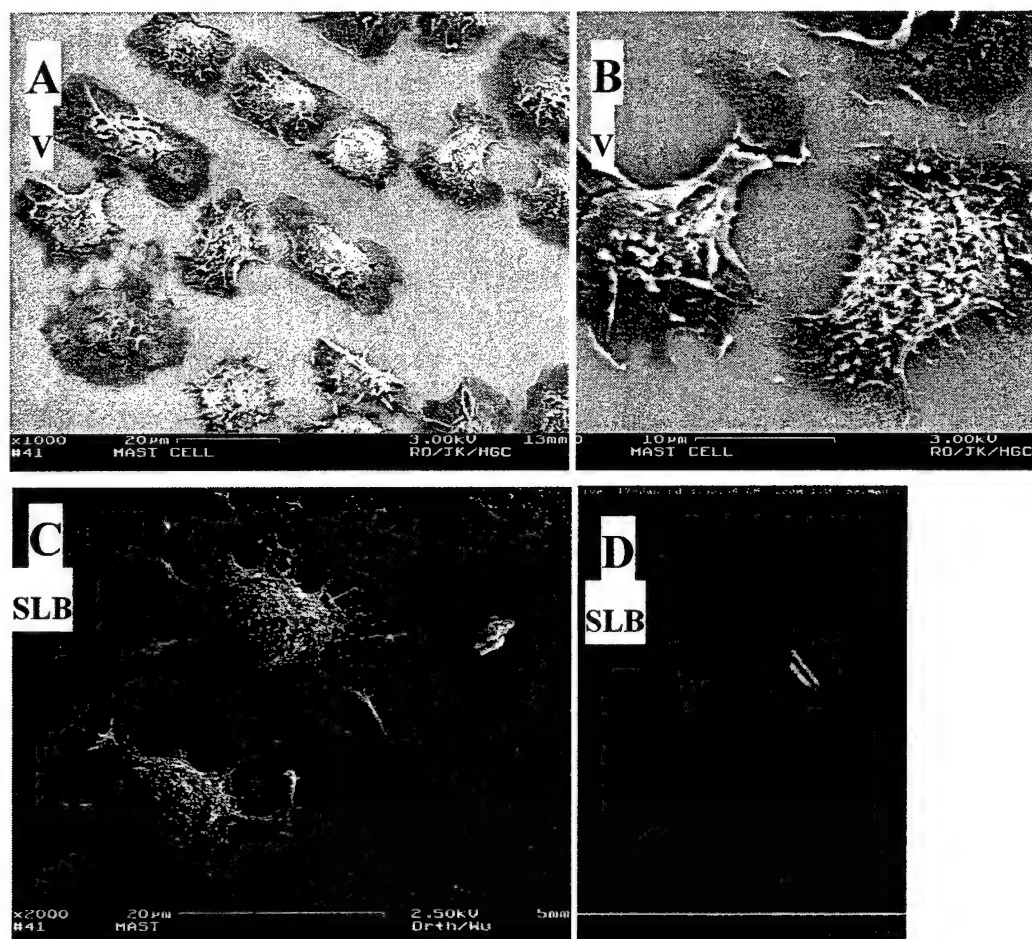
Figure 6.11. SEM and epifluorescence images of anti-DNP, Alexa 488-conjugated IgE (green) sensitized RBL cells interacting with 10% DNP micropatterned supported lipid bilayers (red) on a silicon substrate.

The following images display unique morphology: (A-B) Stimulated RBL cell on micropatterned vesicle lines. (C) Stimulated RBL cell on micropatterned supported lipid bilayer lines. (D) Epifluorescence image of RBL cells with aggregated IgE-FceRI on the micropatterned supported lipid bilayer lines. The "V" represents patterned vesicles. The "SLB" represents patterned supported lipid bilayer.
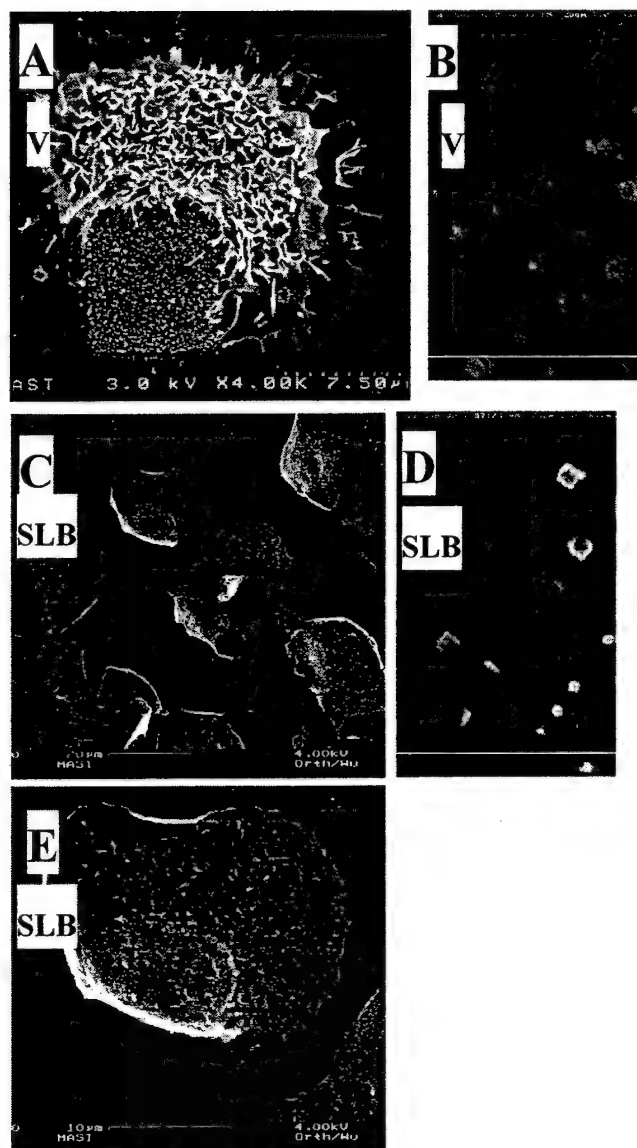
Figure 6.12. RBL cells over squares.
SEM and epifluorescence images of anti-DNP IgE sensitized RBL cells interacting with 10% DNP micropatterned lipid vesicles (A-B) and supported lipid bilayers (C-E) on a silicon substrate. Each of these images illustrate cellular extensions. The following images display unique morphology: (A) Stimulated RBL cell on 8.4 μm micropatterned vesicle square. (B) RBL cells with aggregated IgeRI (green) around 8 μm patterns. (C) RBL cells over supported lipids bilayer patches (sizes are not known). (D) RBL cells with aggregated IgeRI around 8 μm squares. (E) RBL cells over supported lipids bilayer patches. Size is estimated to be 12 μm. The "V" represents patterned vesicles. The "SLB" represents patterned supported lipid bilayer.
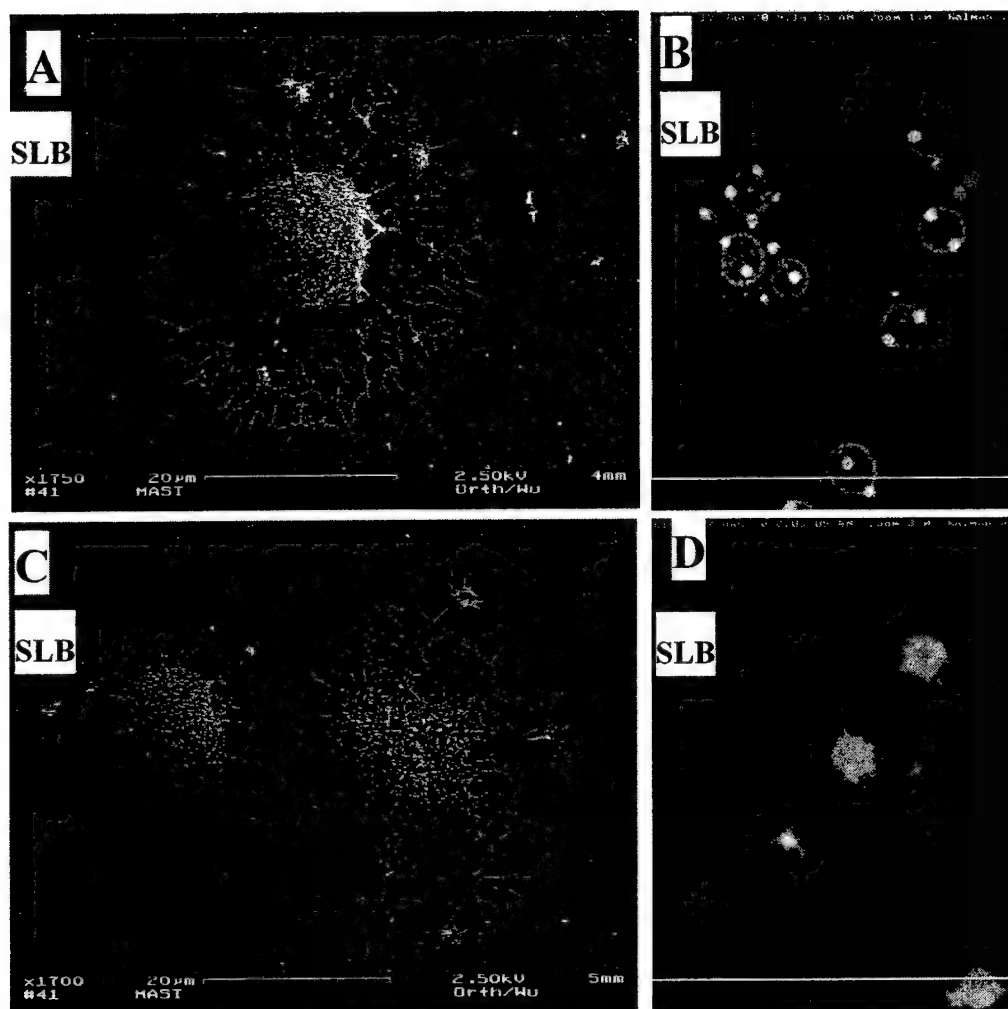
Figure 6.13. RBL cells on squares.
A-D. SEM and epifluorescence images of anti-DNP IgE sensitized RBL cells interacting with 10% DNP micropatterned supported lipid bilayers on a silicon substrate. Each of these images illustrate cellular extensions. The "SLB" represents patterned supported lipid bilayer.
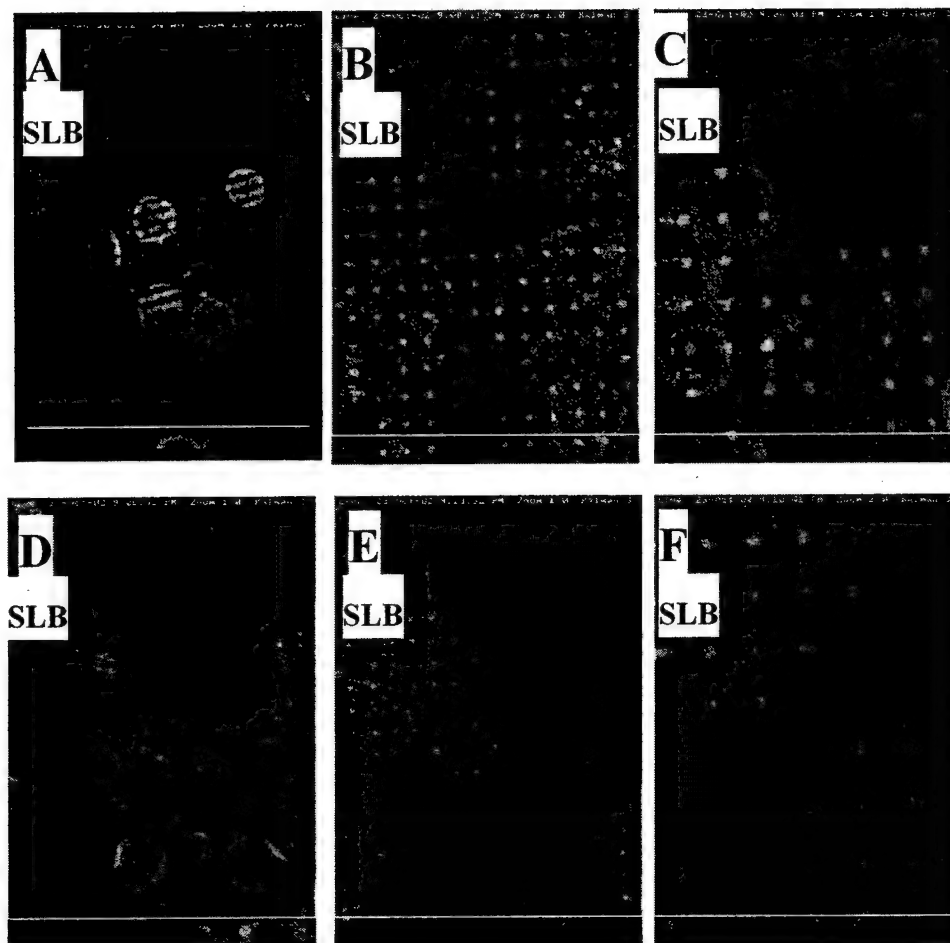
Figure 6.14. RBL cells on pattern with no DNP.
(A-F) SEM and epifluorescent images of anti-DNP IgE sensitized RBL cells interacting on a surface with no DNP in the micropatterned supported lipid bilayers on a silicon substrate. Each of these images illustrate cellular extensions. The cells appear unresponsive to the patterned lipids. The "SLB" represents patterned supported lipid bilayer.

References

[1] Bromley, S. K., W. R. Burack, K. G. Johnson, K. Somersalo, T. N. Sims, C. Sumen, M. M. Davis, A. S. Shaw, P. M. Allen, and M. L. Dustin. 2001. *Annu. Rev. Immunol.*, 19:375-396.

[2] Lanzavecchia, A., G. Lezzi, and A. Viola. 1999. *Cell*, 96:1-4.

[3] van der Merve, P. A. 2001. *Immunity*, 14:665-668.

[4] Weiss, A. and D. R. Littman. 1994. *Cell*, 76:263-274.

[5] Daeron, M. 1997. *Annu. Rev. Immunol.*, 15:203-234.

[6] Holowka, D. and B. Baird. 1996. *Annu. Rev. Biophys. Biomol. Struct.*, 25:79-112.

[7] Brown, D. A. and E. London. 1998. *Annu. Rev. Devel. Cell Biol.*, 14:111-136.

[8] Simons, K. and E. Ikonen. 1997. *Nature*, 387:569-572.

[9] Baird, B., E. D. Sheets, and D. Holowka. 1999. *Biophys. Chem.*, 82:109-119.

[10] D. Holowka and B. Baird. 2001. *Sem. in Immunol.*, 13:99-105.

[11] R. Xavier and B. Seed. 1999. *Curr. Opin. Immunol.*, 11:265-269.

[12] D. Holowka, E. D. Sheets, and B. Baird. 2000. *J. of Cell Science*, 113:1009-1019.

[13] McConnell, H. M.; Watts, T. H.; Weis, R. M.; Brian, A. A. 1986. *Biochim. Biophys. Acta.*, 864:95-106.

[14] E. Sackmann. 1996. *Science*, 271:43-48.

[15] S. G. Boxer. 2000. *Curr. Opin. Chem. Biol.*, 4:704-709.

[16] Johnson, S. J., T. M. Bayerl, D. C. McDermott, G. W. Adam, A. R. Rennie, R. K. Thomas, and E. Sackmann. 1991. *Biophys. J.*, 59:289-294.

[17] Barsumian, E. L., C. Isersky, M. K. G. Petrino, and P. R. Siraganian. 1981. *Eur. J. Immunol.*, 11:317-323.

[18] Bieri, C., O. P. Ernst, S. Heyse, K. P. Hofmann, and H. Vogel. 1999. *Nat. Biotechnol.*, 17:1105-1108.

[19] Brown, D. A. and E. London. 1998. *Annu. Rev. Devel. Cell Biol.*, 14:111-136.

[20] Chen, C. S., M. Mrksich, S. Huang, G. M. Whitesides, and D. E. Ingber. 1997.

Science, 276:1425-1428.

[21] Cornish, T., D. W. Branch, B. C. Wheeler, and J. T. Campamelli. 2002. *Mol. Cell Neurosci.*, 20:140-153.

[22] Groves, J. T. and S. G. Boxer. 2002. *Acc. Chem. Res.*, 35:149-157.

[23] Groves, J. T., N. Ulman, and S. G. Boxer. 1997. *Science*, 275:651-653.

[24] Ilic, B. and H. G. Craighead. 2000. B*iomedical Microdevices*, 2:317-322.

[25] James, C. D., R. C. Davis, L. Kam, H. G. Craighead, M. Isaacson, J. N. Turner, and W. Shain. 1998. *Langmuir*, 14:741-744.

[26] James, C. D., R. Davis, M. Meyer, A. Turner, S. Turner, G. Withers, L. Kam, G. Banker, H. G. Craighead, M. Isaacson, J. Turner, and W. Shain. 2000. *IEEE Trans Biomed Eng*, 47:17-21.

[27] Kam, L. and S. G. Boxer. 2001a. *J. of Biomedical Materials Research*, 55:487-495.

[28] Kam, L., W. Shain, J. N. Turner, and R. Bizios. 2001b. B*iomaterials*, 22:1049-1054.

[29] Kulcysiski, A. and H. Metzger. 1974. *J. Exp. Med.*, 140:1675-1695.

[30] Liu, F.-T., J. W. Bohn, E. L. Ferry, H. Yamamoto, C. A. Molinaro, L. A. Sherman, N. R. Klinman, and D. H. Katz. 1980. *J. Immunol.*, *124*:2728-2737.

[31] Metzger, H. 1992. *J. Immunol.*, *149*:1477-1487.

[32] Oliver, J. M., J. Seagrave, R. F. Stump, J. R. Pfeiffer, and G. G. Deanin. 1988. *Prog. Allergy*, <u>42</u>:185-245.

[33] Pierini, L., D. Holowka, and B. Baird. 1996. *J. Cell Biol.*, 134:1427-1439.

[34] Reviakine, I. and A. Brisson. 2000. *Langmuir*, 16:1806-1815.

[35] Simons, K. and E. Ikonen. 1997. *Nature*, 387:569-572.

[36] Mallavarapu, A. and T. Mitchison. 1999. *J. of Cell Biology*, 146:1097-1106.

[37] Vasioukhin, V. C. Bauer, M. Yin, and E. Fuchs. 2000. *Cell*, 100:209-219.

[38] Frame, M. C. V. J. Fincham, N. O. Carragher, and J. A. Wyke. 2002. *Nature Reviews Molecular Cell Biology*, 3:233-245.

[39] Mitchison, T. J. and L. P. Cramer. 1996. *Cell*, 84:371-379.

[40] Ramirez-Weber, F.-A. and T. B. Kornberg. 1999. *Cell*, 97:599-607.

[41] Chiou, W.-F., A. Y.-C. Shum, C.-H. Peng, C.-F. Chen, and C.-J. Chou. 2003. *European J. of Pharmacology,* 458:217-225.

NANOMETER-SCALE ANTIBODY PATTERNING FOR DIRECTED EOSINOPHIL IMMOBILIZATION AND STIMULATION[1]

Immunoglobulin G antibodies (IgG) are patterned for the precise immobilization and stimulation of eosinophil cells. We demonstrate that the antigen bovine serum albumin (BSA) can be patterned on silicon using a photolithographically patterned polymer lift-off technique [Ilic]. The micro- and nanoscale patterns are realized as the polymer is mechanically peeled away in one contiguous piece in aqueous solution. Anti-BSA IgG are bound specifically to BSA to create a pattern of oriented AB that provides a surface for eosinophil immobilization and degranulation. The width of the patterns ranged from submicron to 76 μm, appropriate dimensions for the 10-14 μm diameter eosinophil cells. This method provides a new technique for immobilizing cells onto nano- and micrometer scale patterns for analyzing cellular biochemical cascade events such as degranulation and studying cellular morphological changes in response to defined nanoscale antigenic stimulus.

Introduction

Eosinophilic granulocytes (eosinophils) play an important role in the host immune defense against parasite invasion [1]. These exocytotic cells synthesize cytotoxic proteins and store these proteins in secretory granules, where they are ready to be released onto the surface of a parasite [2]. Eosinophils contribute to the

---

pathophysiology of bronchial asthma [3] with activation of allergen-specific IgG1 and IgG3 induced through the F_c portion of the immunoglobulin molecules ($Fc_\gamma RII$) [4]. Eosinophil cell F_c and complement receptor numbers vary dramatically between healthy patients and patients with eosinophilia [5]. Eosinophils are stimulated and degranulate in response to zymosan (yeast cell walls) [6], IgG- coated Sephadex beads [7], IgA coated beads [8], and lipid mediators leukotriene B_4 (LTB_4) and platelet activating factor (PAF) [9]. Whole cell patch-clamp technique has been used to study the discrete electrical impedance changes during compound exocytosis and cumulative fusion [10]. Cellular adhesion through the B_2 integrin is an important step in eosinophil activation and accumulation as demonstrated by eosinophil binding to IgG coated sepharose beads and by binding inhibition with membrane antibodies against CD18 and CD11b--the B_2 integrin ligands [11].

Micron-scale patterning of biomolecules is an active area of research as the microelectronics technology merges with biology [12]. Patterning biomaterials on the micro- and nanometer scales allow a more focused method for cell stimulation than bath application of the biomaterial. Several different methods have been used to micropatterned biomaterials and chemicals on solid substrates for cell interrogation. Photopatterning has been used to spatially distribute biomolecules, such as enzymes, antibodies, and nucleic acids, for the development of biochips on silicon, glass, and plastic substrates [12]. A printing technique called microcontact printing (μCP) process uses a poly(dimethyl siloxane) (PDMS) elastomeric stamp to pattern a wide array of and biomaterials [14], [15], [16]. Microfabrication techniques were used to micropattern bovine serum albumin and horseradish peroxidase [17]. μCP has been used to pattern cell adhesion proteins to immobilize and direct neuronal and astroglial cell growth on glass substrates [18]. Deep plasma etching and photoplastics were used

to create PDMS stamps to pattern different cell suspensions to specific locations of a tissue culture substrate [19].

Many different cell types have been exposed to patterned biomaterials on solid substrates. *E.coli* O157:H7 cells were captured from a solution using PDMS stamped anti- *E.coli* O157:H7 for a diffraction grating biosensor [20]. Neuronal and glia cells were patterned using light-assisted functionalized photoresists [22]. A silicon micromachined flow-through chamber has been designed for the 'entrapment' of chick embryo spinal cord neurons as a model system for biological neural networks [23]. Differentiated B104 neuroblastoma cells were micropatterned on four substrates to determine the preferred support substrate [24].

This paper presents a method for patterning a surface with antibodies that serve as a stimulus for eosinophil immobilization, activation and degranulation. A patterned BSA:anti-BSA IgG complex serves as a model stimulus for eosinophils. Vapor deposited Parylene, di-para-xylylene, is conformally deposited over the silicon substrate and used as a pinhole-free barrier between the solution and the substrate. Conventional photolithography and reactive ion etching (RIE) are used to pattern the polymer [25]. After the BSA incubation, the samples are incubated with Alexa-594-conjugated anti-BSA IgG solution. The immunospecificity of the antigen allows Alexa-594-conjugated anti-BSA IgG molecules to bind specifically to the patterned substrate. The samples are subsequently immersed in buffer solution and the Parylene layer is mechanically removed. Micro- and nanometer square patterns are formed using a polymer lift-off method [26] (Fig. 7.1). Eosinophils are pipetted onto the patterned surface (Fig. 7.2). Time series epifluorescence microscopy occurs immediately after cell addition to detect real time cell immobilization, morphological changes, and degranulation.

1a. Photolithography

1b. Reactive Ion Etching

1c. APTS Addition

1d. BSA and IgG Incubation

1e. Parylene Removal

1f. Eosinophil Immobilization

Legend:
- Photoresist
- Parylene
- Silicon Substrate
- 3-APTS
- BSA
- Anti-BSA IgG-Alexa 594
- Eosinophil
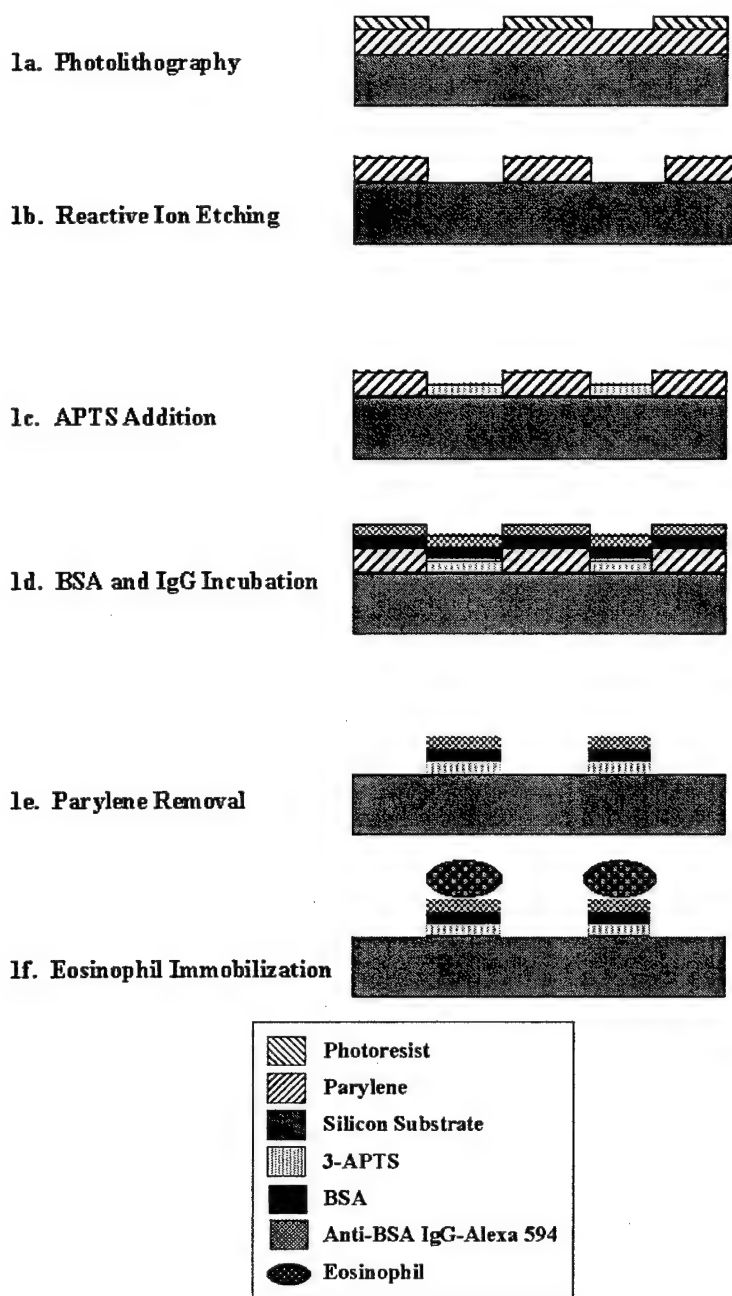
Figure 7.1. Process flow schematic of the fabrication steps.
(A) Patterning of 1.5 μm of OCG OiR 897-12i photoresist (OCG Chemical Company, West Patterson, NJ) using optical lithography. (B) Reactive ion etching of 1.0 μm layer of Parylene C dimer and subsequent removal of the top photoresist layer. (C) Application of 3-aminopropyltriethoxysilane layer to a plasma cleaned silicon substrate. (D) Application of 100 μg/mL BSA and 50 μg/mL anti-BSA IgG. (E) Mechanical Parylene removal with tweezers, resulting in a surface with patterned Alexa 594-BSA-anti-BSA complex. (F) Immobilization of eosinophils to the patterns Fc(IgG) surface.
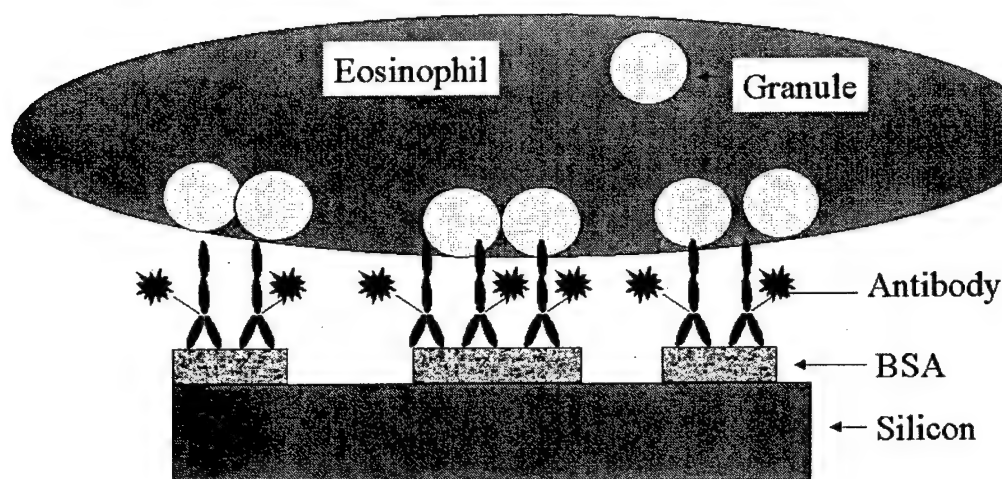
Figure 7.2. Schematic detailing the eosinophil cell binding to F_c tail of Alexa 594 conjugated anti-BSA IgG on silicon substrate.

Experimental Section

Silicon Wafer Preparation. Parylene is deposited on silicon substrates and photolithographically patterned as detailed in Chapter 3 using OCG OiR 897-12i photoresist (OCG Chemical Company, West Patterson, NJ) with a 1.3 µm Parylene thickness. 3-aminopropaltriethoxysilane (3-APTS, Sigma-Aldrich, Milwaukee, WI) solution is prepared in a 50-ml amber bottle using 0.5-ml of 3-APTS and 24.0 mL of acetone in a nitrogen purged glovebox to create a 2% silane solution. The silanization step began by cleaning 1 cm^2 silicon chips in a Harrick Plasma Cleaner/Sterilizer PDC 3-G for 1 min. The chips are removed and placed in 100°C Milli-Q filtered water for 30 min. The silicon chips are nitrogen dried then quickly inserted into the bottled silane solution and incubated in a closed container for 30 min. The chips are removed, washed in acetone for 5 min, immersed in isopropyl alcohol and deionized water, and baked on a hotplate at 70°C.

BSA and Anti-BSA IgG Preparation. Bovine Serum Albumin (BSA) (Sigma-Aldrich, Milwaukee, WI) is reconstituted to 10 mg/mL and used to create 100, 10, and 1 µg/mL dilutions. A 30 µl drop of 2 mM BSA solution is placed on the Parylene-

patterned substrate for 60 min, as illustrated in Fig. 7.1D. Polyclonal, mouse anti-BSA IgG molecules (Sigma-Aldrich, Milwaukee, WI) and stained with NHS-Alexa 594 dye (Molecular Probes, Eugene, OR). The IgG stock solution is diluted to 100 μg/mL, 7.4 pH in phosphate buffered saline (PBS). Samples are incubated in 35-mm plastic Petri dishes (Fisher Chemicals, Pittsburgh, PA). Alexa 594-conjugated anti-BSA IgG is applied onto the pattern and incubated for 30 min. After the incubation, the sample remains immersed in aqueous solution while being transferred to a second Milli-Q water beaker in a 35-mm Petri dish. The Parylene is removed mechanically by peeling it off the substrate with tweezers in solution. The polymer film is shed easily in one contiguous piece from the substrate. The resulting sample contains patterned antigen-Ab complexes as illustrated in Fig. 7.1D.

Eosinophil Cell Preparation and Immobilization. Fresh blood is drawn from the jugular veins of horses, eosinophils are isolated, and are purified over discontinuous Percoll gradients as previously described [26]. Purified eosinophils are suspended in Medium 199 (Sigma-Aldrich, Milwaukee, WI) containing 4 mM glutamine, 4.2 mM NaHCO3 and penicillin/streptomycin (Sigma-Aldrich, Milwaukee, WI) (pH 7.2-7.3)] stored at room temperature and used within 24 h. The cell suspension is incubated for 45 min in LysoTracker Green (Molecular Probes, Eugene, OR). The samples are placed in the bottom indentation of 35mm Petri dish (Mat Tek, Ashland, MA) containing 2 mL of PBS buffer. 50 μl of 1.9×10^6 cells/mL solution is pipetted directly onto the patterned silicon chips. Time series epifluorescence imaging begins immediately after cell application using an Olympus AX 70 upright microscope with a 60X water immersion objective and Omega Optical filter sets (Brattleboro, VT). Alexa 594 dye is observed with a 510-590-nm excitation/590-nm emission filter set and LysoTracker Green is observed with a 450-490-nm excitation/520-nm emission filter set. Images are captured using a Spot CCD camera (Diagnostic Instruments, Inc.,

Sterling Heights, MI). Cells are fixed with 3.7% paraformaldehyde (Sigma, Milwaukee, WI) for long-term storage.

Results

In this report, we describe the micro- and nanometer scale arrays of patterned Ab for cell stimulation, test the patterned surface antigenicity with functional antibodies, develop a method for immobilizing eosinophil cells to the pattern, analyze the cells' preferential binding to the patterned surface, and detect eosinophil degranulation events after cell incubation on the pattern.

Fig. 7.3A illustrates Alexa 594-conjugated anti-BSA IgG squares with 700-nm widths on the lower right to 76-μm squares on the upper left) on a silicon substrate using the Parylene lift-off technique. This matrix of patterns demonstrates the wide range of sizes attainable with this patterning technique. 500 nm resolution is approximately the lowest photopatterning threshold attainable using the 10X stepper. A statistical analysis showed that the average relative aerial density of fluorescently-labeled antigen to the background is at least 150 times greater in the exposed regions than in the lift-off regions [28].

Fig. 7.3B illustrates the immobilization of horse eosinophils to the BSA-anti-BSA IgG complexes. Horse eosinophils were used since they have large granules that are easy to visualize during microscopy. This binding is similar to the experiments using immunoglobulin coated Sepharose beads detailed in the introduction. This method provides information that Sepharose beads do not offer. First, this method can be used to determine the spatial distribution and size of patterned F_c stimuli required for eosinophil activation and degranulation. Second, this technique allows eosinophil migration to be analyzed over the planar patterned surface.

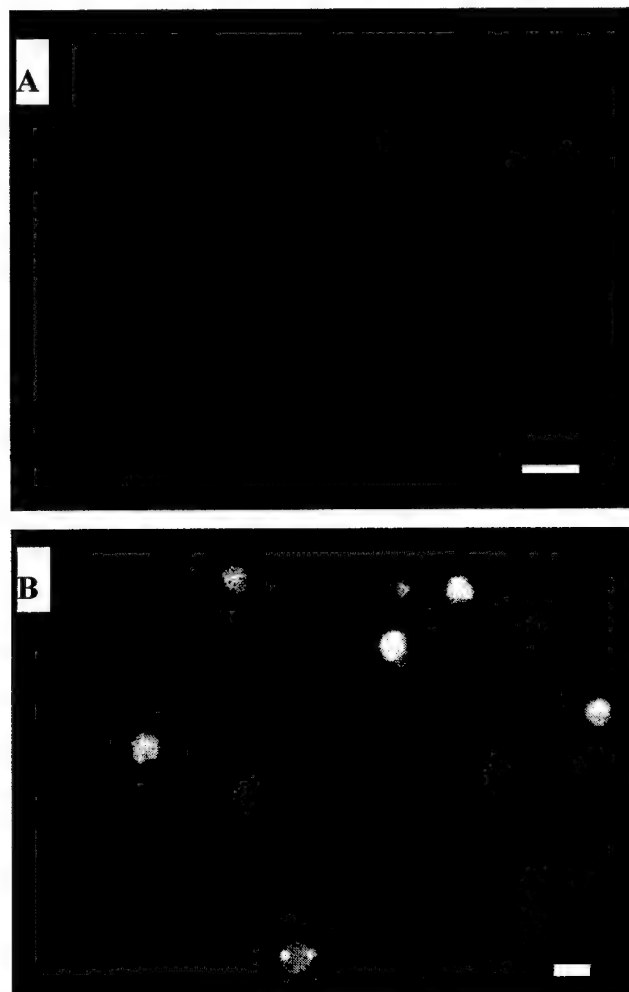Figure 7.3. Epifluorescent images of patterned Alexa-594 conjugated anti-BSA antibodies on silicon.

(A) Epifluorescent image of patterned Alexa-594 conjugated anti-BSA antibodies specifically bound to patterned BSA on silicon substrate. Scale bar is 70 μm and the largest square is 67 μm. (B) Eosinophil cells (green) immobilized to the patterned antibody matrix. Scale bar is 19 μm and the period between dots is 9.6 μm.

Fig. 7.4A shows the initial state and Fig. 7.4B shows the same region after 5 min. These images demonstrate clear morphological changes are occurring on the substrate. Consequently, the circled regions in this image show possible fusion and/or degranulation events may be occurring. Further experimentation with patch clamp amperotometry will be required to confirm that these changes are taking place.

Discussion

This technique may be useful to determine if fusion events and degranulation events may be occurring on the patterned substrate using fluorescence imaging. The signal observed in unpatterned regions is comparable to the signal observed on a blank, new silicon wafer surface. Thus, the unpattterned regions show negligible binding. Uniformity of the final patterned biomaterial relies upon an optimized photoresist thickness of 1.5 μm and Parylene thickness 1.0 μm, photolithography precision, optimized RIE duration to prevent under- and overetching, and sufficient biomaterial incubation time. Application of 1 μm of Parylene and 1.5 μm of photoresist provided optimal conditions for polymer removal and resolution.

Anti-BSA Ab are used to confirm the specificity of the binding onto the patterned BSA and provide a surface rich in F_c fragments onto which eosinophils can bind and be stimulated. The patterned antigen did not spread from the confined pattern regions and were still isolated after a month of storage in aqueous solution.

The Parylene lift-off technique offers a rapid and precise way to create supported micro- and nanometer-scale patterns. These patterns can be used to capture other biomaterials from solution and integrated into biosensors, bioMEMS, and biological assay systems.

There are several advantages of this technique. The Parylene film removal can be performed at any step during the processing. Therefore, multiple reagents can be
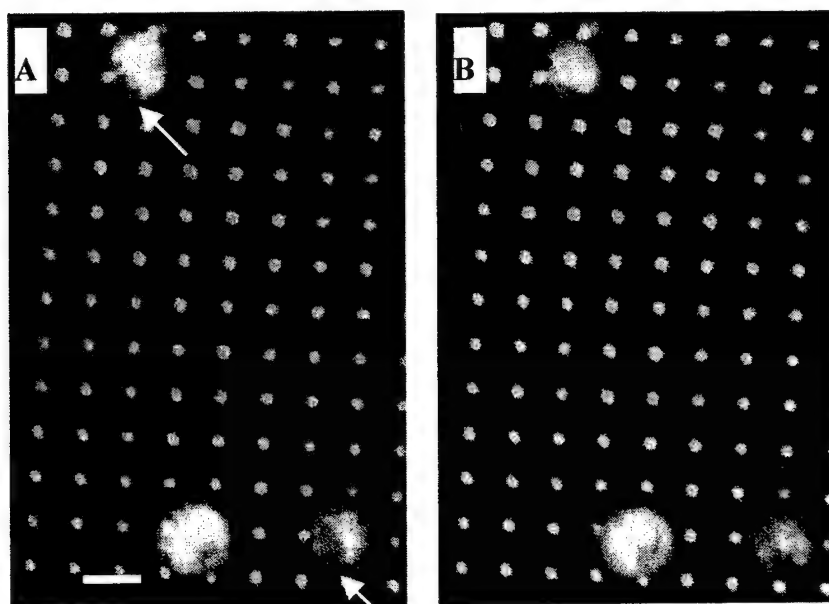
Figure 7.4. Epifluorescence images of eosinophils interacting with the patterned substrate.
(A) Eosinophil interaction with the substrate 1 min after application. (B) Eosinophil interaction with the substrate 6 min after application. Morphological changes can be observed in the cells with white circles. The cell with the top arrow appears to lose a green granule at its base. The cell with the lower arrow appears it may have degranulated from its center onto the pattern. Patch clamp amperotometry will be required to confirm that these changes are taking place. The scalebar is 15 μm.

added to the initial patterned surface prior to Parylene removal. This would allow subsequent reagents to be added at high concentrations and maximal binding without concern for nonspecific binding on unpatterned surface areas. Parylene is a biologically compatible polymer, provides a conformal coating with low permeability, and can be removed with a one-step mechanical lift-off. This technique permits the sample to remain submerged in solution so that the functional molecules are not denatured when dried. Parylene does not have a permanent bond with the substrate, thus allowing easy removal in one piece. The conformal film of Parylene is pinhole-free, so no unwanted patterning occurs in unexposed regions.

Conclusion

We have demonstrated a method for precise patterning antigen at the micro- and nanometer scale for cell stimulation. The antigenicity is confirmed by binding fluorescent antibodies onto the patterned surface. Eosinophil cells are effectively immobilized on the patterned surface. The eosinophils demonstrated preferential binding to the patterned surface. Time course imaging provides a means to study spatial-temporal changes associated with stimulation and degranulation. This technique offers a new versatile tool to pattern antigen and other biomaterial onto solid substrates with feature sizes as low as 1 μm.

References

[1]   Klein, J. and V. Horejší, *Immunology.* Oxford: Blackwell Science Ltd., 1998, p. 52.

[2]   Scepek, S., R. Moqbel, and M. Lindau. Compound exocytosis and cumulative degranulation by eosinophils and their role in parasite killing. 1994. *Parasitology Today*, 10:276.

[3]   Butterfield, J. H., K. L. Leiferman, and G. J. Gleich. "Eosinophil-associated diseases," in *M. M. Samter's Immunological Diseases,* 1, M. M. Frank, K. F. Austen, H. N. Claman, and E. R. Unanue, Eds. Boston: Little, Brown and Company, 1994, 501-527.

[4]   Kaneko, M., M. C. Swanson, G. J. Gleich, and H. Kita. Allergen-specific IgG1 and IgG3 through Fc gamma RII induce eosinophil degranulation. 1995. *J. Clin. Invest.*, 95:2813-2821.

[5]   Winqvist, I., T. Olofsson, I. Olsson, A. M. Persson, and T. Hallberg. Altered density, metabolism and surface receptors of eosinophils in eosinophilia. 1982. *Immunology*, 47:531-539.

[6]   Archer, G. and J. Hirsch. Mation picture studies on degranulation of horse eosinophils during phagoctosis. 1963. *J. Experimental Medicine*, 118:287-313.

[7]   Winqvist, I., T. Olofsson, and I. Olsson. Mechanisms for adherence of eosinophils to an antibody-coated surface. 1985. *Scand J. Haematol*, 35:88-95.

[8]   Abu-Ghazaleh, R. I., T. Fujisawa, J. Mestecky, R. A. Kyle, and G. J. Gleich. IgA-induced eosinophil degranulation. 1989. *J. Immunol.*, 142:2393-2400.

[9]   Kroegel, C., T. Yukawa, G. Dent, P. Chanez, K. F. Chung, and P. J. Barnes. Platelet-activating factor induces eosinophil peroxidase release from purified human eosinophils. 1988. *Immunology*, 64:569-561.

[10] Lindau, M., J. Hartmann, and S. Scepek. Three distinct fusion processes during eosinophil degranulation. 1994. *Annals of the New York Academy of Sciences*, 710:232-247.

[11] Kaneko, S., S. Horie, M. Kato, G. J. Gleich, and H. Kita. A crucial role for b2 Integrin in the activation of eosinophils by IgG. 1995. *J. Immunology*, 155:2631-2541.

[12] Branch, D. W., B. C. Wheeler, G. J. Brewer, and D. E. Leckband. Long-term maintenance of patterns of hippocampal pyramidal cells on substrates of polyethylene glycol and microstamped polylysine. 2000. *IEEE Transactions on Biomedical Engineering*, 47:290-300.

[13] Dontha, N., W. B. Nowall, and W. G. Kuhr. Generation of biotin/avidin/enzyme nanostructures with maskless photolithography. 1997. *Anal. Chem.*, 69:2619-2625.

[14] Biebuyck, H. A., N. B. Larsen, E. Delemarche, and B. Michel. Lithography beyond light: microcontact printing with monolayer resists. 1997. *IBM J. Res. Develop.*, 41:159-170.

[15] Xia, Y. and G. M. Whitesides. Soft lithography. 1998. *Angewandte Chemie*, 37:550-575.

[16] Yang, P., T. Deng, D. Zhao, P. Feng, D. Pine, D. F. Chmelka, G. M. Whitesides, and G. D. Stucky. Hierarchically ordered oxides. 1998. *Science*, 282:2244-2246.

[17] Britland, S., E. Perez-Arnaud, P. Clark, B. McGinn, P. Connolly, and G. Moores. Micropatterning proteins and synthetic peptides on solid supports: A novel application for microelectronics fabrication technology. 1992. *Biotechnol. Prog.*, 8:155-160.

[18] James, C. D., R. C. Davis, L. Kam, H. G. Craighead, M. Isaacson, J. N. Turner, and W. Shain. Patterned protein layers on solid substrates by thin stamp microcontact. 1998. *Langmuir*, 14:741-744.

[19] Kam, L., W. Shain, J. N. Turner, and R. Bizios. Correlation of astroglial cell function on micro-patterned surfaces with specific geometric parameters - hepatocytes and 3T3 fibroblast. 1999. *Biomaterials*, 20:2343-2350.

[20] Folch, A., A. Ayon, O. Hurtado, M. A. Schmidt, and M. Toner. Molding of deep polydimethylsiloxane microstructures for microfluidics and biological. 1999. *J. Biomech. Eng.*, 121:28-34.

[21] St. John, P. M., R. Davis, N. Cady, J. Czajka, C. A. Batt, and H. G. Craighead. Diffraction-based cell detection using a microcontact printed antibody grating. 1998. *Anal. Chem.*, 70:1108-1111.

[22] Nicolau, D. V., T. Taguchi, H. Taniguchi, H. Tanigawa, and S. Yoshikawa. Patterning neuronal and glia cells on light-assisted functionalized photoresists. 1999. *Biosens. Bioelectron.*, 14:317.

[23] Martinoia, S., M. Bove, M. Tedesco, B. Margesin, and M. Grattarola. A simple microfluidic system for patterning populations of neurons on silicon micromachined substrates. 1999. *J. Neurosci. Methods*, 87:35-44.

[24] Corey, J. M., A. L. Brunette, M. S. Chen, J. A. Weyhenmeyer, G. J. Brewer, and B. C. Wheeler. Differentiated B104 neuroblastoma cells are a high-resolution assay for micropatterned substrates. 1997. *J. Neurosci. Methods*, 75:91-98.

[25] Ilic, B. and H. G. Craighead, "Topographical patterning of chemically sensitive biological materials using a polymer-based dry lift-off," 2000. *Biomedical Microdevices*, 2:317-322.

[26] Orth, R., T. G. Clark, and H. G. Craighead. Avidin-biotin micropatterning methods for biosensor applications. 2003. *Biomedical Microdevices*, 5:29-34.

[27] Scepek, S. and M. Lindau. Focal exocytosis by eosinophils--compound exocytosis and cumulative fusion. 1993. *EMBO J.*, 12:1811-1817.

[28] Orth, R. B. Ilic, T. G. Clark, and H. G. Craighead. Patterning micro- and nanometer scale lipid bilayers using a polymer-based lift-off. 2003. *Biophysical J.* (Accepted pending revisions).

CHAPTER 8

PATTERNING MITOGEN AND BACTERIA FOR MACROPHAGE AND LYMPHOCYTE IMMOBILIZATION AND PROLIFERATION

In this study, I demonstrate a new *in vitro* assay using microfabrication techniques to pattern mitogen and bacteria on a planar substrate. Patterned mitogen and bacteria serve as epitopes that are recognized by macrophages and lymphocytes. The mitogen and bacteria are patterned using the polymer lift-off technique detailed in Chapter 3 to create features ranging from 76 μm to ~1 μm resolution. While significant work has been done in the past with these cells in culture, this process provides a new technique to control the stimuli, and to visualize how the macrophages and lymphocytes respond to mitogen and bacteria in a spatially defined manner. Mouse monoclonal antibodies against equine membrane cell receptors include anti-major histocompatibility (MHC) class II, anti-CD4, anti-CD3, and anti-leukocyte function associated-antigen (LFA)-1. Alexa 488-Nanofluorogold antibodies were used as secondary antibodies to stain the primary antibodies bound to the respective cell receptors. Scanning electron microscopy (SEM) imaging was used to visualize the dynamic cellular responses of the macrophages and lymphocytes on micropatterned bacteria and mitogen patches. This imaging provided evidence for macrophage recognition and clearance of bacteria, lymphocyte-macrophage interaction, and extension of filopodia by both the macrophages and lymphocytes. This imaging provides a detailed view of the complex immune reaction of the professional antigen presenting cells (APCs) deliver of processed antigen to lymphocytes, with subsequent activation of the adapted arm of the immune response.

142

Introduction

Lymphocytes and macrophages arise from hematopoietic stem cells, and serve essential roles in host immunity through their cytokine release and specific cellular functions. Lymphocytes can be found both in the blood stream, in organized lymphoid tissue, and in tissues at the site of inflammation. A critical facet of the lymphocyte function is its interaction with the extracellular matrix (ECM). Integrins on the surface of lymphocytes enable these cells to bind to the blood vessel cell wall in the proximity of a pathogen insult. T lymphocytes interact with components of the ECM by virtue of B1-integrin receptors [5]. The primary B1-integrin receptors expressed by T lymphocytes include a4B1 (CD49d/CD29) and a5B1 (CD49e/CD29), a3B1 (CD49c/cd29), and a6B1 (CD49f/CD29) [6], [7]. Adhesion mediated by integrin receptors on T lymphocytes is regulated by extracellular stimuli (inside out signaling), which causes rapid changes in the functional activity of these molecules [5]. Extracellular stimulation of inside out signaling occurs in T cells during the binding of L-selectin, which induces intracellular signals that regulate the affinity of B1 and B2 integrins [8], [9]. Outside-in signaling takes place in T lymphocytes where ligand binding by integrins can produce intracellular signals that modifying the cell's functional activity [5]. For example, binding of aLB2 to ICAM-1 decreases the ability of a4B1 integrin to bind fibronectin [10].

Macrophages play a critical role in the host immune response. In addition to dendritic cells, they are frequently the first cells of the immune system to confront foreign invading substances. Macrophages play a primary role for the immune system of phagocytosis of dead/dying cells, opsonized substances, and material lacking self markers. Phagocytes determine what to devour by way of two mechanisms [11]. First, via pattern receptors on their cell surfaces that recognize structures characteristic of pathogens or abnormal cells, which are absent on healthy cells. These include

lectins that recognize pathogen carbohydrate structures, and scavenger receptors that recognize anionic polymers on apoptotic cells. Second, they carry F_c receptors and complement receptors for opsonins, which are immunoglobulins and complement fragments that bind to the pathogen's surface and mark it as foreign. Macrophages also serve as a key player, if not the primary player in directing an immune response through the release of cytokines. Macrophages exist in three states: resting, primed, and activated. Macrophages are activated mainly by their interaction with TH1 helper cells (inflammatory T cells). The macrophages secrete interleukin (IL)-1 and IL-12. IL-12 activates T cells, which in turn release IFN-γ. Macrophages also serve as professional antigen presenting cells of the foreign material they have phagocytosed using the exogenous pathway of antigen processing and MHC class II presentation.

Immunity is maintained in organisms through a complex interplay among hematopoietic cells that each perform their immune functions by responding to the discrete stimuli of their microenvironment. Images shown in this work hope to shed light on the role of cellular extentions, including filopodia, cytonemes, lamellapodia, and podosomes on how cells sense their microenvironment. There has been an increasing amount of research recently looking at these cellular extensions [12], [13], [14], [15], [16], and [17].

Experimental Section

Lymphocyte, Macrophage, and *Staphylococcus aureus* Preparation. For monocyte-derived macrophage isolation, 40 mL of peripheral blood was collected from horses via jugular venipuncture in vacuum tubes containing heparin. Mononuclear leukocytes were isolated using Ficoll-Paque gradient centrifugation (Amershan Biosciences, Piscataway, NJ). Leukocytes (5×10^6 cells) were washed with phosphate buffered solution (PBS), and cultured in 15 ml of fresh RPMI 1640 medium (Gibco

Invitrogen Co., Grand Island, NY) with 5% heat-inactivated fetal calf serum (FCS) at 37° C and 5% CO_2 for 3 days. Monocyte-derived macrophages adhere to the plastic surface of culture flasks during this period. After discarding the supernatant containing the non-adhering leukocytes, 2 ml of 0.25% Trypsin and 1 mM EDTA solution (Gibco Invitrogen Co., Grand Island, NY) were added to the flask for 3 minutes. The cells were washed 3 times with PBS and resuspended in phenol-free RPMI 1640 with 10% FCS, 1X Penicillin-Streptomycin, 2.5 μg/mL amphotericin B (RPMI-PenStrep-AmpB) (Gibco Invitrogen Co., Grand Island, NY) at 0.5 x 10^6 cells/mL. The cell solution was placed in siliconized tubes and kept on ice until use.

For isolation of lymphocytes, 40 mL peripheral blood from the same horse was collected in heparinized tubes on the same day of monocyte-derived macrophage final preparation. Lymphocytes were isolated using iron micropowder (Sigma, St. Louis, MO) and Ficoll gradient centrifugation. The cells were washed 3X in PBS, and resuspended in RPMI-PenStrep-AmpB at 2 x 10^6 cells/mL.

For the proliferation analysis, 1.5 x10^7 lymphocytes resuspended in 1mL PBS were labeled with 0.25μM CFSE in a gentle mixer, at room temperature, and in the dark for 10 min. The reaction was blocked by adding equal volume of FCS for 1 min. Heat killed *Staphylococcus aureus* (SA), pokeweed mitogen (PWM), concanavalin A (conA), and phytohemagglutinin (PHA) (Sigma-Aldrich, Milwaukee, WI) were stained using Alexa 594 protein labeling kit (Molecular Probes, Eugene, OR). 500 μL of 2 mg/mL SA are incubated in 1M bicarbonate. This volume is added to a vial containing Alexa 594 dye (Sigma-Aldrich, Milwaukee, WI). The vial is stirred at 200 rpm for 60 min. The excess dye is removed using Micro Spin microcentrifuge gel separation columns (BioRad, Hercules, CA).

Silicon Wafer Preparation and Biomaterial Patterning. Parylene is deposited on 3 inch silicon wafers and photolithographically patterned as detailed in Chapter 2 using

OCG OiR 897-12i photoresist (OCG Chemical Company, West Patterson, NJ) with a 1.3 μm Parylene thickness. A diamond scribe is used to dice a silicon wafer into 1 cm^2 pieces that each contain nine of the patterns shown in Fig. 3.X. Mouse anti-*staphylococcus aureus* IgG (αSA-IgG, RDI, Flanders, NJ) was reconstituted to 10 mg/mL and used to create a 100 μg/mL dilution. 30 μL of 100 μg/mL αSA-IgG, conA, PWM, or PHA were pipetted on the Parylene-patterned substrate and incubated for 60 min at 37°C, as illustrated in Figure 8.1C. Incubation was performed in a humidified incubator to prevent drying-out of the small volume samples. The samples were washed 3X in PBS. 100 μg/mL of Alexa-594-conjugated SA were pipetted onto the silicon chips and incubated for 1 h at 37°C in a humidified container. The samples were washed 2X in PBS and RPMI-PenStrep-AmpB. 75 μL of macrophages (5 x 10^5 cells/mL) were pipetted onto the samples and incubated for 12 h at 37°C in a humidified container. The samples were washed 3X in RPMI-PenStrep AmpB. 75 μL of lymphocytes (2 x 10^6 cells/mL) were added onto each chip and incubated for 12 h at 37°C in a humidified container.

Macrophage and Lymphocyte Receptor Labeling. 50 μL of one of the following unlabelled mouse monoclonal antibodies against horse proteins (anti-CD4, anti-LFA-1, anti-CD3, and anti-MHC class II) were added to the samples for 1 hour at room temperature. The samples were washed 2 times in 1% bovine serum albumin (Sigma, St. Louis, MO) in PBS (BSA-PBS). The samples were incubated with anti-mouse Alexa 488-NANOGOLD® (Fluoronanogold) reagent diluted 1/100 (10 μg/mL) in PBS-BSA for 30 min at room temperature. The samples were washed 3X in PBS. The samples were fixed by placing them in 3.7% formaldehyde in PBS for 15 min. The samples were subsequently placed into 1% BSA-PBS solution for 10 min to quench the formaldehyde reaction. The samples were washed 2 X in PBS, and rinsed 2X in deioniozed (DI) water (1 min each rinse). The samples were developed in
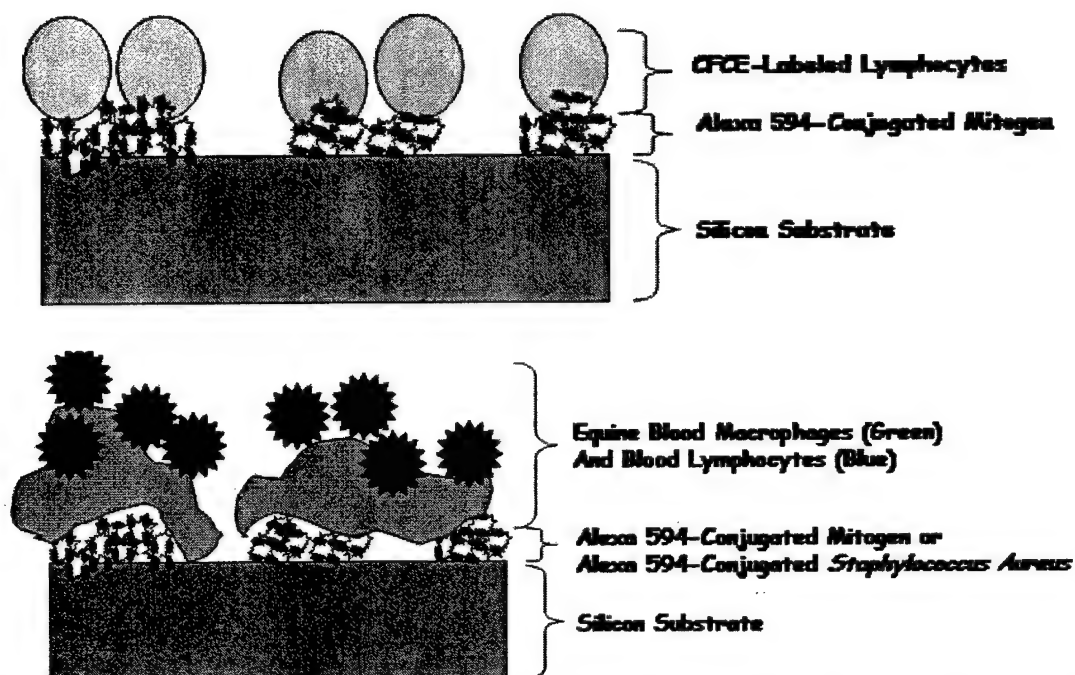
Figure 8.1. Schematic illustrating leukocyte adhesion to micropatterned surfaces.

(A) Schematic illustrating the adhesion of CFSE-stained peripheral blood lymphocytes to Parylene micropatterned Alexa-594-conjugated mitogen (pokeweed, concavalin A, or PHA). (B) Schematic illustrating the adhesion of peripheral blood macrophages and lymphocytes to Parylene micropatterned Alexa-594-conjugated mitogen (pokeweed, concavalin A, or PHA) or *Staphylococcus Aureus (SA)* to anti-SA IgG.
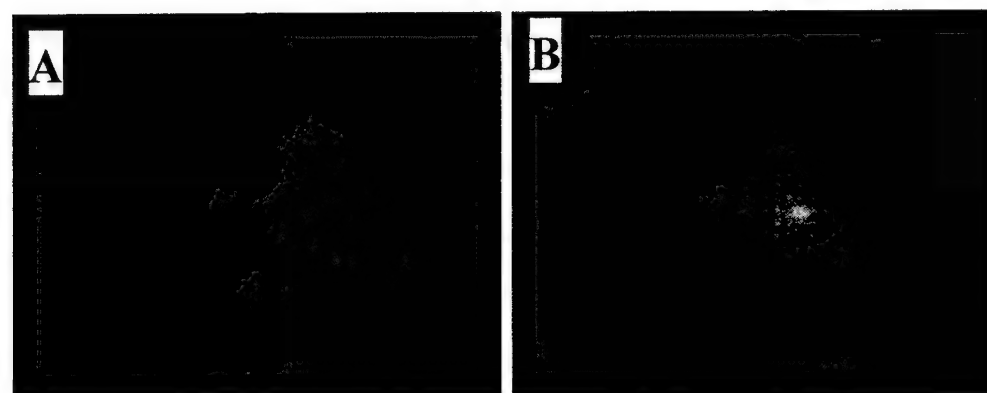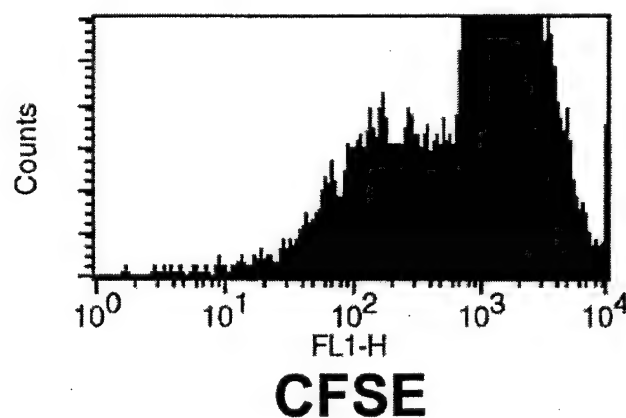
Figure 8.2. Epifluorescent images of Alexa CFSE-conjugated equine lymphocytes (green) on micropatterned Alexa 594-conjugated pokeweed mitogen (red).
(A) Sample with image taken of the cells in the focal plane of the pattern. (B) Sample with image taken of the cells above the focal plane of the pattern. A plume of cells can be observed which serves as evidence for proliferation on the pattern. (C) CFSE flow cytometry analysis of cells harvested from the micropatterned surface.

freshly mixed Li Silver enhancement developer for 5-30 min depending upon the desired silver nucleation thickness (about 20 min). The samples were rinsed 3X in DI water, thereafter dehydrated in 100% ethanol, and critical point dried as described in Chapter 6.

Microscopy. Optical microscopy was performed using an Olympus AX 70 upright microscope as detailed in chapter 3. The microscopy was performed to observe the secondary anti-mouse, Alexa-488 Fluoronanogold IgG bound to the primary antibodies used to label cell surface receptors on the cells. The samples were prepared for scanning electron microscopy (SEM) as detailed in Chapter 6 and imaged using a Hitachi 4500 SEM.

Results and Discussion

The initial objective of the project was to create spatially defined mitogen to serve as stimuli for the lymphocytes. After observing favorable results with this experiment, the experiments were expanded to the patterning of a variety of mitogen and bacteria for interaction with lymphocytes by themselves and with macrophages and lymphocytes together. To achieve precise patterning, the Parylene lift-off technique [2] was implemented since it could pattern biological materials at centimeters to hundreds of nanometer features size. The Parylene lift-off method provided a temporary stencil that was ideal for the patterning of antibodies, mitogen, and bacterial on the silicon substrate. The pattern used for the experimentation consisted of features ranging from ~700 nm to 76 μm, as detailed in Chapter 3. The range of the features offered a method analyze a differential response of the lymphocyte and macrophage. There appeared to be more prominent cellular extensions in the regions with a large areas of bacteria in comparison to areas with less.

To characterize the efficacy of the patterning method, the mitogen and SA were stained with the Alexa 594. The Alexa 594 fluorescence allowed these biomaterials to be observed on the substrate after the patterning step. Fig. 8.1A depicts the binding of lymphocytes to the patterned, Alexa 594-conjugated mitogen. Fig. 8.1B demonstrates the binding of macrophages and lymphocytes to the patterned, Alexa 594-conjugated mitogen or SA to the αSA-IgG.

Lymphocyte Response to Mitogen Micropatterned Surface. Cells respond to the microenvironment in which they reside. The mitogens were patterned to determine if they could elicit a response by the lymphocytes. Fig. 8.2A-B shows the effective patterning of Alexa 594 conjugated pokeweed mitogen. The patterns indicated that the mitogen remained in their spatially defined locations during the 3d incubation. Prior to application on the patterned substrates, the lymphocytes were stained with CFSE. Proliferation was analyzed by epifluorescence microscopy, flow cytometry, and SEM analysis. Lymphocyte proliferation was recognized in cells off the focal plane of the pattern. When rising approximately 40 μm off the surface, numerous plumes (clonal proliferation) of cells could be observed. The haze seen in the center of the image is a plume in which the lymphocytes have either proliferated or aggregated in response to the patterned antigen. After the lymphocytes had been incubated on the surface for 3 days, the cells were vigorously agitated, and the cells were harvested. Fig. 8.2C shows a CFSE fluorescence histogram from the cells harvested from containers. The CFSE fluorescence measurement performed in a flow cytometry system shows a positive indication that proliferation happened. When cells divide, daughter cells have half of the fluorescence of the parent cell. Fig. 8.2C shows a decrease in CFSE fluorescence in the population of cells after 3 days of incubation in the mitogen-patterned container.

SEM imaging provided a detailed view of the interaction between the lymphocytes and the micropatterned mitogen. The images in Fig. 8.3A-E show the
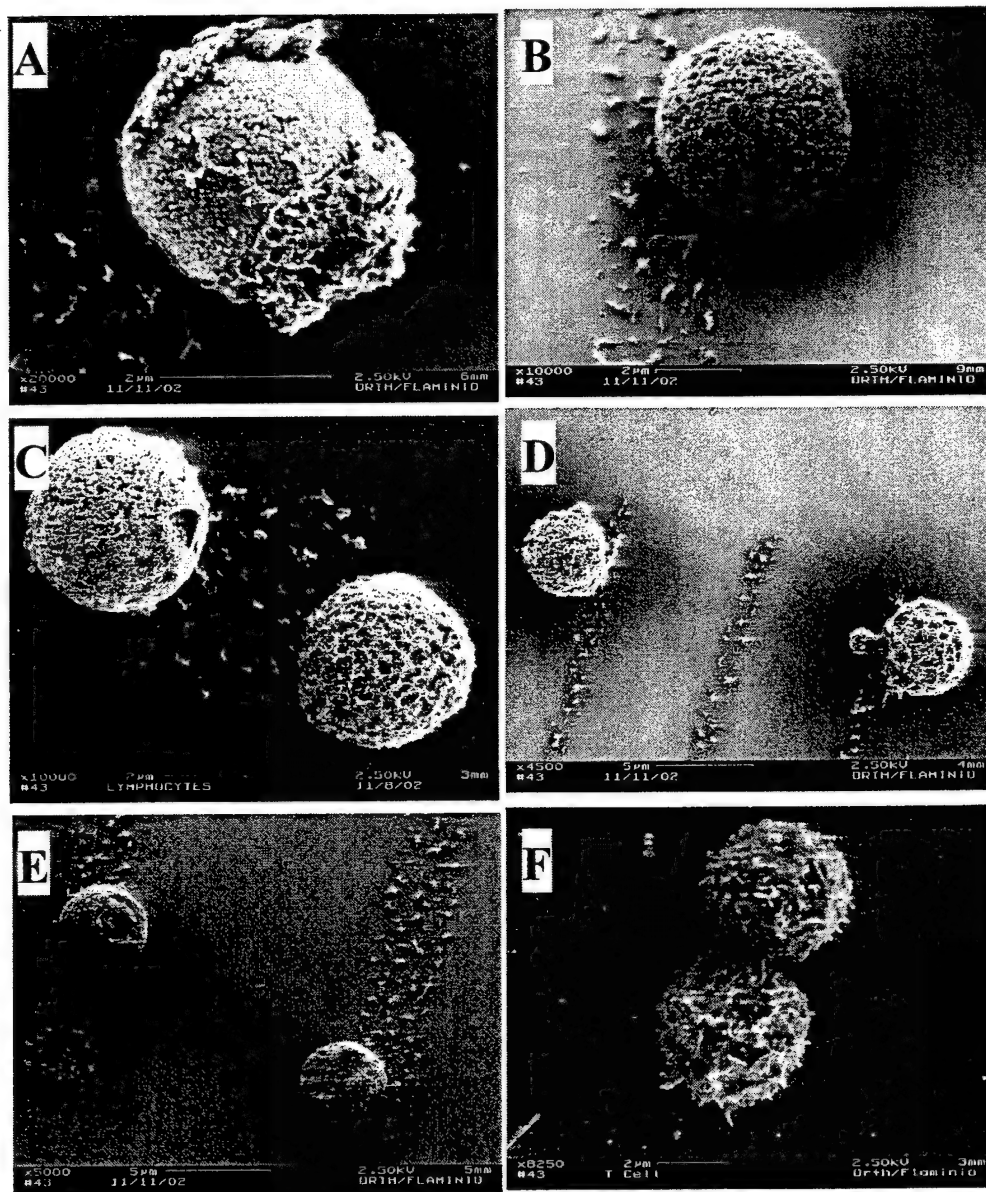
Figure 8.3. SEM images of equine peripheral blood lymphocytes interacting with micropatterned pokeweed mitogen on a silicon substrate.

Each of these images illustrate lymphocytes with extensions. The contacts are formed through integrin adhesion. The following images are lymphocytes bound to different patterns of pokeweed mitogen patterns: (A) 10 μm square (note the adhered extracellular matrix from prior a adhesion). (B) 3 μm line. (C) 4.2 μm square. (D) 1.5 μm line. (E) 3 μm lines.

lymphocyte responses to the patterned pokeweed mitogen. In comparison to the epifluorescent imaging of the cells where a continuous carpet of cells was observed, the SEM images showed that the samples that went through the dehydration and critical point drying steps showed a marked decrease in the number of cells. The cells observed in the SEM images were generally bound onto the patterned regions and not onto the atomically smooth silicon dioxide substrate. The cells are potentially attached at their bases. The patterns can be discerned since they contain numerous previous attachments. A contributing factor to the large number of the adhesion tendrils prior attachments could be the use of 3-aminopropyltriethoxysiane was used to adhere the mitogen to the substrate. Perhaps the amine groups of this silane served as nonspecific adhesion points for the cells. Prior to the critical point drying, the number of cells on the surface was significantly higher. *In vivo*, lymphocytes are generally thought to be circulating cells that sample microenvironments and circulate through lymphoid tissues. They may form temporary attachments at the site of surveillance during their immunological performance before they flow back to the lymphatic system. Fig. 8.3F shows two lymphocytes bound to one another, either as a result of cell division or the formation of an immune synapse.

Of particular interest are processes extending out from the lymphocytes as shown in Fig. 8.4. Cellular outgrowths are typically composed of actin (thinner, ~60 nm) and microtubule components (thicker, ~200 nm). These images show prominent extensions that fall into both of these size ranges. The larger outgrowths appear to adhere the cells to the substrate and to each other. The smaller features may be serving as a sensory role, which is commonly associated to filopodia in neuron and other cell types. Small distinct extensions exist in many cell types, including neuronal cells, epithelial cells, and are frequently referred to cytoneme like filopodia [16]. The lymphopodia frequently are submicron in size, ranging from 200 nm to 2 μm. These
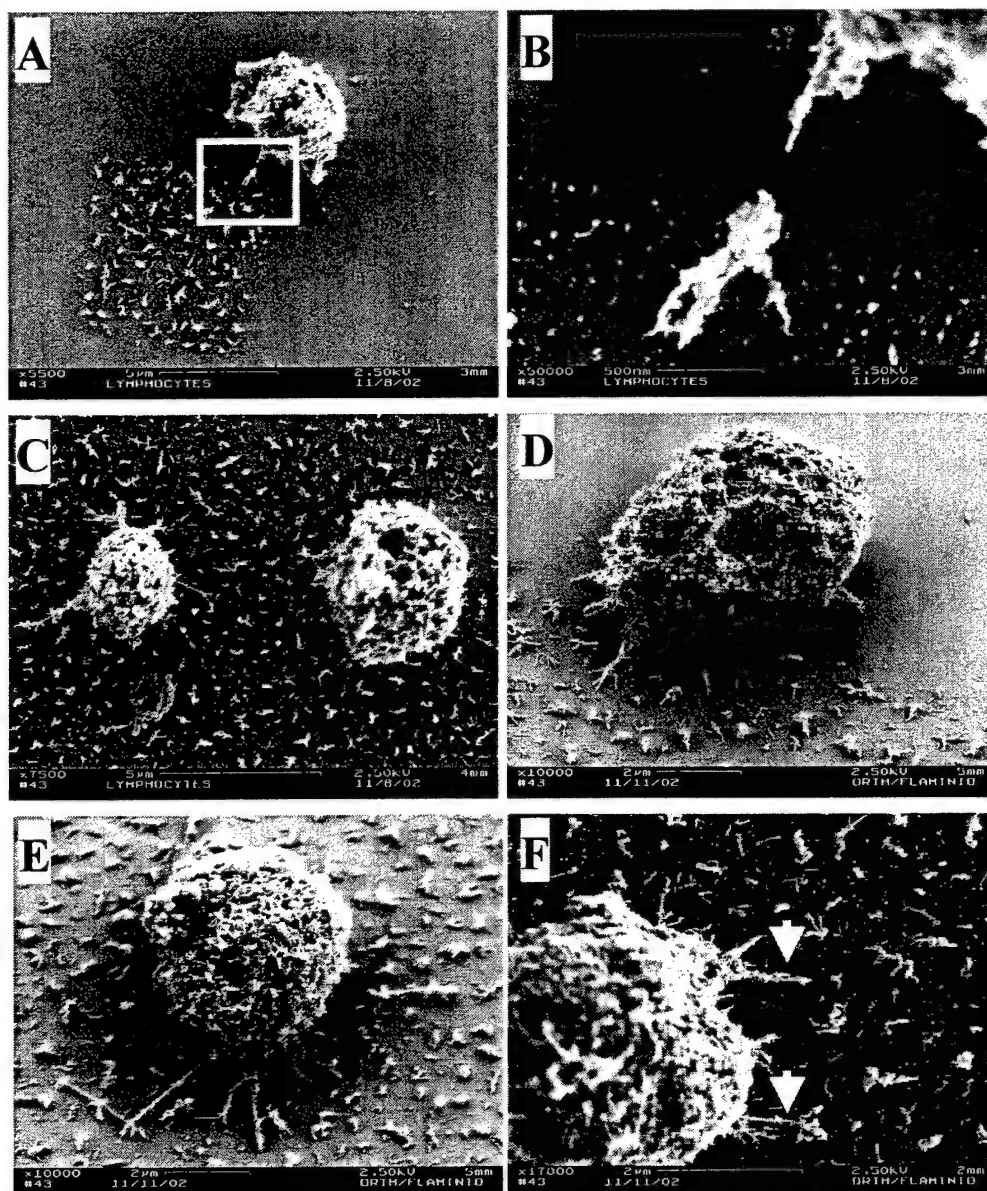
Figure 8.4. Lymphocytes with filopodia extension on micropatterned surface.

SEM images of equine peripheral blood lymphocytes interacting with micropatterned pokeweed mitogen on a silicon substrate. Each of these images illustrate lymphocytes with extensions. The contacts are formed through integrin adhesion. (A) Image showing an integrin adhesion "foot." (B) A magnified view of the square shown in image A. (C) Cells adhered to the silicon substrate. The cells on the left has 30 nm filopodia. (D) Lymphocyte either retracting away from the patterned surface or toward the patterned surface. (E) Lymphocyte with multiple filopodia extensions, ranging from 50 nm (leftmost extension) to 80 nm (center extensions below cell). (F) Lymphocyte with 80 nm (upper) and 40 nm (lower) filopodia.

extensions also demonstrate distinct orientation toward patterns on the surface (Fig. 8.5). A close view of the extension reveals that there are periodic bulbous portions of these extensions. These could either be sensing nodes or, more likely, bundles of cytosolic materials being shuttled to the distal end of the cellular extension. Fig. 8.5 A-B displays fibers that may have traveled away from the cell toward the patterned mitogen. It also indicates the path that the cells have taken. Fig. 8.5C-F shows cells with a range of attachments. The cell in Fig. 8.5C could be traveling toward or away from the attachment point. Fig. 8.5D has several extensions in different directions, so they could be extending to sense the environment. Fig. 8.5 E-F and Fig 8.6A-F all show images of lymphocytes bound to the substrate in clusters with an extensive network of fibrous extensions. It is currently not known why these attachments form, but it can be speculated that these may serve for attachment at the site of a pathogen invasion, sensing of a pathogenic tissue region, anchoring to precede a site of proliferation, or anchoring as a means to aggregate cells to release cytokines in a pathogenic region.

Lymphocyte and Macrophage Interaction on Micropatterned *Staphylococcus Aureus (SA)*. The initial objective for this experiment was to determine if an interaction between the lymphocytes and the macrophages could be established on a patterned bacteria microenvironment. In this experiment, SA are commonly ingested by horses on the grass they eat. For this reason, it can be assumed that the horse that provided the blood for the experiments will have been presensitized to this bacterium. From the results of what has been observed with this reaction, we propose detailed six phase activation sequence for the macrophages and lymphocytes on our patterned surface.

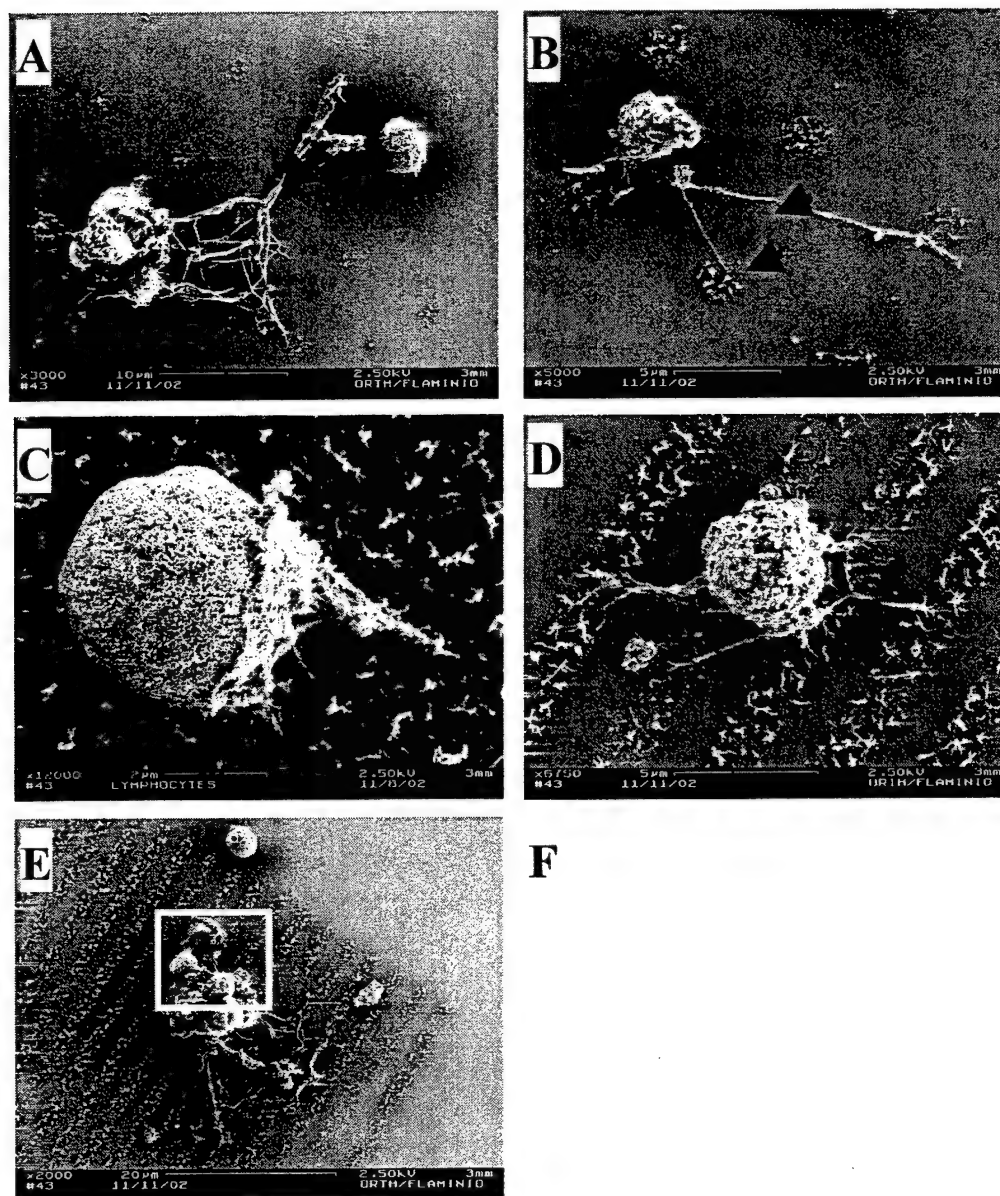(1) Unstimulated lymphocytes with few filopodia and small ruffles (Fig. 8.7).

Figure 8.5. SEM images of equine peripheral blood lymphocytes interacting with micropatterned pokeweed mitogen on a silicon substrate. Each of these images illustrate lymphocytes with extensions.

The contacts are formed through integrin adhesion. (A) Lymphocyte with large scale extensions demonstrating an oriented migration toward the patterned pokeweed mitogen 340 nm wide at the arrow. (B) Lymphocyte with oriented filopodia that are 110 nm (upper) and 60 nm (lower) wide at the point of the arrows. (C) Lymphocyte demonstrating an adhesion where the cell's outer membrane appears to be sloughing off or extending toward the surface. (D) Lymphocyte with multiple extensions to different mitogen patterns. (E) Lymphocytes anchored to the substrate. (F) A magnified view of the square shown in image A.
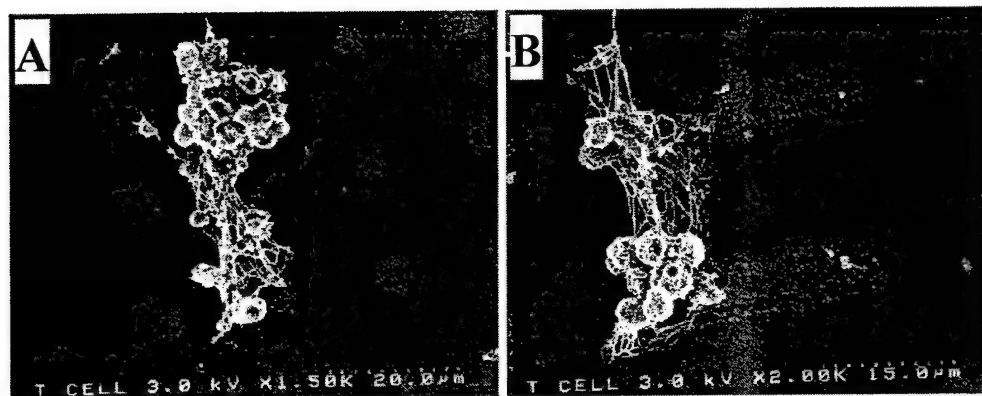
Figure 8.6. SEM images of equine peripheral blood lymphocyte clusters on a pokeweed mitogen micropatterned silicon substrate.
(A) Lymphocyte cluster on 5.5 μm patterns of mitogen with 100 to 300 nm extensions. (B) Lymphocyte clusters on 7 mm lines of mitogen with filopodia anchoring the cluster to the mitogen. (C) Lymphocyte clusters on 1 μm mitogen patches with numerous oriented extensions to neighboring cell clusters. (D) Lymphocyte cluster on 2.2 μm mitogen lines. (E) Lymphocytes cluster on 1.7 μm patterns of mitogen. (F) Lymphocyte cluster on 1.6 μm lines of mitogen.

A

B

Figure 8.7. SEM images of equine peripheral blood lymphocyte and macrophage clusters on a silicon substrate.
(A) Macrophages on the silicon substrate with no micropatterned stimuli. (B) Macrophages and lymphocytes on the silicon substrate with no micropatterned stimuli.

(2) Macrophages encounter bacteria, upregulate filopodia, moderate ruffles (Fig. 8.8 to 8.11).

(3) Macrophages phagocytose bacteria, high filopodia, large ruffles; lymphocyte may contribute to the filopodia network. (Fig. 8.10 to 8.12, 8.13 A-C).

(4) Macrophages send our fibrous extensions that interact with neighbors (Fig. 8.12).

(5) The filopodia network promotes lymphocyte-macrophage interaction. (Fig. 8.13 to 8.14).

(6) Lymphocytes bound to macrophages increase their microvilli-like extensions (Fig. 8.15, especially D-E).

Phase 1: Unstimulated cells. Macrophage cells incubated in a bacteria free solution remain in one of two forms, either flattened or rounded. Fig. 8.7A shows macrophages on a silicon substrate that was patterned polymer but did not have any patterned SA bacteria. When lymphocytes are added to the solution, the macrophages flatten out significantly and are in contact with most of the lymphocytes (Fig. 8.7B).

Phases 2 and 3: The images in Fig. 8.9 to 8.9 show Alexa-594 conjugated SA patterned using the Parylene lift-off method detailed in Chapter 3. The images in Fig. 8.8A-B show bacteria patterns that are relatively undisturbed. These images were taken near the edge where few cells were present during the incubation. The cells migrate to the center of the chip after application to the surface, as they probably drawn to one another chemotactically and desire contact with one another. Fig. 8.8C-D, on the other hand, show the SA patterns significantly disturbs, as a result of significant phagocytosis by the macrophages. Fig. 8.9 shows several examples of macrophages phagocytosing the bacteria from the patterns. In these images, the macrophages are always the brightest features, as they have internalized a significant
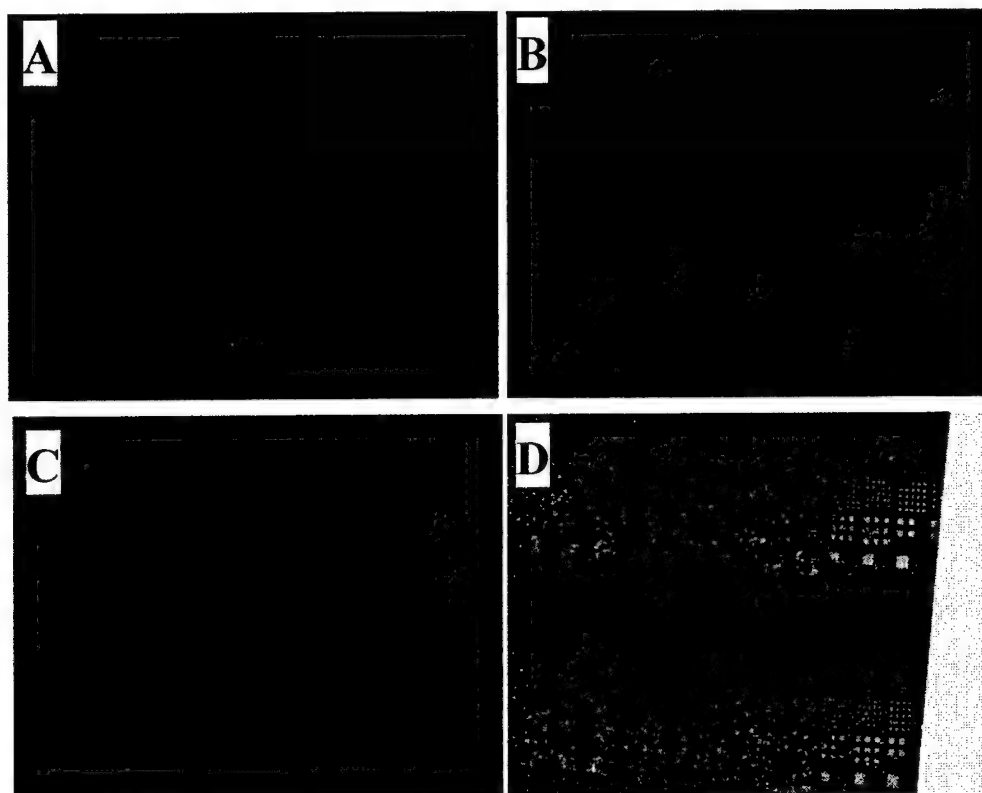
Figure 8.8. Epifluorescent images of Alexa 488 Nanofluorogold conjugated equine lymphocytes and macrophages (green) obtain from a bronchial lavage incubated on patterns of Alexa 594-conjugated SA (594-SA, red).

(A) Pattern of 594-SA near the edge of the pattern and consequently relatively undisturbed by macrophages. (B) Pattern of 594-SA also near the edge relatively undisturbed. (C) Closer to the center of the sample, the pattern becomes more difficult to distinguish as the macrophages phagocytose more of the SA. (D) The pattern is undistinguishable near the center where the macrophages have phagocytosed the majority of the SA, compared to the edge where it remains relatively undisturbed.
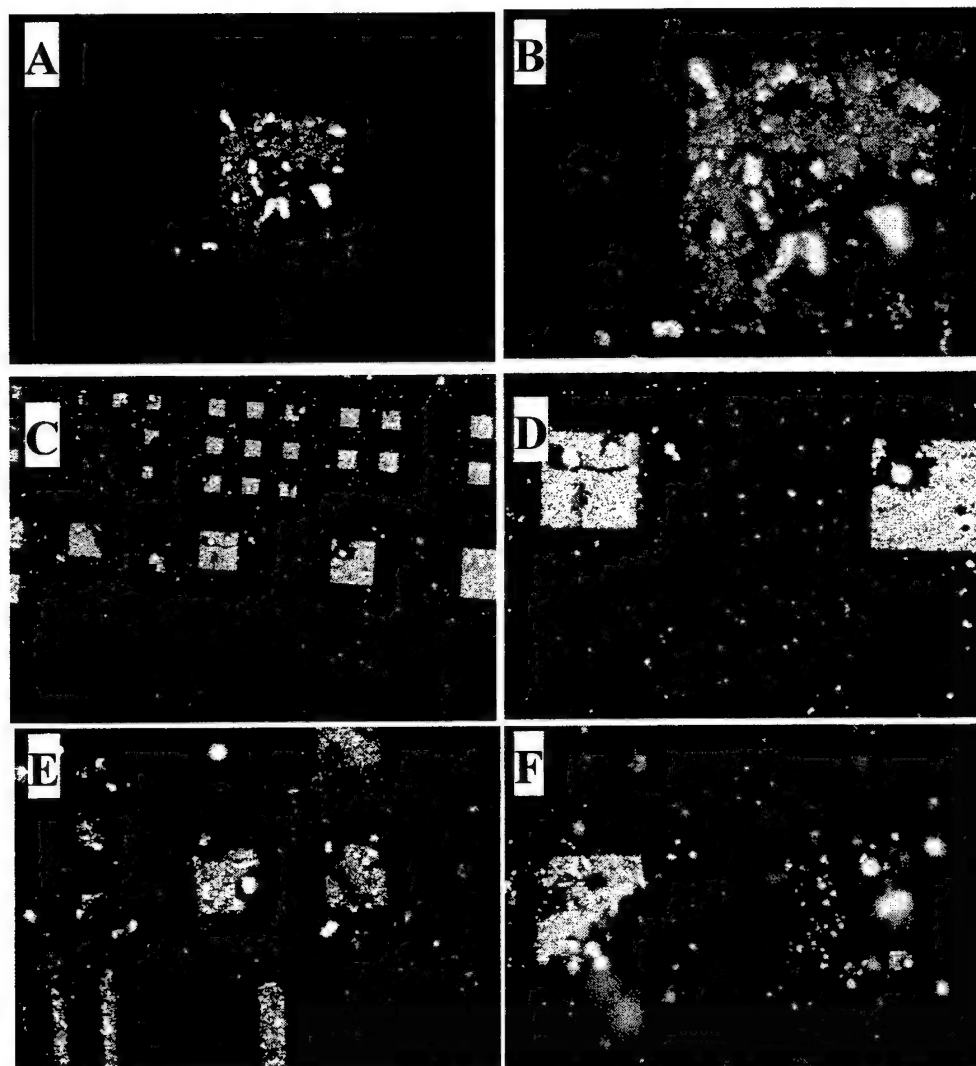
Figure 8.9. Epifluorescent images of Alexa 488 Nanofluorogold conjugated equine peripheral blood lymphocytes and macrophages (green) incubated on patterns of Alexa 594-conjugated SA (red).

All these imaged demonstrate macrophages phagocytosing the micropatterned bacteria. (A) Image taken with a 50X objective demonstrates the macrophages consuming the bacteria on the near proximity of the cells. The unlabelled macrophages are bright red from their phagocytosis of the Alexa-594 conjugated SA. (B) This is the same image as in A taken with a 100X objective. (C) Image demonstrating phagocytosis over the different patterned regions. This image was taken with a 20X objective. (D) The same field of view as C except taken with a 50X objective. (E-F) Images showing varying degrees of phagocytosis of the patterned surface.
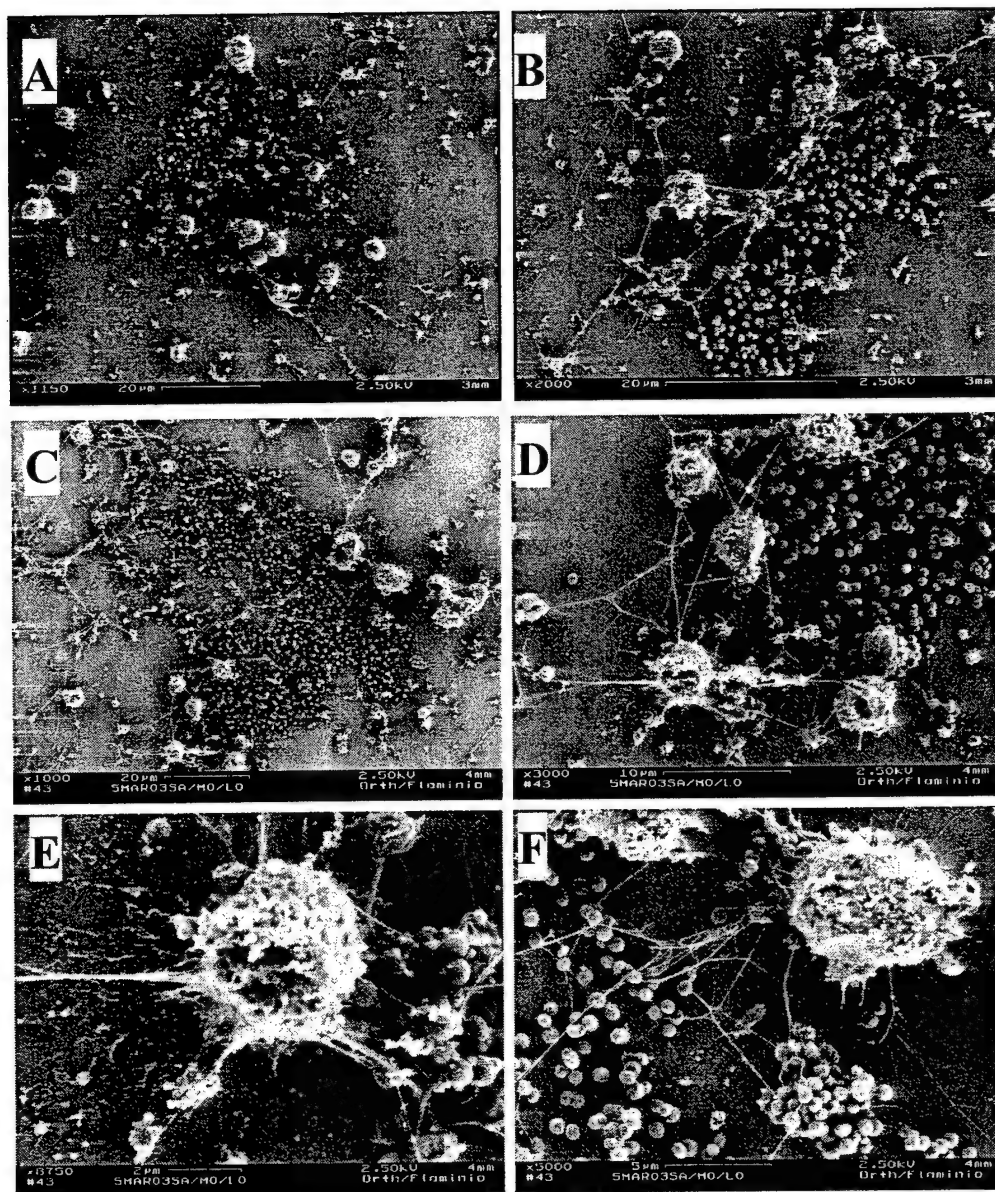
Figure 8.10. SEM images of equine peripheral blood lymphocyte clusters on a pokeweed mitogen micropatterned silicon substrate.
(A-C) Micropatterned squares of bacteria with macrophages actively clearing the surface. (D-E) These images are magnified views of magnified view of Fig. 8.10C displaying the macrophage clearing the bacteria via a "fishnet" approach. (F) Another view of the bacteria being cleared in clusters via the "fishnet" clustering technique.
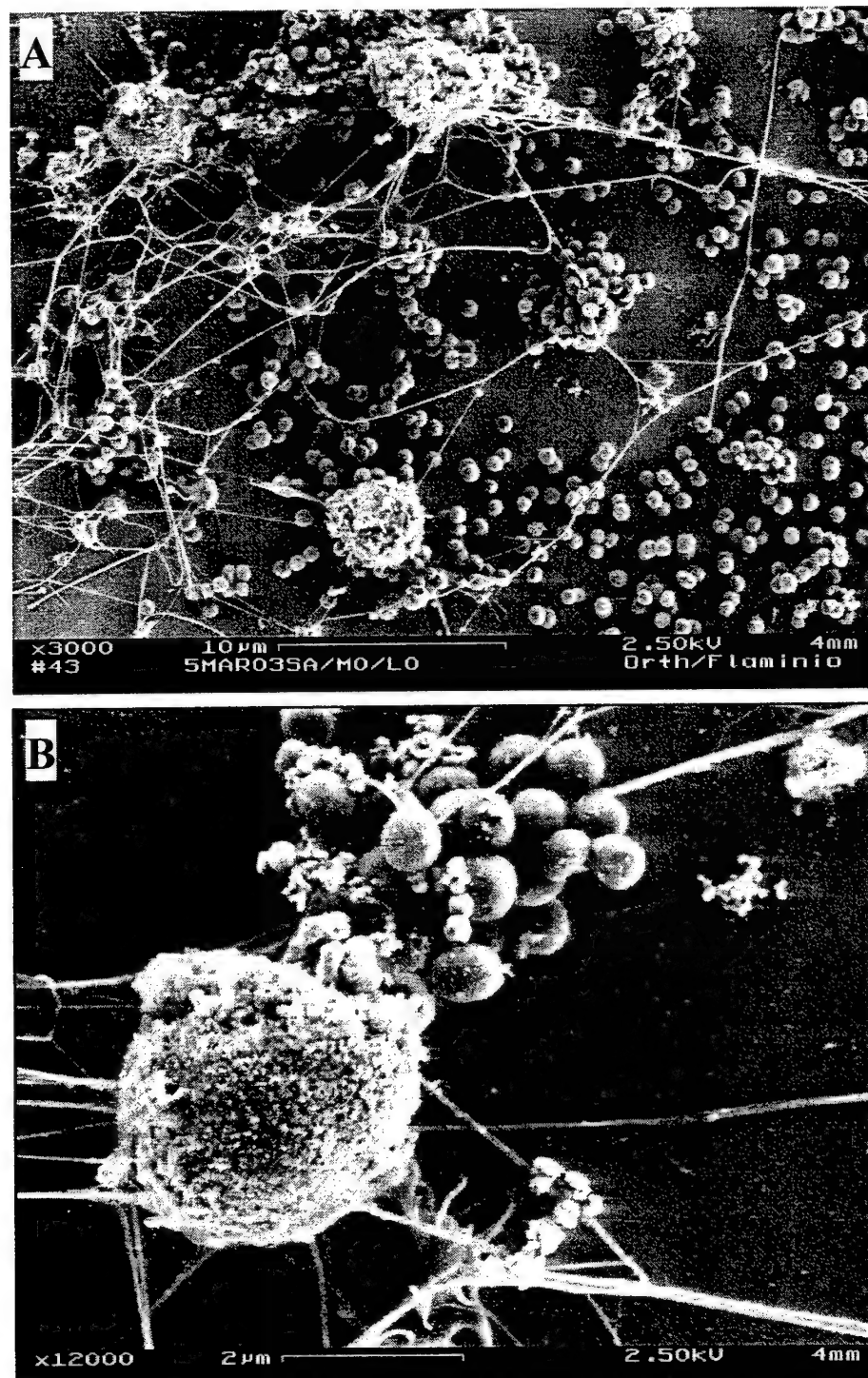
Figure 8.11. (A-B) SEM images of equine peripheral blood lymphocyte clusters on a staphylococcus aureus mitogen micropatterned silicon substrate.
These images show the aggregation of these bacteria via cellular extensions from cells.
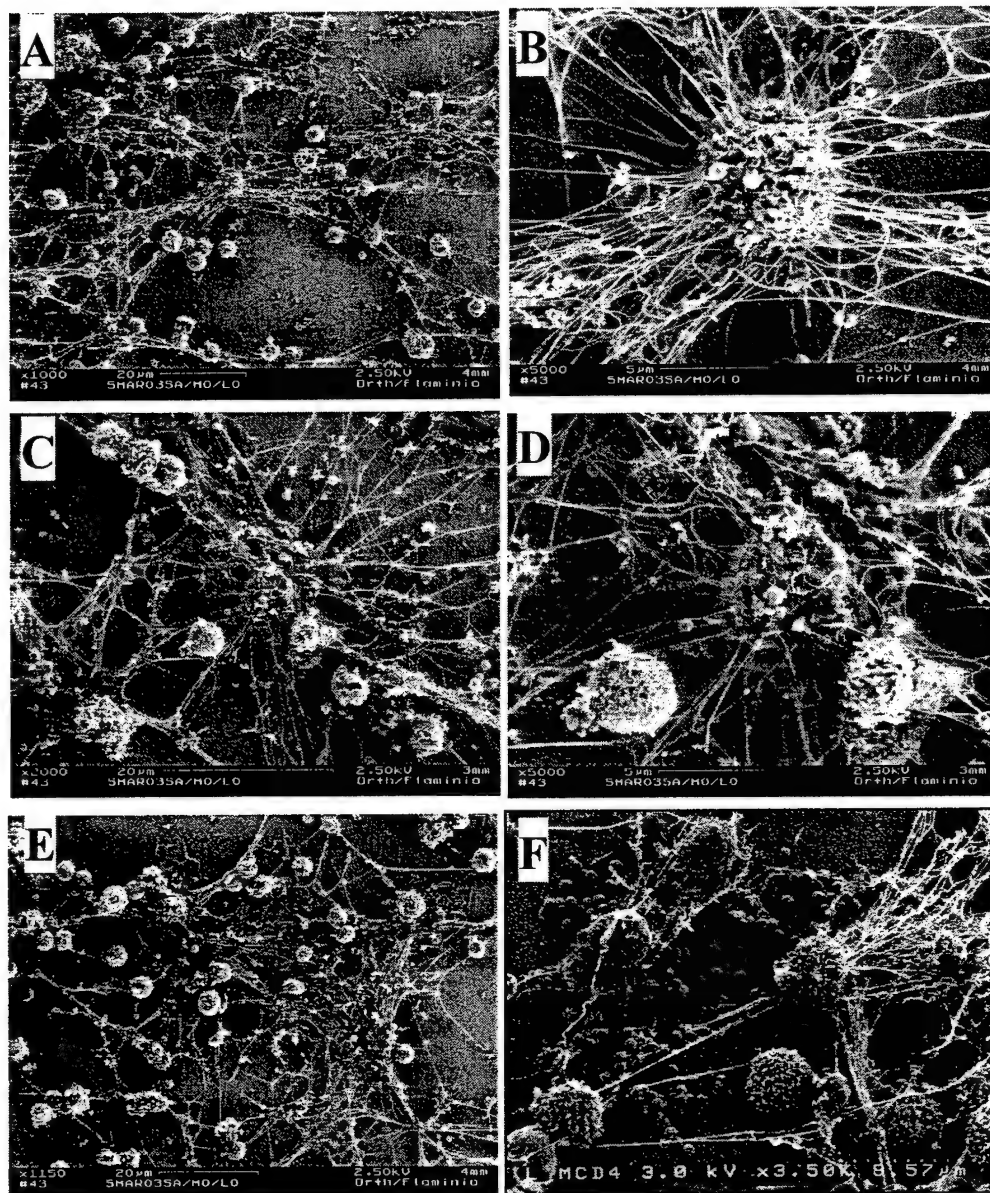
Figure 8.12. SEM images of equine peripheral blood lymphocyte clusters on a pokeweed mitogen micropatterned silicon substrate.
(A-E) Macrophages and lymphocytes with filapodia-like projections in a region filled with patterned SA.
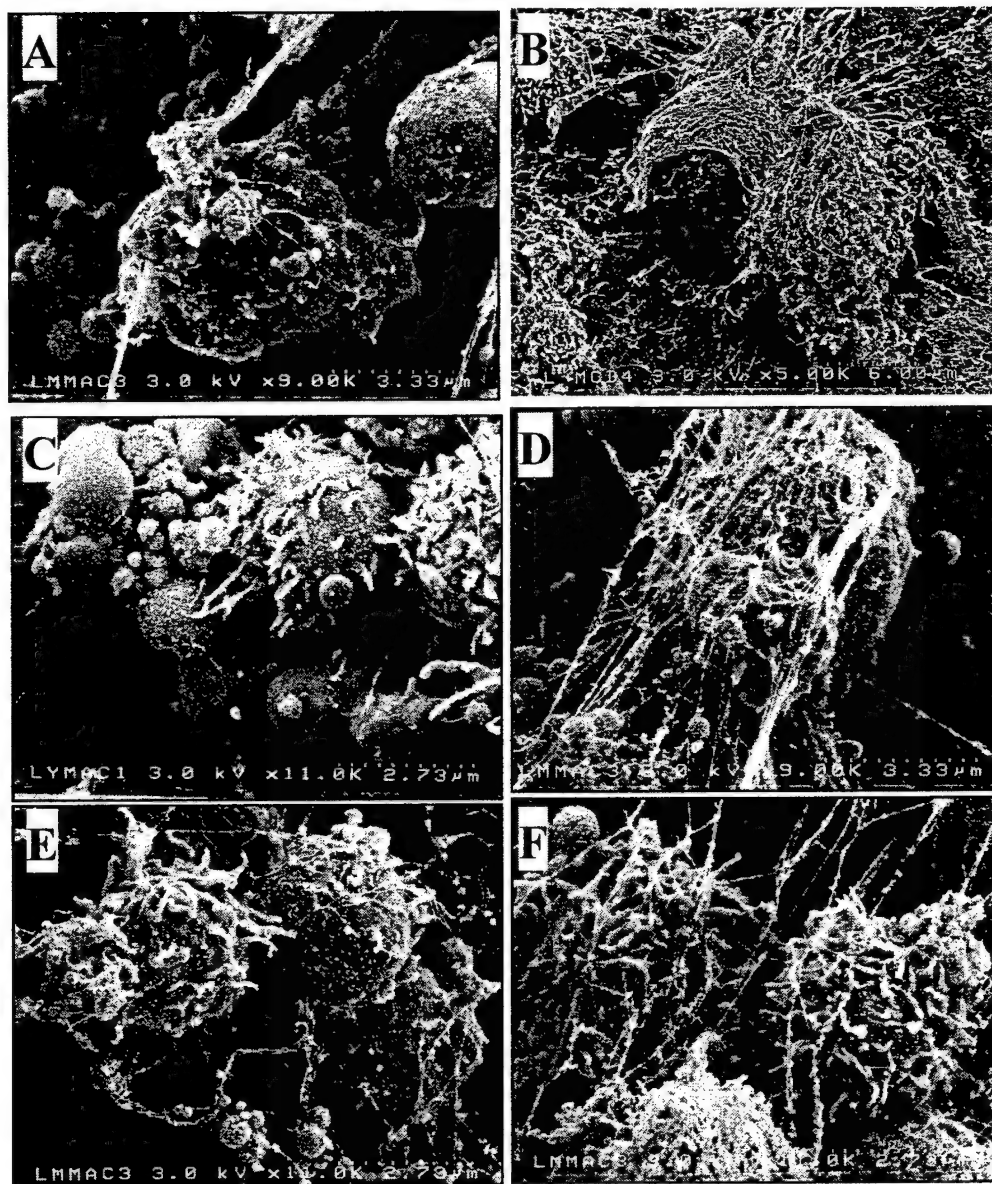
Figure 8.13. SEM images of equine peripheral blood lymphocyte clusters on a pokeweed mitogen micropatterned silicon substrate.
Macrophages and lymphocytes with filapodia-like projections in a region filled with patterned SA. (A-C) Macrophags can be observed phagocytosing the bacteria. (C-E) Lymphocytes appear to contribute to the fiber extensions.
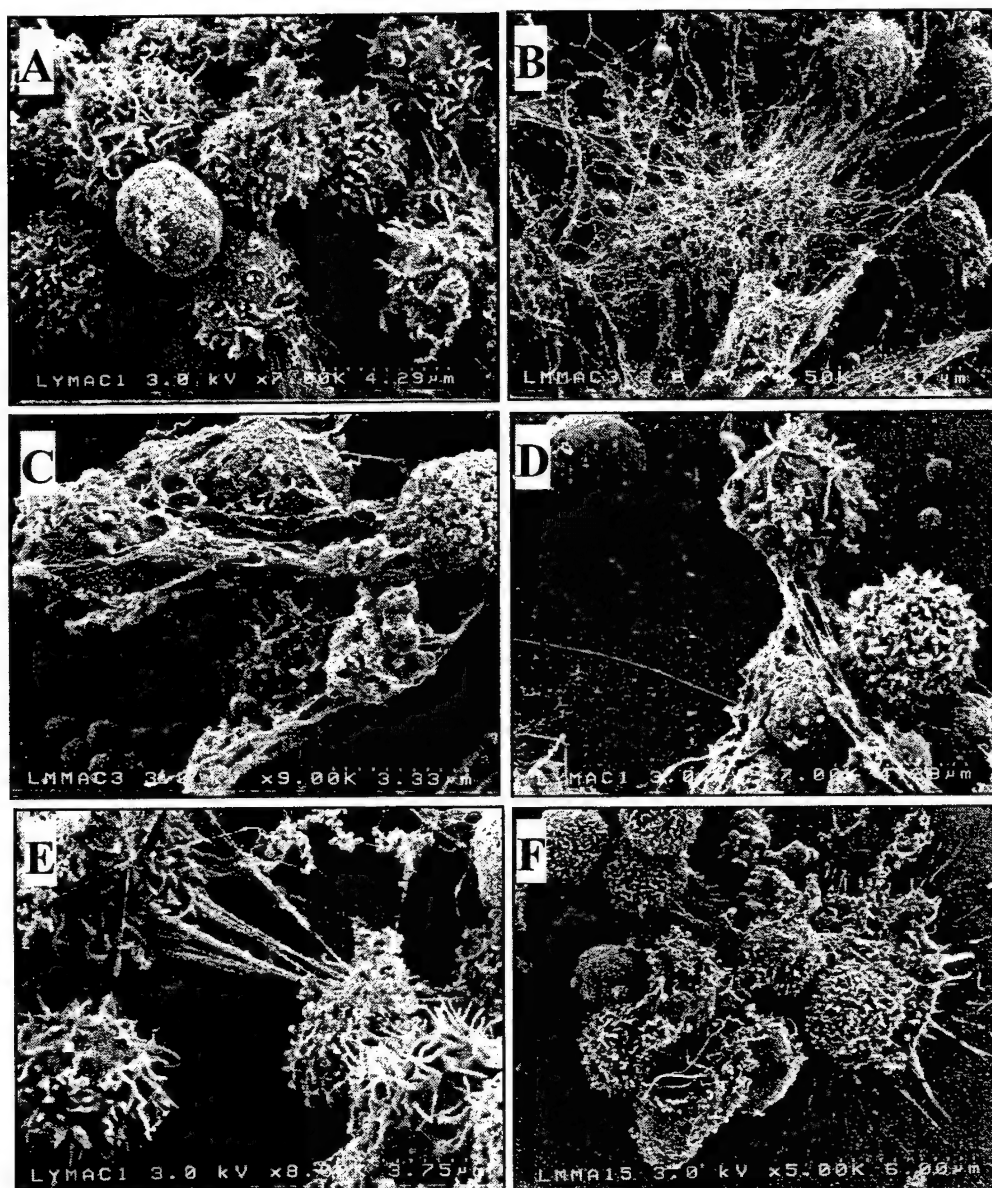
Figure 8.14. SEM images of equine peripheral blood lymphocyte clusters on a pokeweed mitogen micropatterned silicon substrate.
Macrophages and lymphocytes with filapodia-like projections in a region filled with patterned SA. (A-C) Macrophags can be observed phagocytosing the bacteria. (C-E) Lymphocytes appear to contribute to the fiber extensions.
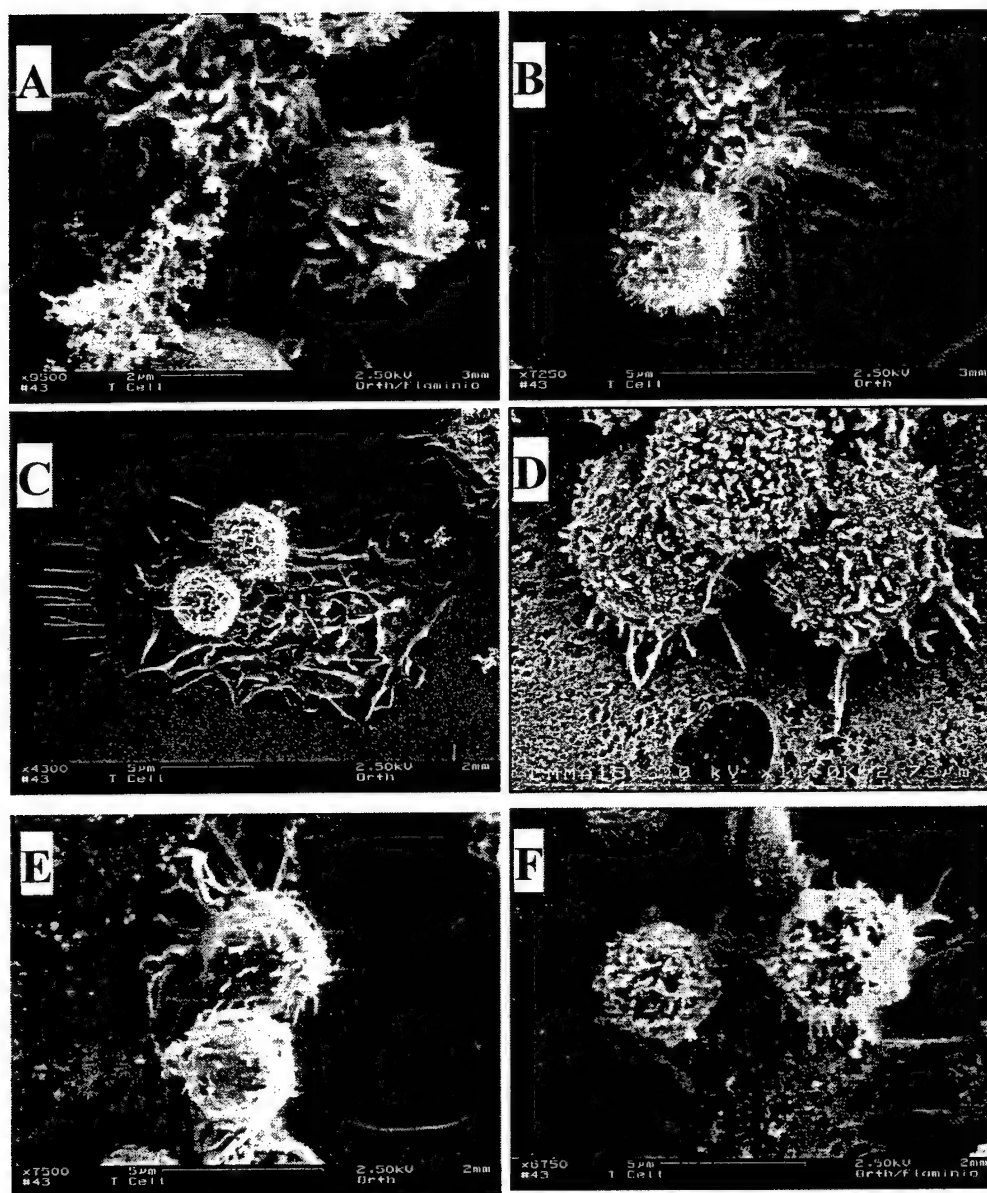
Figure 8.15. SEM images of equine peripheral blood lymphocytes anchored to macrophages.
(A) Ruffled macrophage interaction with lymphocytes at an early phase prior to macrophage adhesion and flattening on the substrate. (B) Macrophage with more extensive process formation, potentially in the middle of surface adhesion. (C) Adhesion in a ruffled state with bound lymphocytes. (D-F) Adhesion of lymphocytes after the ruffled phase.

amount of the Alexa 594 dye by phagocytosing the bacteria. This is most apparent in Fig. 8.9A where the green intensity for the image is low. Of particular interest in these images is the empty halo around the macrophages. This empty area is quite common, as the cells have developed a mechanism to clear areas that measure 0.5 to 2 cell diameters. Fig. 8.10 shows the dynamic activity macrophages undergo in the process of clearing bacteria from a region. The macrophages appear to send out processes in order to initially make contact with the bacteria (Fig. 8.10A-C). In the process, the extensions cluster the bacteria (Fig. 8.10D, F), and the macrophages migrate toward the bacteria (Fig. 8.10E), and bind to the clustered bacteria (Fig. 8.10E, F). Fig. 8.11 shows clustering of the bacteria via the extensions and the cell interaction with the clusters of cells. The actual mechanism occurring needs to be studies further, but this finding could shed light onto how macrophages clear bacteria efficiently over large areas. Fig. 8.12 shows macrophages sending out fibers that interact with neighboring cells.

Phase 4. After the macrophages encounter and phagocytose the bacteria, they start to send out filopodia, potentially to look for more bacteria interact with lymphocytes and/or to alert neighboring cells (Fig. 8.10 to 8.12, 8.13 A-C). This image shows that there are a significant number of fibers that form between macrophages.

Phases 5 and 6. After or concurrent with Phase 4, lymphocytes also begin to associate with macrophages. During this interaction, the macrophages can be seen as migratory (Fig. 8.15A), partially immobilized (Fig 8.15B), or fully immobilized (Fig. 8.15C). Fig. 8.15A shows a migratory macrophage interacting with a minimally lymphocyte, as determined by the small external processes. Fig. 8.15B shows a lymphocyte interacting with a macrophage that is more adhered to the surface. This

lymphocyte appears more stimulated than the one in Fig. 8.15A. This macrophage may be in the process of flattening down on the surface. The lymphocyte may be providing a signal to the macrophage that is required for the macrophage to flatten onto the surface. Fig. 8.15C shows a ruffled macrophage with bound to cells that are most probably macrophages. Macrophage-macrophage binding does occur, as was seen in the control in Fig. 8.7A-B. Fig. 8.15D shows a fairly mature macrophage with a number of adhered lymphocytes, each lymphocyte showing different levels of potential activation. Fig. 8.15E-F show stimulated lymphocytes on unruffled macrophages. In these images, the lymphocytes are sending out processes to the macrophages. The purpose of these extensions has yet to be determined. Fig 8.16 shows more lymphocytes binding to the macrophages. Of particular interest is the large number of lymphocytes that adhere to the macrophages.

The fluorescent staining was used to visualize specific molecules on the cells surfaces. LFA-1, present on both T cells and macrophages, provided a means to visualize the cells and their relative proximity to the patterned SA (Fig. 8.17). The fluorescent staining was also used to observe interactions between the cells. In a similar manner, staining for MHCII, CD3 and CD4 provided a means to separate the T cells from the macrophages (Fig. 8.18). When observing MHCII, CD3, and CD4 we observe regions where there were bright patches, and this was assumed to be an interaction between macrophages and lymphocytes. These images indicate that there is the presence of these molecules on the cell surface.

Fig. 8.19 displays images of immunogold labeling of the samples with the Alexa 488 Fluonanogold. An anti-mouse antibody that contain a 1.5 nm gold particle at the disulfide bond was used. The samples were incubated in a silver enhancement solution that nucleates silver off the gold particle a sphere measuring 10-100 nm. As a result, the antibodies used to tag cell surface molecules (i.e. MHCII, CD3, CD4, and
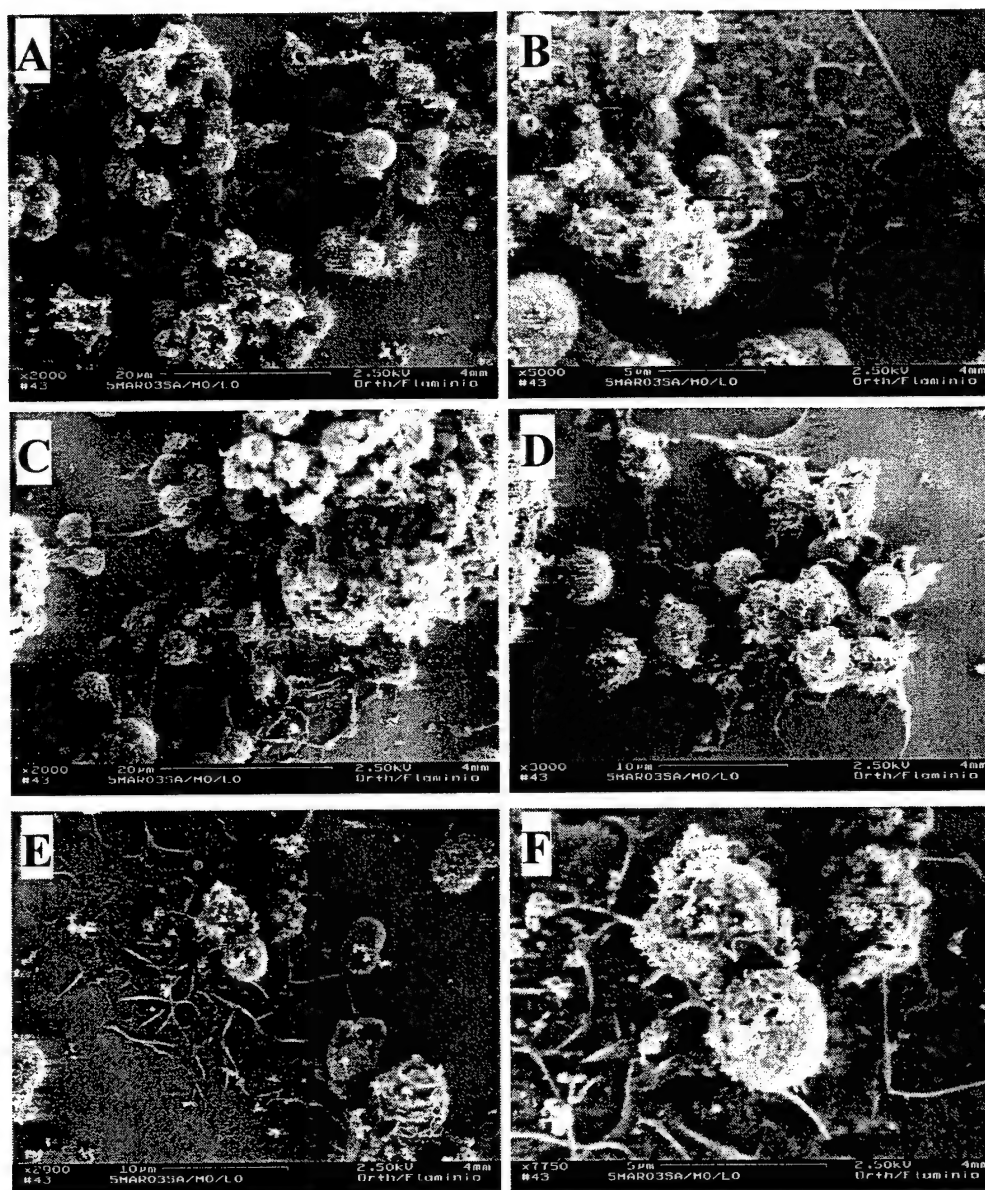
Figure 8.16. SEM images of equine peripheral blood lymphocytes anchored to macrophages.
(A) Ruffled macrophage interaction with lymphocytes at an early phase prior to macrophage adhesion and flattening on the substrate. (B) Macrophage with more extensive process formation, potentially in the middle of surface adhesion. (C) Adhesion in a ruffled state with bound lymphocytes. (D-F) Adhesion of lymphocytes after the ruffled phase.
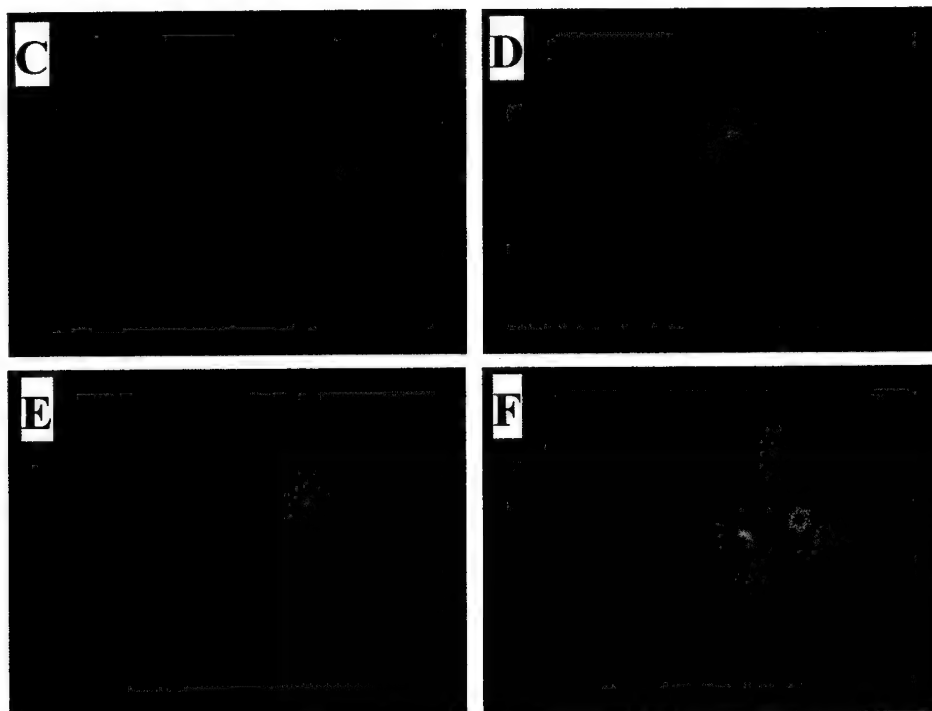
A

B

C

D

E

F

Figure 8.17. Epifluorescence images of equine peripheral blood lymphocyte clusters on a pokeweed mitogen micropatterned silicon substrate.
(A-F) Anti- LFA-1 staining.

A   B

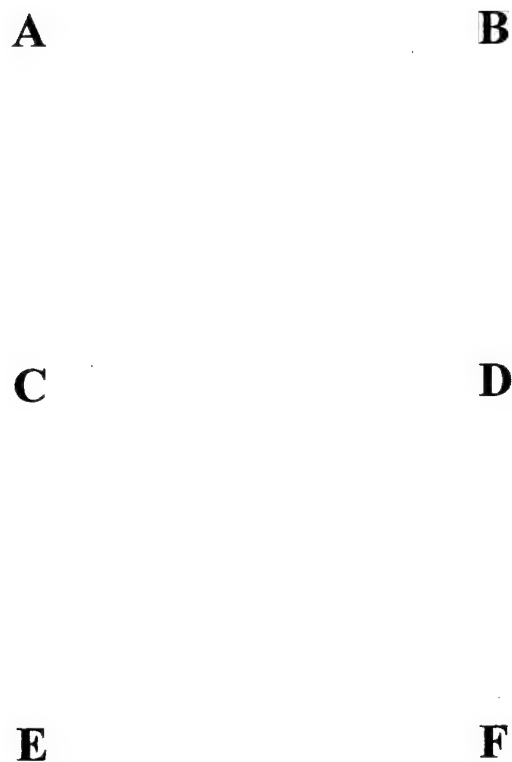C   D

E   F

Figure 8.18. Epifluorescence images of equine peripheral blood lymphocyte clusters on a pokeweed mitogen micropatterned silicon substrate.
(A-C) Staining of anti-MHC II antibodies. (D) Staining of anti-CD4. (E-F) Anti-CD3.

A   B

C   D

E   F

Figure 8.19. SEM images of equine peripheral blood lymphocyte clusters on a pokeweed mitogen micropatterned silicon substrate.
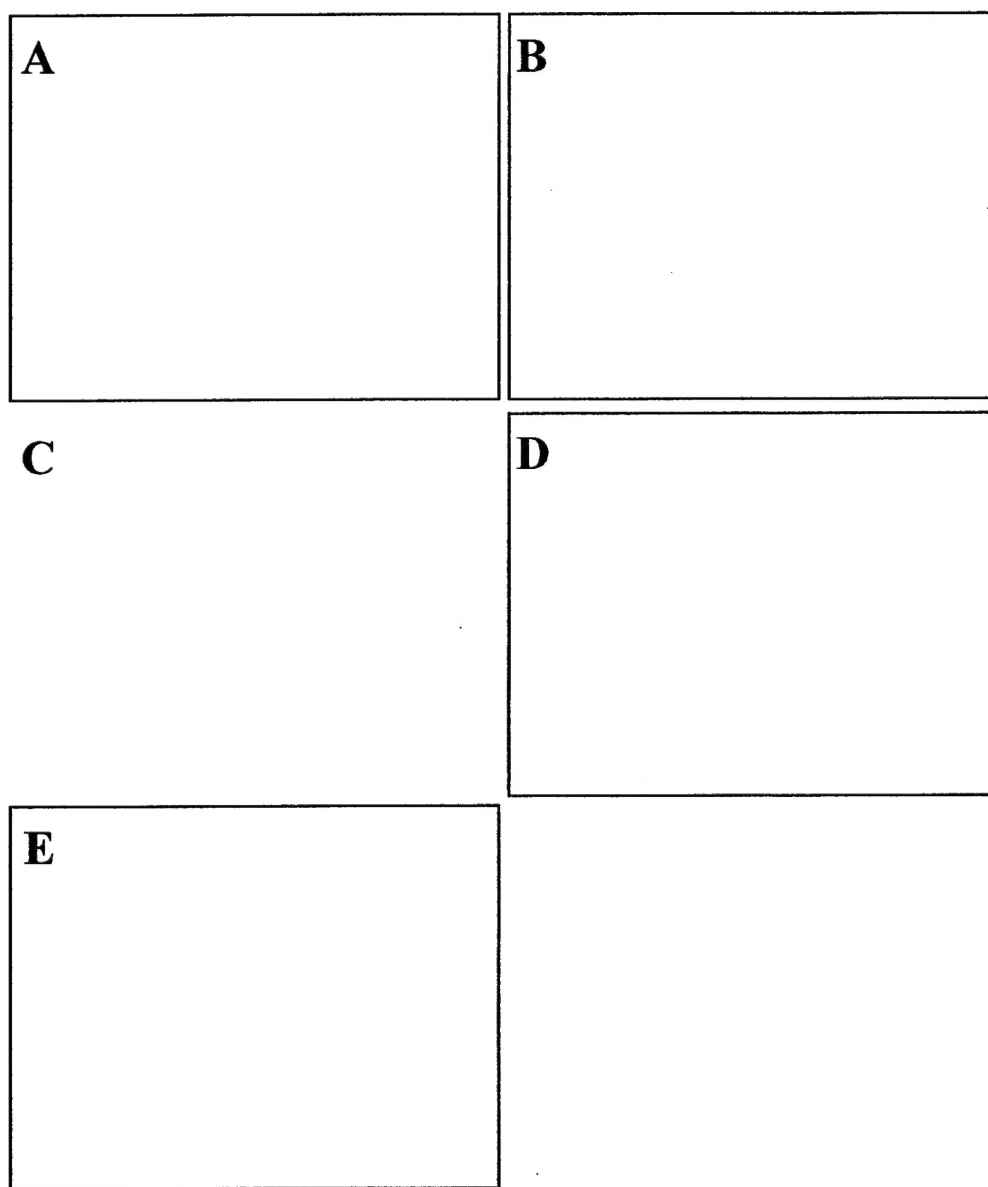(A-B) Lymphocyte with labeled LFA-1 (C-D) Label marking CD3. (E-F) Label marking CD4.

Figure 8.20. SEM images of equine peripheral blood lymphocyte clusters on a pokeweed mitogen micropatterned silicon substrate.
(A-E) Additional noteworthy images.

LFA-1) could be detected on the surface.   Fig. 8.20 display additional interering images that have yet to be characterized.

Conclusion

This research procedure provides a method for analyzing macrophage and lymphocyte responses to different isolated antigen spatially patterned at the micro- and nanometer scale. It allows control over the antigenic surface density, the surface area covered by antigen, the spacing between features, and the feature dimensions to submicron resolution. The mitogen and SA serve as a model of interaction of immune cells and their surroundings. SEM imaging provides a clear view of morphological changes to the mitogen stimuli. This augments the information gathered from fluorescent imaging, provides new insight to what occurs at the immune synapse and gives a better understanding of how immune cells interact with their environment.

References

[1]   Grakoui, A., Bromley, S. K., Sumen, C., Davis, M. M., Shaw, A. S., Allen, P. M. & Dustin, M. L. 1999. *Science,* 285:221-227.

[2]   Ilic, B. and H. G. Craighead. 2000. *Biomed. Microdevices,* 2:317-322.

[3]   Orth, R. N., Wu, M., Holowka, D. A., Craighead, H. G., Baird, B. A. 2003. *Langmuir,* 19:1599-1605.

[4]   Simons, K. and E. Ikonen. 1997. *Nature,* 387:569-572.

[5]   Li, S. S., A. Ivanoff, S.-E. Bergstrom, A. Sandstrom, B. Christensson, J. van Nerven, J. Holgersson, D. Hauzenberger, I. Arencibia, and K.-G. Sundqvist. 2002. *Eur. J. Immunol.,* 32:1069-1079.

[6]   Makgoba, M. W., M. E. Sanders, G. E. Ginther, M. L. Dustin, T. A. Springer, E. A. Clark, P Mannoni, and S. Shaw. *Nature,* 331:86-88.

[7]   Elices, M. J., L. Osborn, Y. Takada, C. Crouse, S. Luhowskyi, M. E. Helmer, R. R. Lobb. 1991. *Cell,* 60:577-584.

[8]   Giblin, P. A., S. T. Hwang, T. R. Katsumoto, and S. D. Rosen. 1997, *J. Immunol.,* 159:3498-3507.

[9]   Hwang, S. T., M. S. Singer, Giblin, P. A., T. A. Yednock, K. B. Bacon, S. I. Simon, S. D. Rosen. *J. Exp. Med.,* 184:1343-1348.

[10]   Porter, J. C. and N. Hogg. 1997. *J. Cell Biol.,* 138:1437-1447.

[11]   Klein, J. and V. Horejší, *Immunology.* Oxford: Blackwell Science Ltd., 1998, p. 52.

[12]   Mallavarapu, A. and T. Mitchison. 1999. *J. of Cell Biology,* 146:1097-1106.

[13]   Vasioukhin, V. C. Bauer, M. Yin, and E. Fuchs. 2000. *Cell,* 100:209-219.

[14]   Frame, M. C. V. J. Fincham, N. O. Carragher, and J. A. Wyke. 2002. *Nature Reviews Molecular Cell Biology,* 3:233-245.

[15]   Mitchison, T. J. and L. P. Cramer. 1996. *Cell,* 84:371-379.

[16]   Ramirez-Weber, F.-A. and T. B. Kornberg. 1999. *Cell,* 97:599-607.

[17]   Chiou, W.-F., A. Y.-C. Shum, C.-H. Peng, C.-F. Chen, and C.-J. Chou. 2003. *Eur. J. Pharm.,* 458:217-225.

[18]   Flaminio, M. J. B. F., B. Rush, E. G. Davis, K. Hennessy, W. Shuman, and
M. J. Wilkerson. 2002. Veterinary Research Communications 26:85-92.